Eva-Maria Köhler, BSc

Recombinant expression of new HNL enzymes in Escherichia coli and Pichia pastoris and their biochemical characterization

MASTERARBEIT

zur Erlangung des akademischen Grades

Diplom-Ingenieurin

Masterstudium Biotechnologie

eingereicht an der

Technischen Universität Graz

Betreuer

Ao.Univ.-Prof. Mag.rer.nat. Dr.rer.nat. Anton Glieder

Institute of Molecular Biotechnology

Graz, Oktober 2016

EIDESSTATTLICHE ERKLÄRUNG

Ich erkläre an Eides statt, dass ich die vorliegende Arbeit selbstständig verfasst, andere als die angegebenen Quellen/Hilfsmittel nicht benutzt, und die den benutzten Quellen wörtlich und inhaltlich entnommenen Stellen als solche kenntlich gemacht habe. Das in TUGRAZonline hochgeladene Textdokument ist mit der vorliegenden Masterarbeit identisch.

25.10.2016

Datum

Unterschrift

Danksagung

An dieser Stelle möchte ich mich bei all jenen bedanken, die durch ihre fachliche und persönliche Unterstützung zur Anfertigung dieser Diplomarbeit beigetragen haben.

An erster Stelle gilt mein Dank Herrn. Prof. Dr. Anton Glieder, für die Bereitstellung des interessanten Themas und die Möglichkeit es im Rahmen dieses ACIB Projekts zu verwirklichen.

Frau Dr. Margit Winkler danke ich für die ausführliche Korrektur und die hilfreichen Anregungen und Vorschläge zur Durchführung meiner wissenschaftlichen Arbeit.

Ein ganz besonderer Dank auch an Elisa Lanfranchi, die immer ein offenes Ohr für meine täglichen Fragen hatte und mir eine große Hilfe bei der praktischen Arbeit im Laboralltag war. Danke für den offenen Austausch und dass du mir bei meinen zahlreichen Fragen immer mit viel Geduld hilfreich zur Seite standst.

Frau Dr. Mandana Gruber danke ich für die fachliche und freundliche Unterstützung bei der Durchführung der Synthese Experimente am Institut für Organische Chemie.

Besonders bedanken möchte ich mich auch bei meiner lieben Studienkollegin Katharina Dokulil, mit der gemeinsam im Labor zu arbeiten jeden Tag eine Freude war und in der ich während der Studienzeit eine gute Freundin fand.

Danke auch an meine Studienkollegen der Gliedergroup und allen Mitarbeitern des ACIB Teams, besonders unserer Frühstücksrunde, die mir immer hilfsbereit zur Seite stand.

Abschließend möchte ich meiner Familie danken. Meinen Geschwistern David und Kerstin, besonders meiner Schwester Sophie, die mich nach langen Arbeitstagen oft noch mit Selbstgekochtem überrascht hat sowie meinen Eltern, die mich seit der Schulzeit immer in meinen Entscheidungen bekräftigt haben und die es mir ermöglichten mein Studium durch ihre Unterstützung abzuschließen.

This project has received funding from the European Union's Seventh Framework Programme for Research, technological development, and demonstration under grant agreement no. 289646

Abstract

Hydroxynitrile lyases (HNLs) are a highly diverse group of enzymes, distinct in their sequence and structure, which catalyse the enantioselective cleavage and synthesis of cyanohydrins. Products of HNL catalysed reactions find several applications in the pharmaceutical and fine chemical industry.

In this study, novel HNLs from the fern Davallia tyermannii were recombinantly expressed in Escherichia coli and Pichia pastoris as intra- and extracellular proteins and then biochemically characterized. Purification of E.coli produced enzymes was performed by affinity chromatography followed by the enzyme's biochemical characterization including several spectrometric screenings in order to determine the optimal reaction conditions for DtHNLs and kinetic parameters.

In a comparison with intracellular enzymes, glycosylated enzyme variants, secreted by P. pastoris, showed three times less specific activity but increased stability characteristics with almost similar physiological optima for pH and temperature. It was shown that the purified, as well as extracellularly produced DtHNLs offer a notable option as promising biocatalysts that are both easy to produce, to purify, and they also have good properties in view of the reaction conditions required for cyanohydrin synthesis reactions.

Kurzfassung

Hydroxynitrillyasen (HNLs) katalysieren die enatioselektive Spaltung sowie Synthese von Cyanohydrinen. Hinsichtlich ihrer Sequenz und Struktur stellen sie jedoch eine sehr heterogene Gruppe von Enzymen dar. Die Produkte HNL katalysierter Reaktionen finden verschiedenste Anwendungen in der Pharma- und Feinchemieindustrie.

Der Schwerpunkt dieser Arbeit lag in der biochemischen Charakterisierung vier neu identifizierter HNLs des Farns Davallia tyermanii (DtHNLs). Für die Expression wurden sowohl Escherichia coli als auch die methylotrophe Hefe Pichia pastoris verwendet. Die Aufreinigung der in E. coli produzierten Enzyme erfolgte per Affinitätschromatographie, gefolgt von deren Charakterisierung mittels spektrophotometrischer Screenings zur Bestimmung ihrer optimalen Reaktionsbedingungen und kinetischen Parameter.

Im Vergleich mit den intrazellulär produzierten Enzymen zeigten die glycosylierten Enzymvarianten, die durch P. pastoris sekretiert wurden, eine etwa dreimal geringere spezifische Aktivität jedoch erhöhte Stabilitätseigenschaften sowie ähnliche physiologische Optima hinsichtlich pH und Temperatur. Es wurde gezeigt, dass die aufgereinigten, sowie extrazellulär hergestellten DtHNLs eine interessante Option als vielversprechende Biokatalysatoren bieten, die sowohl einfach zu produzieren und reinigen sind, als auch gute Eigenschaften im Hinblick auf die in Synthesereaktionen notwendigen Reaktionsbedingungen aufweisen.

Contents

1 Introduction

1.1 Hydroxynitrile lyases

Hydroxynitrile lyases (HNLs) catalyse the enantioselective cleavage and synthesis of cyanohydrins into the corresponding aldehyde or ketone and cyanide (figure1) [1], [2].

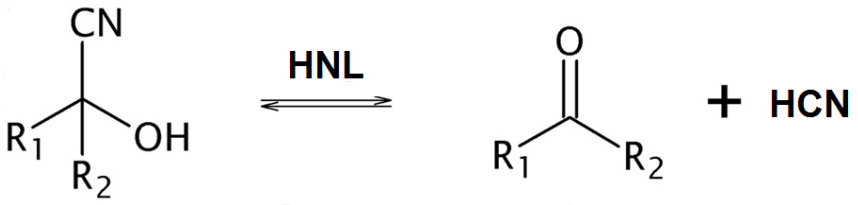

Figure 1: Schematic representation of the Hydroxynitrile lyase redox reaction [2].

At the time when this thesis was started, six different protein families had been identified by crystal structure determination: cupin [3], GMC oxidoreductase [4], alpha/beta hydrolase [5], [6], peptidase S10 [7] and the bet v 1 [8] family respectively. Furthermore, an HNL from the zinc-binding dehydrogenase family was described [9]. Finally, a heterogeneous group of HNLs with unsolved structure includes a recently discovered HNL from millipede [10], which sequence suggests a new protein fold. Several other HNLs have been isolated but no sequences or structures are known. Some examples are the HNLs from *Phlebodium aureum* [11], *Prunus amygdalus turcomanica* [12], *Xymenia americana* [13] and *Passiflora edulis* [14].

HNLs take parts in the last step of the cyanogenic pathway a peculiar defence mechanism of plants and arthropods against herbivores or microbial attack [15]. Specifically the unstable cyanohydrin is stabilized by glycosidic linkage with up to three sugar residues. The resulted cyanogenic glycoside (CG) is stored in the cell vacuole. Upon of the disruption of the plant tissue (e.g. leaf or kern), the CG is released and get in contact with β-glucosidases and hydroxynitrile lyases that are present in the cytoplasm or secreted to the intercellular space. First, the glycosidic linkage in aryl and alkyl β-glucosides is cleaved by β-glucosidases with the result

that the corresponding cyanohydrin dissociates spontaneously or enzymatically in the presence of a hydroxynitrile lyase to HCN and an aldehyde or ketone [16], [17].

In contrast, cyanogenic arthropods either sequester cyanogenic glycosides from their food plants (several plant bugs of the *Jadera* family) or biosynthesize their own [17], [15]. Centipedes for example produce a defensive secretion consisting of mandelonitrile, benzoyl cyanide, benzaldehyde and benzoic acid [18]; and polydesmoid millipedes store mandelonitrile in oily droplets in dorsal storage chambers. When they are jolted, the mandelonitrile is mixed with degrading enzyme in a reaction chamber [19]. The enzymes known to be involved in arthropods cyanogenic glycoside metabolism are β-glucosidases and α-hydroxynitrile lyases, as known from plants. The entire pathway of cyanogenic glycoside biosynthesis is therefore suggested to be highly similar to that known from plants. An explanation is probably an effect of convergent evolution [15], where an independent evolution of similar features in species of different lineages is observed. Analogous structures of similar form or function are created that did not exist in their last common ancestor [20].

The substrate scope of hydroxynitrile lyases offers a broad spectrum since HNLs differ in their stereospecificity and substrate range. *Hb*HNL and *Me*HNL for example use a wide range of substrates including aliphatic, aromatic and heteroaromatic aldehydes and ketones. Others catalyse the synthesis of cyanohydrins from either aromatic or aliphatic substrates [2].

The nowadays identified (*R*)- and (*S*)- selective HNLs are used for asymmetric syntheses of enantiomerically pure cyanohydrins, important building blocks for pharmaceutical, agrochemical and cosmetic industry [2], [21], [22]. Products of HNLs synthesis reaction, cyanohydrins, are built of an alcohol that contains a cyano group. Therefore a hydroxyl and a cyano group are attached to the same carbon atom [23]. The functional groups of synthetized cyanohydrins offer a variety of functionalized units for further transformations used in industrial applications. The nitrile group can undergo hydrolysis, solvolysis, and reduction. The hydroxyl or alcohol group can supress or avoid instability, degradation and racemization and the hydroxyl group as well as the carbon centre can further be used for inversion of configurations [24].

Hydroxynitrile lyase from *Davallia tyermannii* (*Dt*HNL)

The HNL sequence from the fern *Davallia tyermannii* has been recently identified in house [25]. The discovering workflow included integration of transcriptomics and proteomics data, retrieved from in gel activity assay developed in our group [8].

Structure and reaction mechanism

The structure of *Dt*HNL showed a Bet v 1 superfamily fold with a sequence related to the birch (*Betula verrucose*) pollen allergen Bet v 1. The enzyme is a dimer, and each subunit consists of a long C-terminal α-helix shrouded by an anti-parallel β-sheet (Figure 2a). The ligands are bound in a deep hydrophobic pocket between the β-sheet and the α-helix surrounded by the side chains of Val44, Val48, Trp47, Val51, Val52, Phe71, Cys73, Ile108, Phe111, Trp138, Leu160 and Ala164 (Figure 2b). The cavity is thereby shaped particularly by the involved valine residues, the Phe71 and Leu160. Polar hydroxyl-, carbonyl or carboxyl-groups of accepted ligands are bound by Tyr101 and Tyr117.

Interaction with (*R*)-mandelonitrile occurs by binding the cyano group with the guanidinum group of Arg69 and the carboxylic acid group of Asp85. Asp85 is thereby protonated in this complex. The polar OH-group of (*R*)-mandelonitrile is assumed to get deprotonated by Tyr101, whose own OH-group is linked to the guanidium group of Arg69 by a water molecule. The deprotonation is thereby facilitated by an additional hydrogen bond from Tyr 117 (Figure 3b). The active site is linked to the protein surface by a channel consisting of five water molecules, whereby the bridging water is the first of the five molecules (Figure 2c). The tunnel is orthogonal to the active site, and supposedly enables the transfer of HCN and works as a proton relay to the bulk solvent [25].

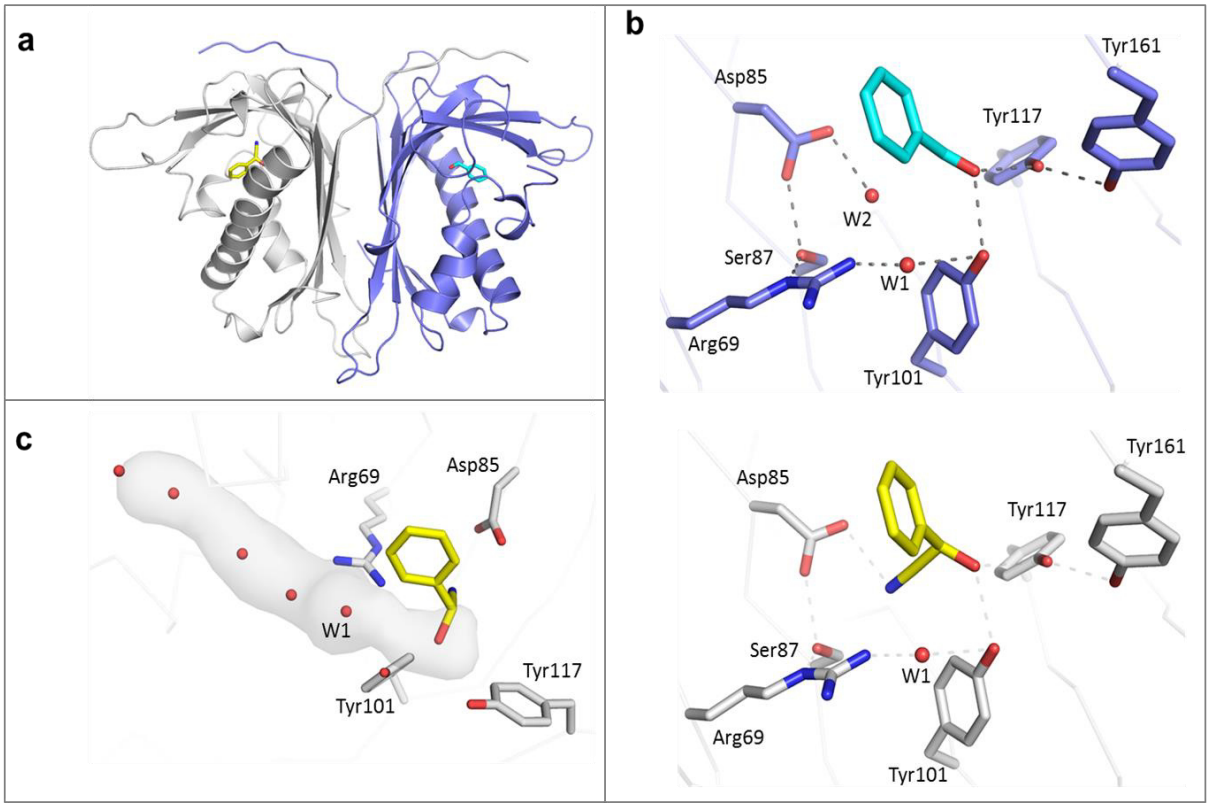

Figure 2: Structure and active site analysis of *Dt*HNL1. a: Three-dimensional structure of *Dt*HNL1 dimer. Respective monomers: ribbon, grey and blue. (*R*)-mandelonitrile: stick, yellow. Benzaldehyde: stick, cyan. b: The active site. Possible hydrogen bonds to (*R*)-mandelonitrile and benzaldehyde are shown as dashed lines. Amino acid residues involved in the catalytic reaction are depicted in stick representation. W1: bridging water. c: Water channel [25].

The distinction of two protons between Tyr101 and Arg69 is possible in three different configurations: a) Tyr-OH, OH^-, Arg^+, b) Tyr-OH, H_2O, Arg^0 or c) Tyr-O^-, H_2O, Arg^+. However, a definition on one of these configurations is not possible; the positive charge of arginine is preferential (Figure 3). Albeit after cyanohydrin cleavage reaction only the configuration Tyr-OH, H_2O, Arg^+ is conform to the structural data. The positively charged arginine residue and a hydrogen bond from the protonated Asp85 stabilize the negatively charged cyano group upon C-C bond cleavage [25].

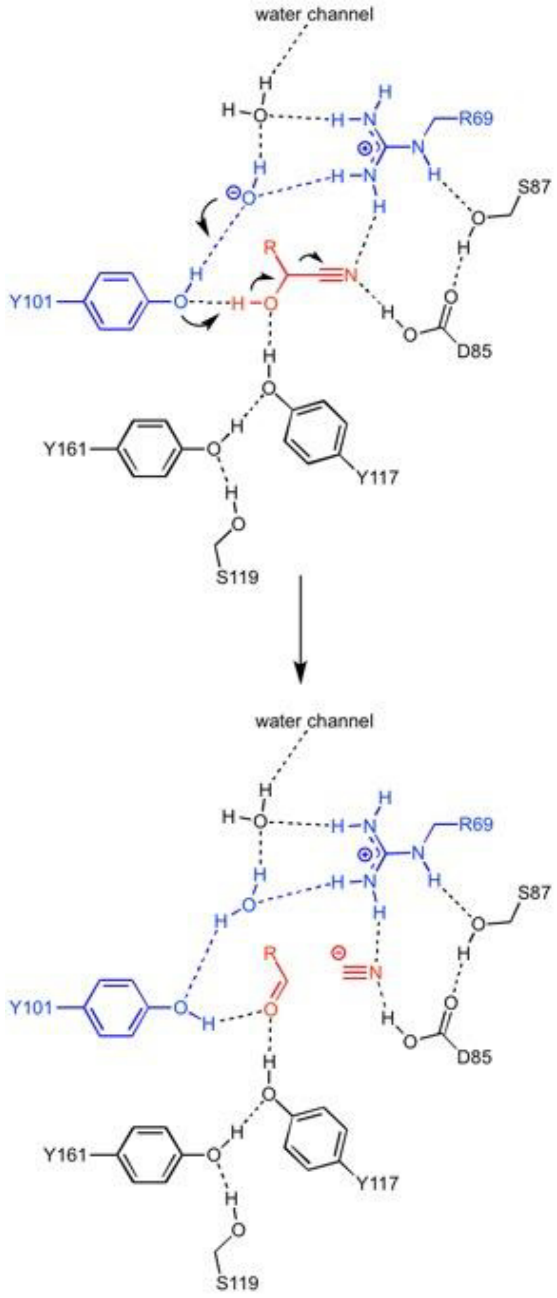

Figure 3: Suggested reaction mechanism for *Dt*HNL1 cleavage reaction of the cyanohydrin (*R*)-mandelonitrile [25].

Prior analysis has shown that *Dt*HNL1 accepts substrates of different aldehyde types (benzaldehyde, 2-chlorobenzaldehyde, 3-Phenylpropanal, 3-Phenylprop-2-enal, Furan-2-carbaldehyde) as well as the ketone 1-phenylethanone, whereby the substrate benzaldehyde showed one of the best conversions, because it is most probably the natural substrate [25]. The enzyme is highly (*R*)-selective with six amino

acid residues involved in substrate binding and catalytic conversion (Arg69, Tyr101, Tyr117, Asp85, Ser87 and Tyr161) [8].

1.2 General techniques used in this work

1.2.1 Protein purification

Purified enzymes are necessary to get specific kinetic enzyme data as well as the enzymes specific activities. They ensure to get clear answers about effects of possible inhibitors, the influence of additional proteins in biochemical properties or the enzymes catalysis. Several chromatographic methods enable the purification of biomolecules according to various differences in their specific properties. Beside affinity chromatography, which is based on bio-recognition of a specific ligand and size exclusion chromatography, which enables the separation of biomolecules according to their size (figure 4), various other techniques are commonly used for protein purification. Hydrophobic interaction and reversed phase chromatography are based on hydrophobicity and ion exchange chromatography enables the separation of proteins according on different charges [26], [27].

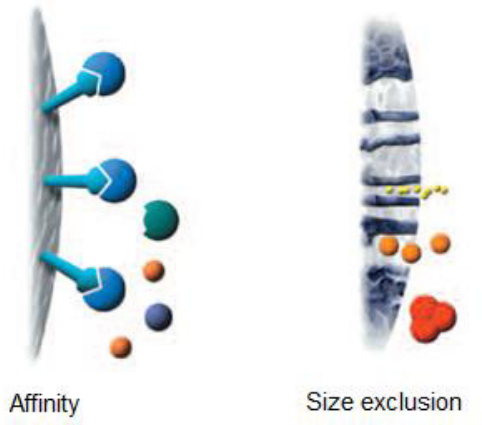

Figure 4: Separation principle of affinity chromatography and size exclusion chromatography for protein purification [28].

The four *Dt*HNL isoenzymes were fused to an N-terminal Histidine-Tag and purified by interaction to the nickel sepharose filling of a HisTrap FF column. The recovery of recombinant HNL enzymes was performed using an increasing concentration of imidazole in the elution buffer. Due to the high toxicity of imidazole and possible adverse influences on *Dt*HNLs enzymatic behaviour in afterwards characterization experiments, the imidazole containing elution buffer was exchanged by subsequent size exclusion chromatography.

1.2.2 Fluorescence based thermal shift assay

Thermal shift assays are based on the energetic coupling of ligand-binding and protein-melting reactions and can be used to screen for optimized buffer conditions by variation of pH, buffer molecules and small-molecule additives [29]. They are a simple, direct, affinity-based tool [30] for the detection of ligand-induced stability enhancement by e.g. different substrates, inhibitors, cofactors or metal ions. These interaction analyses are further used for high throughput drug screening of targets [31], [32].

Changes in the midpoint of protein melting curves are a consequence of the binding of a ligand to the respective protein. The melting temperature (T_m) is thereby directly proportional to the ligand binding affinity (K_a) [31].

Analysis takes place in a real-time PCR machine. Samples are mixed with a respective ligand and a fluorescent dye. Native, folded proteins do not interact with the hydrophobic dye. With increasing temperature the protein starts to unfold and a dye-protein complex is formed. The corresponding increase of the fluorescence intensity is plotted by a CCD detector (figure 5). The melting temperature is defined as the midpoint of the protein unfolding shift. In case of a protein-ligand interaction the melting temperature will shift to a higher value [30], [31].

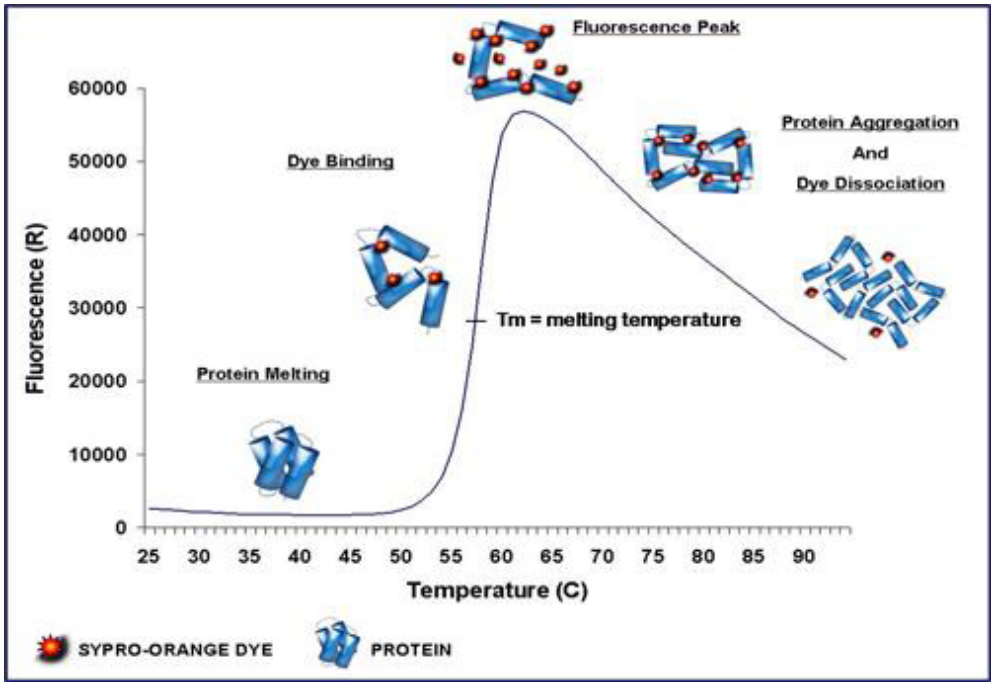

Figure 5: Principle of the fluorescent based thermal shift assay for a proteins melt curve analysis [33].

1.2.3 Gas Chromatography

Chromatographic separation is necessary to identify substrate specificities, specific reaction types, possible side product formatio and unspecific ractions or even unexpected new reaction products. Due to several advantages of gas chromatography (GC) it is one of the most common tecniques for the analysis of mixtures of volatile organic compounds. However, the analyzed substrates and reaction products need to be volatile or made volatile by chemical derivatization, before they can be separated by GC. GC analysis is a repeatable method, that offers a wide range of measurements and detectable components. All gas chromatographs are built of the same components (figure 6).

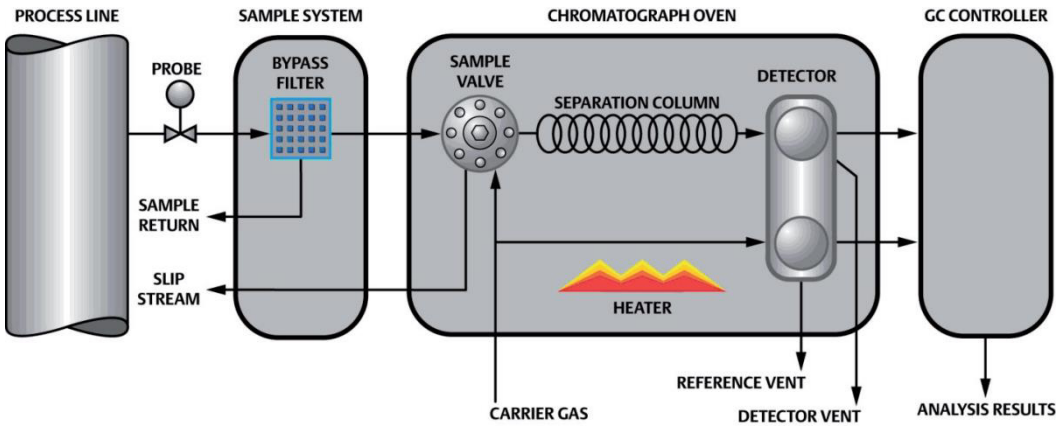

Figure 6: Schematic composition of a gas chromatograph [34].

Separation of the components in a gaseous mixture occurs in the chromatograph column based on their physical characteristics like their boiling points, molecular size or polarity. The stationary phase consists of small support material coated with a thin layer of liquid solvent. Sample gas and carrier gas are transported over the column whereby components with lower boiling points move slower than components with higher ones depending on the temperature of the column. The amount of separation of the components is further determined by the length of the column [34].

For the analysis of converted benzaldehyde to (*R*) - and (*S*)-mandelonitrile in *Dt*HNLs synthesis reaction, a CP-Chirasil-DEX CB column was used. Suitable for chiral compounds the matrix consist of cyclodextrin bonded to dimethylpolysiloxane, which ensures homogeneous enantioselectivity throughout the column. The high resolution factor between isomers leads therefore to a good separation of (*R*) - and (*S*)-mandelonitrile [35], [36].

1.2.4 Michaelis Menten Kinetics

Most enzymatic reactions are well represented by following Michaelis-Menten Kinetics (figure 7). If the initial reaction velocity is blotted against the substrate concentration of the particular reaction, the maximal initial velocity (V_{max}) and the substrate concentration for half-maximal initial velocity (K_M) can be determined [37].

$$\mathbf{v} = \frac{v_{max} * S}{K_M + S}$$

Figure 7: Michaelis Menten equation relating the reaction rate ($\mathbf{v}$) to the concentration of the substrate ($\boldsymbol{S}$) [38].

The formation of a product by decomposition of the enzyme-substrate complex is an irreversible reaction. Its rate constant is known as the turn over number or catalytic constant (k_{cat}), which defines the number of substrate molecules converted to product per unit time by an enzyme saturated with substrate.

The stability of the enzyme-substrate complex and therefore the substrate binding affinity is defined as K_M, since this substrate concentration indicates that half of the enzyme´s active sites are saturated with substrate, whereby the lower the K_M value, the higher the substrate affinity.

The correlation between k_{cat}/K_M is defined as the catalytic efficiency. This ratio is generally used to compare the utilisation of different substrates by a certain enzyme. Higher catalytic efficiencies are thereby preferential [38].

In the current study, the kinetic parameters in both *Dt*HNLs synthesis and cleavage reactions were determined. In synthesis reaction *Dt*HNL1 was used for the conversion of benzaldehyde. Cleavage reaction was carried out using *Dt*HNL1, 2, 3 and 4 for the conversion of (*R*)-mandelonitrile. However, an accurate comparison with other hydroxynitrile lyases is hardly possible, since the reaction conditions often differ in set ups like substrate and buffer compositions or parameters of the biphasic system.

1.3 The *Pichia pastoris* expression system

First identified in 1969 [39], methanol utilizing yeasts were evaluated as a potential source for the efficient production of functional proteins. After establishing pilot scale production of single cell protein research done by the Sibia in collaboration with Phillips Petroleum Company resulted in the establishment of *P. pastoris* as a model eukaryote used in cell biology and an efficient expression system for the production of high levels of heterologous proteins [40].

Advantages offered by the *P. pastoris* expression system compared with mammalian cells include the usage of modest growth medium and culture conditions due to the preference of *P. pastoris* for respiratory growth that facilitates the culturing to very high cell densities. Genetic manipulation is eased since similar techniques are needed for the well characterized yeast *Saccharomyces cerevisiae* and high levels of protein are able to get produced at the intra- or extracellular level while secreted proteins are transported into an almost protein-free medium. Additionally, *Pichia* has the ability to perform higher eukaryotic post translational protein modifications such as glycosylation, proteolytic processing and disulfide bond formation [40], [41], [42] and offers the advantage, that products are free of endotoxins and of oncogenic and viral DNA.

1.3.1 Methanol metabolism

Finally, *Pichia* belongs to one of the four methylotrophic yeasts including *Hansenula, Pichia, Candida* and *Torulopsis*. The first part of the methanol utilisation pathway takes place in the peroxisomes, whereby massive growth of these organelles can be observed in case of methanol induction [43]. Since important key enzymes such as alcohol oxidase, catalase and dihydroxyacetone synthase are located in these organelles, they can take up to 80% of the cytoplasmic volume [39]. Due to these properties, a set of strong and regulatable promoters from methanol metabolism pathway genes is available [44], whereby the promoter of the alcohol oxidase I gene (AOX1) is especially well characterized and therefore commonly used for the production of recombinant proteins [43].

After entering the peroxisome, methanol is oxidized by alcohol oxidase to hydrogen peroxide and formaldehyde. Simultaneously, electrons are transferred to oxygen. The toxic peroxide is oxidized by peroxisomal catalase to water and oxygen while formaldehyde is formed, that can enter two different pathways.

In the subsequent assimilatory pathway, biomass is formed starting with the condensation of formaldehyde with xylulose-5-phosphate. Dihydroxyacetone synthase leads to the production of dihydroxyacetone and glyceraldehyde-3-phosphate. Xylulose-5-phosphate is regained in a cyclic pathway while one-third of glyceraldehyde-3-phosphate leads to the production of biomass and cell constituents.

The dissimilative pathway is responsible for energy production as well as the detoxification of formaldehyde and formate. Formaldehyde enters the cytosol, forms a complex with reduced glutathione and is further oxidized to carbon dioxide by two NAD+ -dependent dehydrogenases. NADH, which is generated in both reactions, is thereby used in energy production when grown on methanol. Detoxification is done by S-formylglutathione hydrolase. It hydrolyses S-formylglutathione, the complex of formaldehyde and glutathione, to formate and glutathione [41], [43], [45].

2 Objectives

Aim of this work was the biochemical characterization of heterologously expressed *Dt*HNL isoenzymes. Histidine-tagged *Dt*HNL enzymes were first expressed in *E. coli* BL-21 (DE3) Star and afterwards purified by affinity chromatography. The enzymatic characterization enabled to determine specific activity, pH and temperature dependence and kinetic parameters described by the Michaelis-Menten model. Furthermore, thermal stability and tolerance against several different compounds were measured.

The second part of this work concerns the production of *Dt*HNLs in *P. pastoris* intracellular and secreted respectively. Specifically, the work focuses on the intracellular expression, while *Dt*HNLs *P. pastoris* secreting strains were provided by a third party (VTU technologies). Thus glycosylated *Dt*HNLs can be obtained as consequence of protein secretion of a protein containing a typical N-glycosylation site. Such glycosylation might influence the biochemical properties of the enzymes. The different recombinant enzyme sources were therefore analyzed with respect to variations on their biochemical characteristics.

3 Material and Method

3.1 Instrument and devices

3.1.1 Centrifuges and associated equipment

Centrifuge 5810R: Eppendorf AG, Hamburg, Germany
Centrifuge 5415R: Eppendorf AG, Hamburg, Germany
Avanti™ centrifuge J-20XP: Beckman Coulter™, Inc, Vienna Austria
JA-10 rotor, fixed angle: Beckman Coulter™, Inc, Vienna Austria
JA-25.50 rotor, fixed angle: Beckman Coulter™, Inc, Vienna Austria
Nalgene®Labware 500ml PPCO Centrifuge Bottles: Thermo Fisher Scientific, Rochester, NY, USA

3.1.2 Electrophoresis and associated materials and devices

Agarose Gel electrophoresis
PowerPac™ Basic Power supply: Bio-Rad Laboratories, Vienna, Austria
Sub-cell GT, Bio-Rad Laboratories: Vienna, Austria
Chroma 43 medium-wave 302 nm: Laborgeräte Vetter GmbH, Wiesloch, Germany
Biozym LE Agarose: Biozym Biotech Trading GmbH, Vienna, Austria
6x DNA Gel loading dye: Thermo Fisher Scientific Inc., Waltham, MA, USA
GeneRuler™ 1kb DNA Ladder: Thermo Fisher Scientific Inc., Waltham, MA, USA

SDS-Page
PowerEase 500 power supply: Invitrogen™ life technologies, Lofer, Austria
XCell SureLock™ Mini-cell: Invitrogen™ life technologies, Lofer, Austria

NuPAGE® Novex 4-12% BisTris Gel, 1.0mm, 15 well/ 10 well: Invitrogen™ life technologies, Lofer, Austria
NuPAGE® MES SDS Running Buffer (20x): Invitrogen™ life technologies, Lofer, Austria
NuPAGE® LDS sample buffer (4x): Invitrogen™ life technologies, Lofer, Austria
NuPAGE® sample reducing agent (10X): Invitrogen™ life technologies, Lofer, Austria
PageRuler™ prestained protein ladder: Thermo Fisher Scientific Inc., Waltham, MA, USA
HP Scanjet 4370 photo scanner: Hewlett-Packard Development Company, L.P., Palo Alto, CA, USA

Native-Page

NativePAGE™ Novex®4-16% Bis-Tris Gel, 1.0mm, 10 well: Invitrogen™ life technologies, Lofer, Austria

NativeMark™ Unstained Protein Standard: Invitrogen™ life technologies, Lofer, Austria

Whatman® filter paper: GE Healthcare Europe GmbH, Vienna, Austria

3.1.3 Electroporation materials

Gene Pulser™: Bio-Rad Laboratories, Vienna, Austria

Electroporation cuvettes 2 mm: Bridge Bioscience™, Rochester, NY, USA

3.1.4 Microplates

PS-Microplate 96-well, flat bottom: Greiner Bio-One GmbH, Frickenhausen, Germany

UV-STAR® MICROPLATTE, 96 WELL, HALF AREA: Greiner Bio-One GmbH, Frickenhausen, Germany

Rotilab® Abdeckfolien für Mikrotestplatten: Carl Roth GmbH+Co KG, Germany

VIEWseal™, sealing film, transparent: Greiner Bio-One GmbH, Frickenhausen, Germany

SILVERseal™, aluminium foil: Greiner Bio-One GmbH, Frickenhausen, Germany

MicroAmp® optical 96-well reaction plate: Applied Biosystems, Foster City, CA, USA

MicroAmp® optical adhesive covers: Applied Biosystems, Foster City, CA, USA

96-well footprint deep well plate, PP: Bel-Art Products, Pequannock, NJ, USA

Cover for deep well plate: Bel-Art Products, Pequannock, NJ, USA

3.1.5 Reaction Tubes

Micro-centrifuge tubes, 1.5 mL with lid: Greiner Bio GmbH, Frickenhausen, Germany

PP-Tube, sterile, cap, 12 ml: Greiner Bio GmbH, Frickenhausen, Germany

PP-Tube, sterile, 15 mL: Greiner Bio GmbH , Frickenhausen, Germany

PP-Tube, sterile, +/- support skirt, 50 mL: Greiner Bio GmbH, Frickenhausen, Germany

3.1.6 Pipettes and devices

GILSON PIPETMAN Classic™ (20 µL, 200 µL, 1000 µL): Gilson, Inc. P.O. Box 620027, Middleton, USA

Eppendorf Research® pipette (adjustable volume), 0.1-2.5 µL: Eppendorf AG, Hamburg, Germany

peqPETTE (1000 µL, 200 µL, 20 µL, 10 µL, 2µL): PEQLAB Biotechnologie GmbH, Erlangen, Germany

Biohit Proline® multichannel electronic pipettor, 8 channels 50-1200 µL: Biohit Plc., Helsinki, Finland

Biohit Proline® multichannel electronic pipettor, 8 channels 5-100 µL: Biohit Plc., Helsinki, Finland

Pipette tips (10 µL, 200 µL, 1000 µL): Greiner Bio-One GmbH, Frickenhausen, Germany

Biohit optifit refill tips 350 µL: Sartorius Stedim Biotech GmbH, Göttingen, Germany

Biohit tips 1200 µL: Sartorius Stedim Biotech GmbH, Göttingen, Germany

INTEGRA Pipetboy: Integra Biosciences AG,Konstanz, Germany

Pipette (5 mL, 10 mL, 25 mL): Sarstedt Aktiengesellschaft & Co., Nümbrecht, Germany

Sartorius™ BIOHIT™ PICUS™ 8-Channel Electronic Pipette (50 – 1200 µL): Thermo Fisher Scientific Inc., Waltham, MA, USA

Finnpipette® Novus 8-Channel Electronic Pipette (30 - 300 µL): Thermo Scientific Inc., Waltham, MA, USA

3.1.7 Platereaders, Photometers and associated materials

DU 800 spectrophotometer: Beckman coulter Inc, Fullerton, CA, USA

NanoDrop 2000c spectrophotometer: peqlab Biotechnologie GmbH, Polling, Austria

Eppendorf BioPhotometer plus: Eppendorf AG, Hamburg, Germany

Synergy Mx monochromator-based multi-detektions-reader: BioTek Instruments, Inc., Winooski, VT 05404, United States

Semi-micro cuvette 10x4x45 mm, Polystyrene: Sarstedt Aktiengesellschaft & Co., Nümbrecht, Germany

Cary 100 UV-Vis Spectrophotometer: Agilent Technologies, Santa Clara, CA, USA

Cary Temperature Controller: Agilent Technologies, Santa Clara, CA, USA

3.1.8 Shaker and Incubators

Titramax 1000: Heidolph Instruments, Schwabach, Germany (1,5mm)

Thermomixer comfort: Eppendorf AG, Hamburg, Germany (3mm)

Multitron II incubator shaker: Infors AG, Bottmingen-Basel, Switzerland

RS 306 rotary shaker: Infors AG, Bottmingen-Basel, Switzerland (50mm)

Certomat® BS1: Sartorius AG, Göttingen, Germany (25mm)

Binder drying oven: Binder GmbH, Tullingen, Germany

3.1.9 Thermocyclers

GeneAmp®PCR System 2700: Applied Biosystems, Foster City, USA

7500 real time PCR system: Applied Biosystems, Foster City, CA, USA

3.1.10 Instruments for FPLC

ÄKTA pure: GE Healthcare Europe GmbH, Vienna, Austria

ÄKTA prime: GE Healthcare Europe GmbH, Vienna, Austria

Sample Pump P-950: GE Healthcare Europe GmbH, Vienna, Austria

His trap™ FF, 5 mL: GE Healthcare Europe GmbH, Vienna, Austria

HiPrep™ 26/10 Desalting 53 mL: GE Healthcare Europe GmbH, Vienna, Austria

Diaphragm pump: VACUUBRAND GMBH + CO KG, Wertheim, Germany

Cellulose acetate filter, 0.2 µm pore size: Sartorius Mechatronics Austria GmbH, Vienna, Austria

Polysulfone reusable bottletop filter holder: Nalgene Nunc International Corporation, Rochester, NY, U.S.A.

3.1.11 Instruments for Syntesis Reaction

PAC III HCN Detector: Dräger Safety AG & Co. KGaA, Lübeck, Germany

HP 6890 GC system: Hewlett-Packard, Palo Alto, CA, USA

PAL autosampler: CTC Analytics AG, Zwingen, Switzerland

CP-Chirasil-DEX CB column (25 m x 0.32 mm, 0.25 mm film): Agilent Technologies, Santa Clara, CA, USA

3.1.12 Other materials and devices

Arium® basic ultrapure water system: Sartorius Stedim Biotech GmbH, Göttingen, Germany

Cryo.s™ freezing tube 2 ml: Greiner Bio GmbH, Frickenhausen, Germany

Hamilton pH electrode: Hamilton Messtechnik GmbH, Höchst, Germany

inoLab® pH720 pH meter: WTW, Weilheim, Germany

Kern scale ABS 220-4: KERN & SOHN GmbH, Balingen, Germany

Membrane filters 0,025 µm: Millipore Corporation, Billerica, MA, USA

MR 3000 magnetic stirrer: Heidolph, Schwabach, Germany

PG12001-S DeltaRange: Mettler-Toledo International Inc., Argentia Road, CA, USA

Rotations-Vacuum-Concentrator RVC 2-18: Martin Christ Gefriertrocknungsanlagen GmbH, Osterode am Harz, Germany

Rotilabo® syringe filters, CME, sterile, Ø 33 mm, 0.22 µm pore size: Carl Roth GmbH + Co. KG, Karlsruhe, Germany

Safe-lock tubes (0.5/1.5/2 mL): Eppendorf AG, Hamburg, Germany

Sartorius BL 120S scale: Sartorius Stedim Biotech GmbH, Göttingen, Germany

VivaSpin 20, 10,000 MWCO PES: Sartorius Stedim Biotech GmbH, Göttingen, Germany

Vortex-Genie 2: Scientific Industries Inc., Bohemia, NY, USA

3.2 Strains, Plasmids and Primers

3.2.1 Strains

Escherichia coli K12 Top10F': (culture collection number: 1482), F'{*lacI*^{q}, Tn*10*(Tet^{R})} *mcr*A Δ(*mrr-hsd*RMS-*mcr*BC) φ80 *lacZ*ΔM15 Δ*lac*X74 *deo*R *rec*A1 *ara*D139 Δ(*ara-leu*)7679 *gal*U *gal*K *rps*L(Str^{R}) *end*A1 *nup*G

Invitrogen corporation, San Diego, USA

Escherichia Coli BL 21 (DE3) Star: F– *omp*T *hsd*SB(rB–, mB–) *gal dcm* (DE3), Invitrogen, Carlsbad, USA

***Pichia pastoris* Mut^{S}**: (culture collection number: 3445), *Δaox1::FRT*

Based on *P. pastoris* CBS7435, engineered at Graz University of Technology [46]

3.2.2 Plasmids

Preexisting plasmids

- pEHisTEV_*Dt*HNL1_E.coli_opt (figure 8)
- pEHisTEV_*Dt*HNL2_E.coli_opt
- pEHisTEV_*Dt*HNL3_E.coli_opt
- pEHisTEV_*Dt*HNL4_E.coli_opt
- pPpT4_S_*Dt*HNL1_Pichia_opt
- pPpB1_*Dt*HNL1_Pichia_opt

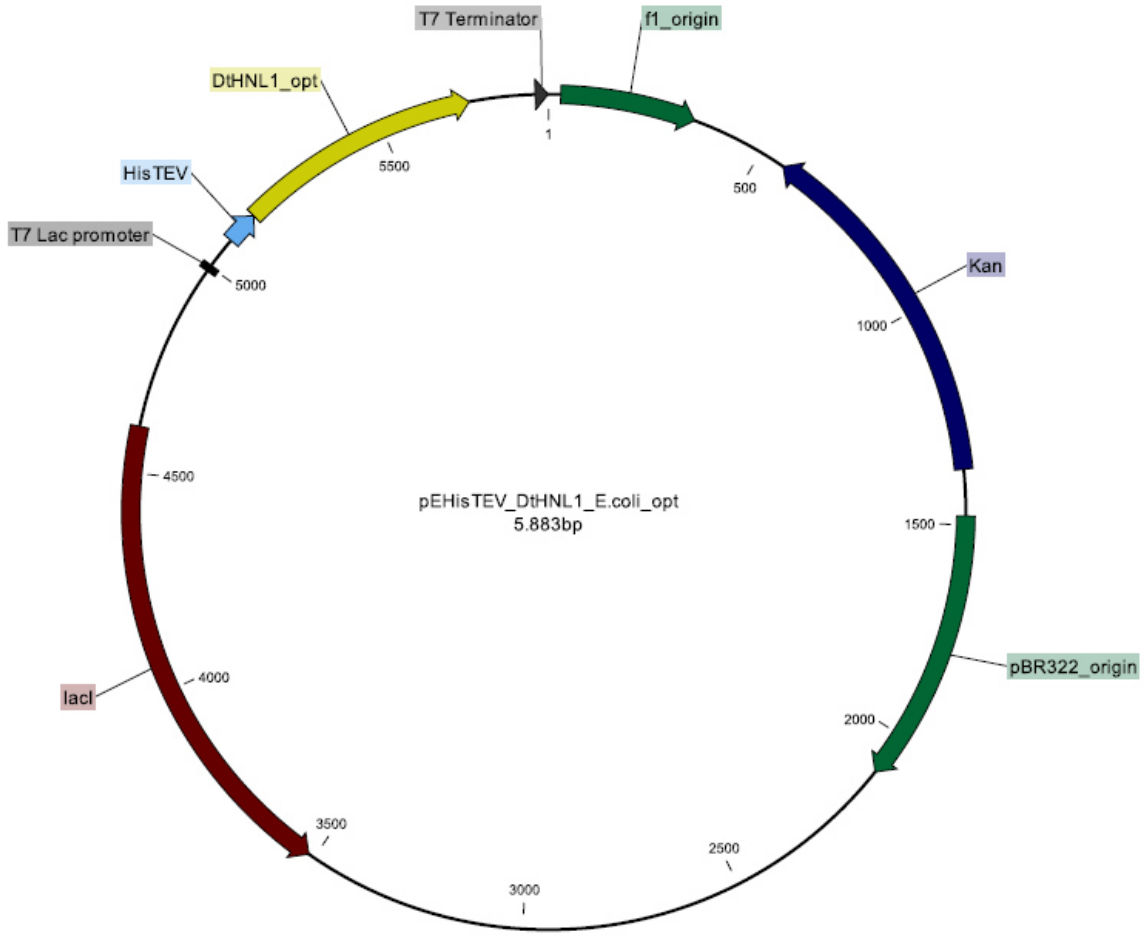

Figure 8: pEHisTEV_*Dt*HNL1_E.coli_opt, Kan: Kanamycin resistance gene, pBR322_origin: pBR322 origin of replication, f1 origin: replication origin of phage f1, lacI: Regulator gene of lac-repressor, T7 lac promoter, T7 terminator, HisTEV: n-terminal tag of GOI, *Dt*HNL1_opt: GOI (vicarious for the four *Dt*HNL isoenzymes) codon optimized for expression in *E.coli*.

Plasmids constructed for this thesis

Preexisting vector backbones pPpT4_S and pPpB1 were constructed by Näätsaari et al. [46] and used for the construction of the following plasmids:

- pPpT4_S_*Dt*HNL2_Pichia_opt (figure 9)
- pPpT4_S_*Dt*HNL3_Pichia_opt
- pPpT4_S_*Dt*HNL4_Pichia_opt

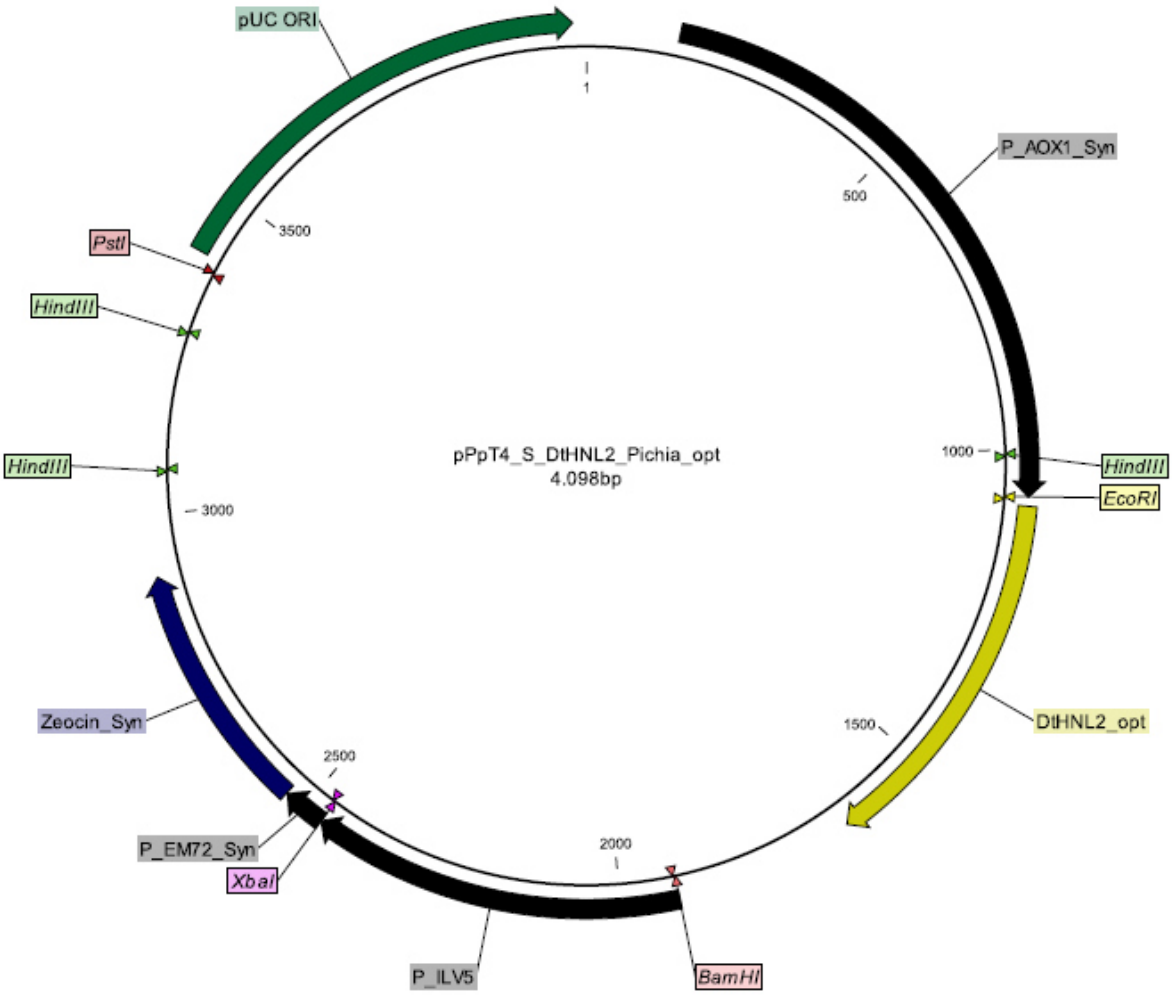

Figure 9: pPpT4_S_*Dt*HNL2_Pichia_opt, Zeocin_syn: Zeocin™ resistance gene, P_ILV5: Eukaryotic promoter, P_EM72 syn: Synthetic prokaryotic promoter, pUC ori: pUC origin of replication, P AOX1 syn: Synthetic AOX1 promoter region, *Dt*HNL2_opt: *Dt*HNL2 (vicarious for *Dt*HNL3 and *Dt*HNL4) codon optimized for expression in *P. pastoris*.

- pPpB1_*Dt*HNL2_Pichia_opt (figure 10)
- pPpB1_*Dt*HNL3_Pichia_opt
- pPpB1_*Dt*HNL4_Pichia_opt

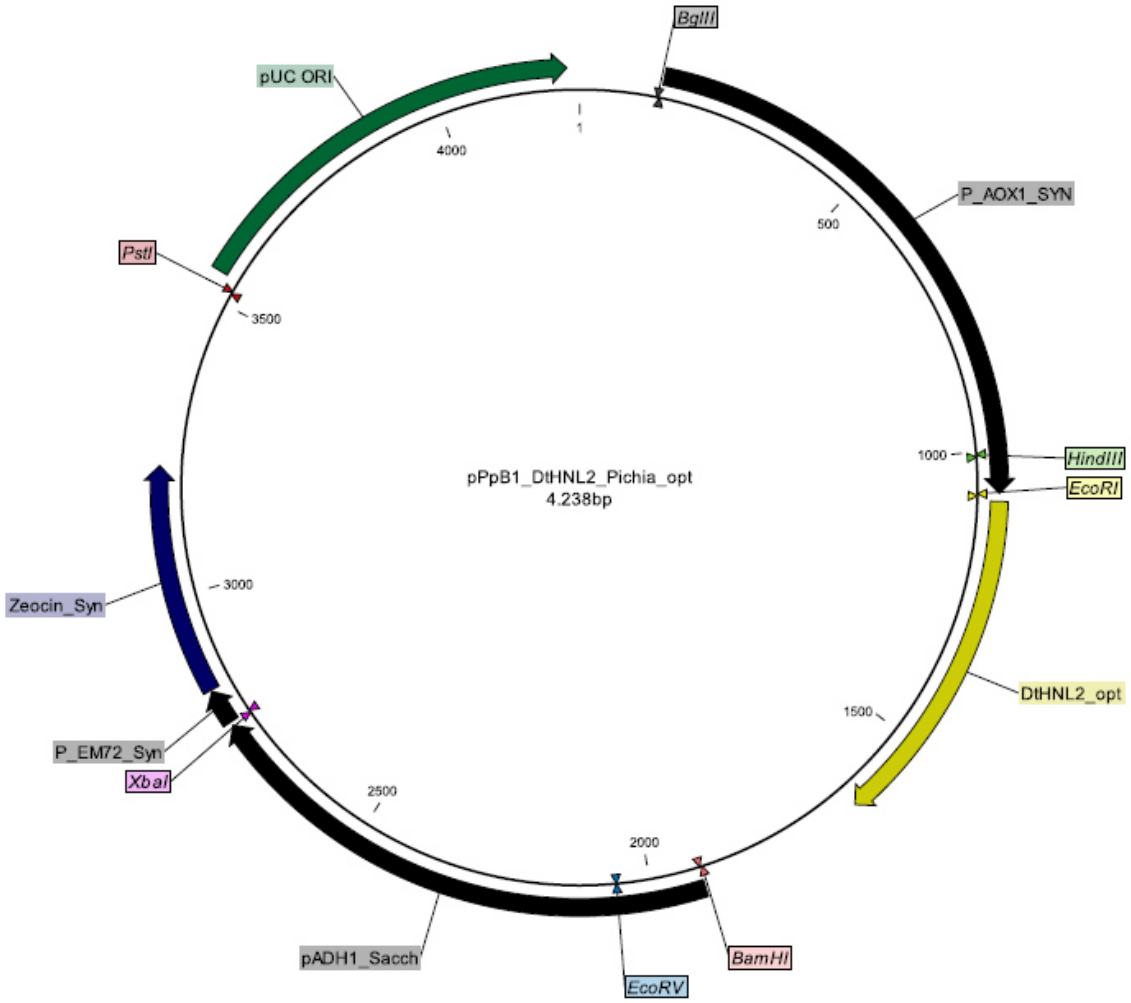

Figure 10: pPpB1_*Dt*HNL2_Pichia_opt, Zeocin_syn: Zeocin™ resistance gene, P_ADH1_Sacch: Eukaryotic promoter, P_EM72 syn: Synthetic prokaryotic promoter, pUC ori: pUC origin of replication, P AOX1 syn: Synthetic AOX1 promoter region, *Dt*HNL2_opt: *Dt*HNL2 (vicarious for *Dt*HNL3 and *Dt*HNL4) codon optimized for expression in *P. pastoris*.

3.2.3 Primers

Table 1: List of primers used

Number	Label	Sequence (5´→3`)	Purpose
P12255	seqRSFC-pAOX1_fwd	GCGACTGGTTCCAATTGACAAGC	Confirmation of plasmids in colony PCR.
P14175	seqRSFC-AOX1TT_rev	CGAGATAGGCTGATCAGGAGCAAG	
P14109 B1	seqpB1_fwd TM 50.2°C	CCTTGTTTCTTTTTCTGCAC	Confirmation of plasmids for intracellular production of *Dt*HNL isoenzymes in *P. pastoris*
P14109 T4	seqpT4s_fwd TM 49.4°C	CACACAATAAGCGTTCATATC	
Mycrosynth standard Primer list	M13	TGTAAAACGACGGCCAG	
	T7 probis	TCCCGCGAAATTAATACG	

3.3 Buffers, Stocks and Media

3.3.1 Buffers and Solutions

3.3.1.1 Buffer solutions for FPLC

Binding buffer: 20 mM $NaPO_4$, 0.5 M NaCl, 10 mM imidazole: 0.593 g/L $NaH_2PO_4.2H_2O$, 2.300 g/L Na_2HPO_4, 29.22 g/L NaCl, 0.681 g/L imidazole

Elution buffer: 20 mM $NaPO_4$, 0.5 M NaCl, 500 mM imidazole: 0.593 g/L $NaH_2PO_4.2H_2O$, 2.300 g/L $Na_2HPO_4.2H_2O$, 29.22 g/L NaCl, 34.04 g/L imidazole

Desalting Buffer: 50 mM $NaPO_4$: 1.811 g/L $Na_2HPO_4.2H_2O$, 4.47 g/L $NaH_2PO_4.2H_2O$, pH 6.5 adjusted with NaOH or o-phosphoric acid (≥ 85 %)

3.3.1.2 Buffer solutions and stock solutions for enzyme characterization

Cleavage Reaction: Kinetic-Assay

50 mM citrate phosphate buffer:

pH 7.0: 0.35 g/L citric acid monohydrate, 3.31 g/L $Na_2HPO_4.2H_2O$

pH 6.5: 0.83 g/L citric acid monohydrate, 2.99 g/L $Na_2HPO_4.2H_2O$

pH 6.0: 1.15 g/L citric acid monohydrate, 2.78 g/L $Na_2HPO_4.2H_2O$

pH 5.5: 1.39 g/L citric acid monohydrate, 2.61 g/L $Na_2HPO_4.2H_2O$

pH 5.0: 1.68 g/L citric acid monohydrate, 2.41 g/L $Na_2HPO_4.2H_2O$

pH 4.5: 1.91 g/L citric acid monohydrate, 2.26 g/L $Na_2HPO_4.2H_2O$

pH 4.0: 2.33 g/L citric acid monohydrate, 1.98 g/L $Na_2HPO_4.2H_2O$

pH 3.5: 2.69 g/L citric acid monohydrate, 1.73 g/L $Na_2HPO_4.2H_2O$

pH 3.0: 3.46 g/L citric acid monohydrate, 1.21 g/L $Na_2HPO_4.2H_2O$

pH 2.5: 4.22 g/L citric acid monohydrate, 0.70 g/L $Na_2HPO_4.2H_2O$

3 mM citrate phosphate buffer: 0.208 g/L citric acid monohydrate, 0.073 g/L $Na_2HPO_4.2H_2O$, pH 3.5

50 mM sodium acetate buffer:

pH 5.0: 3.81 g/L $NaOAc.3H_2O$, 1.06 g/L acetic acid

pH 4.5: 2.67 g/L $NaOAc.3H_2O$, 1.80 g/L acetic acid

pH 4.0: 0.98 g/L $NaOAc.3H_2O$, 2.90 g/L acetic acid

60 mM mandelonitrile solution: 8 µL (*R*) / (*R*/*S*) – Mandelonitrile/mL ddH_2O, Sigma Aldrich

50 mM sodium phosphate buffer: 1.811 g/L $Na_2HPO_4.2H_2O$, 4.47 g/L $NaH_2PO_4.2H_2O$, pH 6.5 adjusted with NaOH or o-phosphoric acid (≥ 85 %)

Cleavage reaction: Endpoint Assay

50 mM citrate-phosphate buffer pH 5.0: 0.50 g/L citric acid monohydrate, 0.89 g/L $K_2HPO_4.2H_2O$

300 mM racemic mandelonitrile: 40 µL racemic mandelonitrile/mL 0.1 M Citric acid

300 mM Acetone cyanohydrin: 27.3 µL Acetone cyanohydrin/mL 0.1 M Citric acid

300 mM Hydroxypivaldehyde cyanohydrin: 77.2 µL Hydroxypivaldehyde cyanohydrin/mL 0.1 M Citric acid

Reaction Mix I: 100 mM N-chlorosuccinimide (13.36 mg/mL), **Succinimide (10x excess)** (133.54 mg/mL), **ddH_2O**

Reaction Mix II: 125 mM Barbituric acid (16 mg/mL), **65 mM Isonicotinic acid** (8 mg/mL), **0.2 mM NaOH**

3.3.1.3 Buffer solutions and stock solutions for Native Page

Running Buffer (10x): 104.6 g/L BisTris, 89.6 g/L Tricine, pH 6.8, pH adjusted with 1M HCl
Sample Buffer (4x): 41.8 g/L BisTris, 10.7 mL/L 6M HCl, 400 g/L Glycerol, 11.7 g/L NaCl, 40 mg/L Ponceau S, pH 7.2
Cathode Additive (20x): 4 g/L Coomassie G-250
Anode Buffer (1x): 100 mL Running buffer 10x, 900 mL Deionized Water
Light Blue Cathode Buffer (1x): 20mL Running buffer (10x), 1 mL Cathode Additive (20x), 179 mL Deionized water.

Native-Page coupled HNL activity assay

Reaction buffer: 100mM Citrate Buffer pH 4.5 (10.44 g/L Citric acid, 294.1 g/L Sodium citrate)
Substrate solution: 15-30 mM racemic mandelonitrile (Sigma Aldrich) in 100mM citrate buffer pH 4.5
Detection paper: Whatman No.1 filter sheets soaked with a 1:1 mixture of 1% (w/v) copper (II) ethylacetoacetate in chloroform and 1% (w/v) of 4,4'-methylenebis (N,N-dimethyl-aniline) in chloroform [47].

Other chemicals and solutions

10x dNTP mix: 20 mM each dATP, dTTP, dCTP, dGTP; 100mM, Fermentas GmbH, St.Leon-Rot, Germany
50x TAE buffer: 242.0 g Tris, 57.1 mL glacial acetic acid ≥99.85 %, 100.0 mL 0.5 M EDTA, dH_2O added to a final volume of 1 L
BEDS solution: 10 mM bicine-NaOH, 3 % (v/v) ethylene glycol, 5 % (v/v) DMSO, 1 M sorbitol, pH 8.3 adjusted with 2 M NaOH, filter sterilized
1 M DTT: 7.71 g dithiothreitol, water added to 50 mL, filter sterilized
Sypro Orange fluorescence dye, 5000x: Invitrogen™ life technologies, Lofer, Austria
Cell Lytic™ B Cell Lysis Reagent: Sigma Aldrich GmbH, Schnelldorf, Germany
SimplyBlue™ SafeStain: Thermo Fisher Scientific Inc., Waltham, MA, USA

3.3.2 Stocks

Kanamycin sulphate (100 mg/mL): Carl Roth GmbH, Karlsruhe, Germany
Zeocin™, 5g Powder: InvivoGen, San Diego, USA
IPTG stock (1 M): Biosynth AG, Staad, Schweiz

3.3.3 *Escherichia coli* media

LB (Low Salt Luria Bertani) Agar: 35 g/L LB-agar (Lennox) (Roth), autoclaved. If needed, antibiotics were added to a final concentration of 25 mg/L Zeocin™ and 50 mg/L kanamycin respectively.

LB medium: 20 g/L LB-medium (Lennox) (Roth), autoclaved. If needed, antibiotics were added to a final concentration of 25 mg/L Zeocin™ and 50 mg/L kanamycin respectively.

SOC medium: 20g/L Bacto™ tryptone, 0.58 g/L NaCl, 5.00 g/L Bacto™ yeast extract, 2 g/L $MgCl_2.6H_2O$, 0.18 g/L KCl, 2.46 g/L $MgSO_4$, 3.81 g/L α-D(+)-glucose monohydrate, autoclaved

3.3.4 *Pichia pastoris* media

Stocks

500x B: 10 mg / 50 mL d-Biotin, filter sterilized

10x D: 220 g/L α-D(+)-glucose monohydrate, autoclaved

10x YNB: 134 g/L Difco™ yeast nitrogen base w/o amino acids, autoclaved

10x PPB: 30.0 g/L K_2HPO_4, 118.0 g/L KH_2PO_4. If needed, pH 6.0 is adjusted with 85 % (v/v) o-phosphoric acid and KOH, autoclaved.

10x S: 182.18 g/L D-sorbitol, autoclaved

10x GY: 100 mL/L ≥ 98 % glycerol, 900 mL/L dH_2O, autoclaved

Y-PER Plus Dialyzable Yeast Protein Reagent: Thermo Fisher Scientific Inc., Waltham, MA, USA

Media for cultivation in 96-deep well plates and 250 mL flasks

YPD (Yeast extract, peptone, dextrose): 10 g/L Bacto™ yeast extract, 20 g/L Bacto™ peptone, 900 mL dH_2O, (15 g/L agar), autoclaved. 100 mL 10x D were added after autoclaving. If needed, Zeocin™ was added to a final concentration of 100 mg/L.

YPD – Agar: 15g/L Bacto™Agar was added to YPD medium before autoclaving.

BMD1 (1 % D-Glucose): 200 mL 10x PPB, 100 mL 10x YNB, 50 mL 10X D, 2 mL 500x B, 650 mL dH_2O

BMM2 (1 % MeOH): 200 mL 10x PPB, 100 mL 10x YNB, 10 mL MeOH, 2 mL 500x B, 690 mL dH_2O

BMM10 (5 % MeOH): 200 mL 10x PPB, 100 mL 10x YNB, 50 mL MeOH, 2 mL 500x B, 650 mL dH_2O

3.4 Enzymes

All enzymes were treated according to the manufacturing recommendations. Deviations are described respectively.

3.4.1 Restriction enzymes

FastDigest® *BamHI* 1 FDU/µL, 10x FastDigest® Buffer, 10x FastDigest® green Buffer: 5' G↓GATCC3', Thermo Fisher Scientific Inc., Waltham, MA, USA

FastDigest® *BglII* 1 FDU/µL, 10x FastDigest® Buffer, 10x FastDigest® green Buffer: 5' A↓GATCT3', Thermo Fisher Scientific Inc., Waltham, MA

FastDigest® *NotI* 1 FDU/µL, 10x FastDigest® Buffer, 10x FastDigest® green Buffer: 5'GC↓GGCCGC3', Thermo Fisher Scientific Inc., Waltham, MA, USA

FastDigest® *EcoRI* 1 FDU/µL, 10x FastDigest® Buffer, 10x FastDigest® green Buffer: 5'G↓AATTC3', Thermo Fisher Scientific Inc., Waltham, MA, USA

FastDigest® *SwaI* (*SmiI*) 1 FDU/µL, 10x FastDigest® Buffer, 10x FastDigest® green Buffer: 5'ATTT↓AAAT3', Thermo Fisher Scientific Inc., Waltham, MA, USA

3.4.2 Polymerases and other enzymes

Phusion® High-Fidelity DNA-Polymerase F530L (5 U/µL), 5x HF buffer: Thermo scientific Inc., Waltham, MA, USA

GoTaq® DNA Polymerase, 5X Green GoTaq® Reaction Buffer: Promega GmbH, Fitchburg, WI, USA

***Endo*H 10 U/µL:** New England BioLabs® Inc., Ipswich, MA, USA

T4 DNA Ligase (5U/µL), 10X T4 DNA Ligase Buffer: Thermo scientific Inc., Waltham, MA, USA

3.5 Software and Webtools

3.5.1 Software

SoftMax Pro 4.8: Molecular Devices, Ismaning, Germany

UNICORN™ 6.3: GE Healthcare Europe GmbH, Vienna, Austria

PrimeView 5.0: Life Sciences, GE Healthcare Europe GmbH, Vienna, Austria

7500 system software version 2.0.4: Applied Biosystems, Foster City, CA, USA

GeneDesigner 2.0.187: DNA 2.0, Menlo Park, CA, USA
CLC MainWorkbench 7.5.1: CLC bio, Boston, MA, USA
SigmaPlot™ 13: Systat Software GmbH, Erkrath, Germany

3.5.2 Webtools

Enzyme information: http://www.brenda-enzymes.org/index.php
Multiple sequence alignment: http://www.ebi.ac.uk/Tools/msa/clustalw2/
Translation: http://web.expasy.org/translate/
Calculation of MW and pI: http://web.expasy.org/compute_pi/
Calculation of molar Ratio: http://bioinfo.clontech.com/infusion/molarRatio.do
Literature search: http://www.ncbi.nlm.nih.gov/, www.scopus.com/home.url,

3.6 Kits and Protocols

3.6.1 Plasmid isolation and DNA purification

Plasmid isolation was done using the GeneJET™ Plasmid Miniprep Kit (Thermo Fisher Scientific Inc., Waltham, MA, USA) according to the manufacturer´s recommendations. Applied deviations were: Cells were scraped from agar plates with a sterile toothpick and final plasmid elution was done with 50 µl prewarmed dH_2O.

Purification of PCR samples and isolated DNA fragments after agarose gel electrophoresis was done with the Wizard® SV Gel and PCR Clean-Up System (Promega GmbH, Mannheim, Germany).

3.6.2 *E.coli* Transformation

Electrocompetent cells (80µl *E.coli* TOP 10F´) and DNA (maximum volume of 10-20 µl) were mixed and incubated on ice for 10 minutes. The suspension was transferred to electro cuvettes and pulsed with 2.5 kV, 25 µF and 200 Ω. Five hundred µl SOC-medium were added immediately and cells were regenerated at 37°C and 500 rpm for 30 – 45 min. Positive transformants were selected by plating aliquots on LB – agar plates containing the appropriate antibiotic. Incubation was done at 37°C overnight.

3.6.3 *E.coli* shake flask cultivation

Precultures of *E.coli* BL21 (DE3) cells were grown in 50 mL Greiner tubes. Therefore 10 mL LB-medium containing the respective amount of Kanamycin were inoculated with a single colony and incubated at 37°C for 16 hours. A 1000 mL baffled shake flask was filled with 400 mL LB-medium containing Kanamycin, inoculated with the preculture to an OD_{600} of 0.1 and incubated under the same conditions. At an OD_{600} of 0.7 – 0.8 protein expression was induced by adding IPTG to a concentration of 0.5 mM. Induced cells were afterwards incubated over night at 25°C. After about 21 hours cells were harvested by centrifugation at 5000 rpm for 10 minutes. Subsequent protein purification by affinity chromatography is described in 3.6.8.

3.6.4 *Cloning strategy for intracellular expression of DtHNL isoenzymes in Pichia pastoris*

Codon optimized, synthetic genes of *Dt*HNL2, 3 and 4 for *P. pastoris*, delivered in pMA-T vectors, were used for transformation of *E.coli* Top10F´ cells. After minipreperation of positive clones and verification by sequencing, all the three plasmids as well as the vector backbones pPpT4s and pPpB1 were cut with *Eco*RI and *Not*I. Digested fragments of *Dt*HNL optimized genes with a size of 555 bp were isolated from a preparative gel, purified and ligated with their respective plasmids using 1U of T4 DNA Ligase. *E.coli* Top 10F´ cells were afterwards transformed with ligated constructs and selected on Zeocin containing LB-plates. Positive clones were verified by colony PCR. Isolated pPpT4-based plasmids were linearized with *Bgl*II, pPpB1-based plasmids were linearized with *Sma*I and additionally transformed in *P.pastoris* CBS 7435 Mut^S. Cultivation of pPpT4s and pPpB1 positive clones was performed in deep-well plates and followed by their screening for (*R/S*)-mandelonitrile cleavage activity.

Construction and cloning of a codon optimized *Dt*HNL1 in *P. pastoris* was formerly done by co-worked Elisa Lanfranchi. The selected clone, that showed highest catalytic activity for (*R/S*)-mandelonitrile cleavage was used for comparison with the strains containing *Dt*HNL2, 3 and 4.

3.6.5 *Pichia pastoris* Transformation

Preparation of electrocompetent *Pichia pastoris* Mut^S cells and transformation of DNA was performed as described by Lin-Cereghino *et al* [48].

A single colony of the respective strain was inoculated to 5 ml YPD medium and incubated over night at 28°C, 175 rpm. The preculture was used to grow a main culture in YPD medium from an OD_{600} of 0.25 to 0.8 – 1.0. The cells were harvested and treated as described by Lin-Cereghino et *al.* For electroporation 80 µl of cell suspension were mixed with approximately 1 µg of linearized DNA, incubated for 5 min on ice and afterwards pulsed with 2.0 kV, 200 Ω, 25 µF. Five hundred µl of 1 M sorbitol and 500 µl YPD medium were added immediately. After 2 hours of regeneration at 28°C, 110 rpm appropriate aliquots were plated on YPD-agar plates containing the respective antibiotic. Cells were incubated for 2 days at 28°C.

3.6.6 Microscale cultivation in deep-well plates

After 2 days of incubation at 28°C positive clones were picked for cultivation in 96- deep well plates similar as described by Weis *et al*. [7]. Cells were grown in 250 µl BMD1 for 60 hours at 28°C, 320rpm and 80% humidity. After adding 250 µl BMM2 cells were cultivated for another 12 h, 24 h and 48 h with respectively addition of 50 µl BMM10 at each time point.

For the final screening the OD_{600} was detected by a SynergyMX plate reader using a clear bottom fluorescence plate.

The cell suspension was harvested by centrifugation at 4000 rpm for 15 minutes. After removal of the supernatant 200 µl Y-PER solution were added per well. Subsequently the plate was vortexed and rested for 40 minutes. After recentrifugation under the same conditions different dilutions of the supernatant were used for the *Dt*HNL enzyme activity assay (3.6.9).

After the first screening the best clones per construct were chosen for a rescreening under the same conditions. The final screening was performed in 50 mL shake flasks. A glycerol stock of the best clone of each construct was frozen at -20°C for further applications.

3.6.7 *Pichia pastoris* shake flask cultivation

Precultures of cells were grown in 50 mL Greiner tubes. Therefore 5 mL BMD1 was inoculated with a single colony and incubated for 24 hours at 28°C, 160 rpm and 80% humidity. Fifty mL BMD 1 was inoculated with the preculture to an OD_{600} of 0.5 in a 250 mL baffled shake flask under the same conditions. To start expression cells were induced with 5 mL BMD10 after 12 hours (methanol concentration of 1%). Henceforth 500 µL methanol was fed after another 12 hours, 24 hours and 48 hours.

Beside determination of OD_{600}, 1 mL of cell suspension was harvested by centrifugation. The incurred pellet was resuspeded in 300 µL 50mM sodium phosphate buffer pH 6.5 with about 0.2 g glass beads (0.1mm diameter). With 10 repetitions the suspension was vortexed for 1 minute and cooled on ice for another minute. After recentrifugation different dilutions of the supernatant were used for the *Dt*HNL enzyme activity assay (3.6.9).

3.6.8 Protein purification

Sample preparation

E.coli strains containing the desired plasmid were cultivated and harvested as described in 3.6.3. Cell material was resuspended in 25 mL binding buffer and disrupted by sonication (80% duty cycle, 7 output, 6 minutes). After centrifugation for 1 hour at 20000 rpm and 4°C the supernatant was filtered through a cellulose acetate filter (0.45 µm) before starting affinity chromatography.

Affinity chromatography

For Affinity chromatography with the ÄKTA pure system 20 mM $NaPO_4$ buffer containing 0.5 M NaCl and 10 mM imidazole (Binding buffer) were used for washing, equilibration and loading. Twenty mM $NaPO_4$ buffer containing 0.5 M NaCl and 500 mM imidazole (Elution Buffer) was used for elution. Cleaning and equilibration of the system and His trap™ FF (5 mL) was done as recommended by the manufacturer. The filtered samples were loaded using the external pump P-950 with a flow of 3 mL/min. Elution was done by replacing the binding buffer (10 mM Imidazole) with a gradient to 100% elution buffer (500 mM Imidazole) for 10 column volumes at a flowrate of 3 mL/min. Absorption at 280 nm, conductivity and concentration of elution buffer were followed with the UNICORN™ 4.12 software. If different protein samples were purified the 5 mL His trap™ was stripped in between each run, washed and equilibrated as recommended by the manufacturer.

After affinity chromatography the fractions were collected, concentrated to volumes smaller than 15 mL with the Sartorius Vivaspin 20 system and desalted by size exclusion chromatography.

Size exclusion chromatography

Exchange of the 20mM imidazole burdened $NaPO_4$ buffer to 50 mM $NaPO_4$ was done by size exclusion chromatography. Washing and equilibration of the HiPrep™ 26/10 Desalting column was done as described in the manufacturers recommendations. Samples were injected using the external loop (15 mL) and loaded with a flowrate of 3 mL/min. The sequence ran with the same flowrate for two column volumes. Absorption at 280 nm and conductivity were followed with the UNICORN™ 4.12 software. The fractions were collected, concentrated with the Sartorius Vivaspin 20 system and aliquots frozen at -80°C. Always fresh, unfrozen samples were used for protein quantification with the BCA assay and subsequent HNL enzyme activity assays.

Purification by gravity flow

Samples were concentrated with the Sartorius Vivaspin 20 system to a volume lower than 50 mL and further treated as described in the manufacturer's Protocol for batch/gravity-flow purification of Histidine-tagged recombinant proteins under native conditions using Ni Sepharose 6 Fast Flow and Empty Disposable PD-10 Columns (GE Healthcare Europe GmbH, Vienna, Austria) with the following deviations.

The nickel containing resin was stored in 20 % EtOH. First washing was done with 100 mL ddH_2O, followed by 50 mL binding buffer. Fifty mL of concentrated sample were added to the resin and incubated at 4°C for 45 min moderate shaking. Subsequent washing was done with 50 mL binding buffer, 50 mL binding buffer containing 30 mM imidazole, 4 mL binding buffer containing 300 mM imidazole and 4 mL elution buffer. All fractions were collected and analysed by SDS-PAGE. Selected ones were pooled, desalted using a PD-10 Desalting Column (GE Healthcare) as recommended by the manufacturer and frozen at –80°C.

3.6.9 Protein quantification

BCA Protein Assay

The colorimetric detection of total protein amount in purified samples was done using the microplate protocol of the Pierce® BCA Protein Assay Kit. Different dilutions of the Albumin standard (BSA) were used to generate a standard curve. After incubating the samples for 30 minutes at 37°C the absorption at 562 nm was detected by a SynergyMX plate reader.

Bradford Protein Assay

The colorimetric detection of total protein amount in glycosylated samples was done using the microplate protocol of the Quick Start™ Bradford Protein Assay. Different dilutions of the Albumin standard (BSA) were used to generate a standard curve. Samples were incubated at room temperature and measured at 562 nm by a SynergyMX plate reader.

3.6.10 Hydroxynitrile lyase enzyme activity assay

All measurements except stability determinations of glycosylated *Dt*HNLs were performed in technical and biological triplicates.

Kinetic assay for activity determination of *Dt*HNLs

For activity determinations of *Dt*HNL measured with mandelonitrile as substrate a kinetic assay was used. The HNL cleaves the mandelonitrile into HCN and benzaldehyde whose production was followed at 280 nm by the Synergy Mx monochromator-based multi-detection-reader.

Required wells of a 96- well UV-STAR® microplate were filled with citrate phosphate buffer (50 mM, pH 5.0) and *Dt*HNL solution from purified enzyme, microscale cultivation or shake flask cultivation. Reference reactions contained 50 mM sodium phosphate buffer instead of diluted enzyme. After a first measurement at 280 nm the reaction was started by adding mandelonitrile (60 mM in 3 mM citrate phosphate buffer, pH 3.5). Immediately the absorption at 280 nm was followed for 10 minutes. The standard reaction temperature was 25°C. Table 2 depicts the standard reaction setup with respective volumes that are needed for the HNL activity assay and its control reaction. Table 3 lists the respective volumes used for stability determinations of glycosylated *Dt*HNLs. Table 4 lists the enzyme amounts of purified *Dt*HNLs in various measurements in µg/reaction. Enzyme amounts of glycosylated *Dt*HNLs are listed in table 5. Values are given in µg/reaction. However, characterization results of glycosylated *Dt*HNLs were determined in relative activities with 0.5 Units/reaction.

Table 2: Standard reaction setup of the Hydroxynitrile lyase activity assay.

Reaction Setup	HNL sample	Control
50 mM citrate phosphate buffer, pH 5.0 (reaction buffer)	130 µl	130 µl
50 mM sodium phosphate buffer, pH 6.5 (storage buffer)	-	20 µl
*Dt*HNL Protein sample	20 µl	-
60 mM Mandelonitrile in 3 mM citrate phosphate buffer, pH 3.5	50 µl	50 µl

Table 3: Reaction setup of the Hydroxynitrile lyase activity assay for stability determinations of glycosylated *Dt*HNLs.

Reaction Setup	HNL sample	Control
50 mM citrate phosphate buffer, pH 5.0 (reaction buffer)	140 µl	150 µl
Glycosylated *Dt*HNL Protein sample	10 µl	-
60 mM Mandelonitrile in 3 mM citrate phosphate buffer, pH 3.5	50 µl	50 µl

Table 4: Enzyme amount of purified *Dt*HNLs in different reaction assays. Amounts are given in µg/reaction. (MM abbreviates Michaelis – Menten)

Assay	Substrate	*Dt*HNL1	*Dt*HNL2	*Dt*HNL3	*Dt*HNL4
Kinetic Assay DWPs	R/S - MNL	0.2 µg	0.2 µg	0.2 µg	0.2 µg
Kinetic Assay Cuvettes	R/S - MNL	0.5 µg	2.0 µg	1.0 µg	1.0 µg
MM - Kinetic Cleavage reaction	R - MNL	0.01 µg	0.01 µg	0.01 µg	0.01 µg
MM - Kinetic Synthesis reaction	R - MNL	50 µg	-	-	-

Table 5: Enzyme amount of glycosylated *Dt*HNLs in different reaction assays. Amounts are given in µg/reaction.

Assay	Substrate	*Dt*HNL1	*Dt*HNL2	*Dt*HNL3	*Dt*HNL4
Kinetic Assay DWPs	R/S - MNL	0.2 µg	0.2 µg	0.2 µg	0.2 µg
Kinetic Assay Cuvettes	R/S - MNL	1.0 µg	1.0 µg	1.0 µg	1.0 µg

The activity was calculated as shown in figure 11 by using the molar extinction coefficient of benzaldehyde (1376 L $mmol^{-1}$ cm^{-1}).

$$\frac{Units}{mL} = \frac{\frac{OD}{min} * V}{v * \varepsilon * d} * f$$

Figure 11: Calculation of volumetric HNL activity. OD/min= slope of benzaldehyde formation in first 3 reaction minutes, V= total reaction volume, v = volume of enzyme solution, $\varepsilon_{280\ nm}$= molar extinction coefficient of benzaldehyde = 1376 L $mmol^{-1}$ cm^{-1}, d = path length, f = dilution factor.

One unit of HNL activity is defined as the amount of enzyme, which converts 1 µmol mandelonitrile per minute in citrate phosphate buffer, pH 5.0, 25°C.

Determination of temperature dependence of *Dt*HNL activities

Activity measurements at certain temperatures were done in quartz glass cuvettes using a Cary 100 UV-Vis Spectrophotometer. Seven hundred µl citrate phosphate buffer (50 mM, pH 5.0) were prewarmed for 5 minutes at certain temperature and mixed with 100 µl enzyme in sodium phosphate buffer (50 mM, pH 6.5). The reaction was started by adding 200 µl mandelonitrile solution (60 mM in 3 mM citrate phosphate buffer, pH 3.5). After vortexing the cuvettes, the reaction was immediately monitored for 5 minutes.

All measurements were performed in technical and biological triplicates. References containing all components except *Dt*HNL were determined twice.

Determination of inhibition effects on *Dt*HNLs activities

Compounds that are known for influencing other HNLs catalytic activity, as *Pm*HNL [49], were assumed also to inhibit *Dt*HNLs. Additives were dissolved in 50mM citrate phosphate buffer, pH 5.0 and used as described in the standard reaction setup of the HNL activity assay (table 2). Components that showed little influence on the catalytic activity of *Dt*HNLs, according to the standard kinetic assay, were treated with a prolonged incubation time of 7 min at 30°C with the respective amount of enzyme and the respective inhibitor prior to the kinetic activity determination.

Endpoint assay for activity determination of *Dt*HNLs

For activity measurements with acetone cyanohydrin and hydroxypivaldehyde an endpoint assay was used. *Dt*HNL cleaves the cyanohydrins into the related carbonyl compound and HCN. The arising cyanide was converted in a three-step-reaction as described in Andexer *et al* [50] and afterwards spectrophotometrically detected by the Synergy Mx monochromator-based multi-detection-reader. N-Chlorosuccinimide oxidizes cyanide anions to cations, which react with isonicotinic acid. The originated dialdehyde is coupled to two molecules of barbituric acid and forms a dye complex that is detected at 600 nm.

In detail, wells of a 96- well UV-STAR® microplate were filled with 140 µl citrate phosphate buffer (50 mM, pH 5.0), 10 µl *Dt*HNL solution (0.1 µg/well) and 10 µl of the respective cyanohydrin (300 mM). The plate was covered with a transparent foil and incubated for 10 minutes at room temperature and moderate agitation on a Titramax 1000 microtiterplate shaker. At particular time points the reaction was stopped by adding 10 µl of reaction mix I. After incubation for another 5 minutes with stronger agitation, the color development was started by adding 30 µL of reaction mix II. Immediately, the reaction was followed for 20 minutes at 600 nm. Reference reactions contained 0.1 M citric acid to follow the possible

spontaneous degradation of cyanohydrin. The activity with different cyanohydrins was calculated relative to mandelonitrile.

3.6.11 Deglycosylation by *Endo*H

Eight Units per enzyme were mixed with 2 µl of denaturation buffer and incubated at 99°C for 10 minutes. Afterwards, 0.5 µl of EndoH, 3 µl of GC-buffer and a respective amount of water were added in a final volume of 30 µl and incubated at 37°C for 24 hours. 4 Units of enzyme were loaded on a SDS-gel and run for 45 min at 250 Volt in MES-buffer. Two µl of EndoH were loaded as a control.

3.6.12 Agarose Gel electrophoresis

For 1 % agarose gel 1xTAE buffer and approximately 2 µl of EtBr (≥98 % ethidium bromide) were used. DNA samples were mixed with 6x Loading Dye. Six µL of 0.1 µg/µL GeneRuler™ 1kb DNA Ladder were used as standard. Control gels were prepared with 200 ml buffer and ran for 30 – 50 minutes at a voltage of 120 V. For preparative gels a volume of 250 ml buffer, a running time of 80 - 100 minutes and a voltage of 80 – 90 V was used.

3.6.13 SDS-Page

If required, glycosylated samples were treated with endoglycosidase H (*Endo*H) according to the manufacturer's recommendations.

Samples were prepared following the Life Technologies™ protocol for NuPAGE® Bis-Tris Mini Gels with reduced samples. Applied deviations were a total volume of 20 µl instead of 10 µl. 20 µl reduced sample were pipetted per well and 5 µL PageRuler™ Prestained Protein Ladder was used as control. The running time using MES Buffer was prolonged up to 50 minutes at 200 V. Staining was performed with SimplyBlue™ SafeStain solution according to the manufacturer´s protocol.

3.6.14 Applied PCR techniques

3.6.14.1 Thermal unfolding experiments

Thermal stability characterizations were performed in 96- well PCR plates using the Applied Biosystems 7500 real-time PCR system. Before starting the measurements a 100 - fold dilution of the Sypro Orange fluorescence dye was prepared in ddH_2O. To determine the appropriate ratio of dye to protein, a set of different proportions were tested prior to the actual unfolding measurements. For *Dt*HNL1 2 µL of the Sypro Orange dilution were mixed with 2 µL of protein (11.6 mg/mL), for *Dt*HNL2 and *Dt*HNL3, 2 µL dye and 1 µL protein (7.4 mg/mL and 14.8 mg/mL) were used and for *Dt*HNL 4 4 µL dye were added to 1 µL of the protein solution (7.7 mg/mL). All wells were filled with the respective buffers listed in table 6 to a total volume of 25 µL. Furthermore blanks were prepared with both protein and buffer (without Sypro Orange) and protein and dye. The plates were covered with optically clear adhesive foils, shaken and measured after shortly spinning down at 1000 rpm. The protein unfolding and the concomitant increase of the fluorescence signal was monitored online using a melt-curve analysis with a heating profile from 25 to 95°C with raising the temperature by 1°C per min. An initial equilibration was done for 2 min at 25°C. All measurements were performed in duplicates.

Table 6: Buffers used for unfolding experiments with the protein thermal shift assay. (JBS Solubility Kit, Jena Bioscience)

Buffer	Molarity	pH
Acetate buffer	50 mM	5.0
		4.5
		4.0
Citrate Phosphate buffer	50 mM	6.5
		5.0
		4.5
		4.0
		3.5
		3.0
		2.5
Potassium Chloride buffer	50 mM	2.0
Sodium/Potassium Phosphate buffer[1]	100 mM	5.0
Sodium Citrate buffer[1]	100 mM	5.5

After correcting the exported data for the dye and protein blank controls the melting temperatures (Tm) were determined by graphic evaluation.

3.6.14.2 Colony PCR with Promega GoTaq polymerase

After transformation of *E.coli* Top10 F´ with pPpB1 and pPpT4 vector based constructs, positive transformants containing the correctly ligated plasmid were identified by colony PCR with GoTaq Polymerase; the plasmids isolated by minipreperation and sent for sequencing with Microsynth. Tables 7 and 8 show the reaction setup and temperature profile for colony PCR.

Table 7: Colony PCR-setup for identification of positive clones.

single reaction		volume of PCR (50 µl):	*50*
Volume (µl)	**Component (µM/l=pmol/µl)**		
29.75	ddH2O (to 50 µl)		
10	5x Green or colourless buffer		
5	dNTPs (2mM [final conc. 0.2 mM each]	final primer concentration (0.5 µM)*	primer stock concentration (pmol/µl)
2.5	forward primer	0.5	*10*
2.5	reverse primer	0.5	*10*
0.25	GoTaq polymerase (0.25 µl per 50 µl reaction)		
add colony	[template DNA (<0.5 µg/50µl = <10ng/µl)]		

Table 8: PCR profile used for colony PCR

Cycle step	Temperature (°C)	Time	Cycles
Initial denaturation	95	2 min	1
Denaturation	95	30 sec	25
Annealing	55	30 sec	
Extension	72	45 sec	
Final Extension	72	7 min	1
	4	∞	

3.6.15 Synthesis reaction

General methods for and the analysis of the synthesis of various cyanohydrins employing HNL were described by Wiedner et al. [51].

Preparation of HCN

4.9 g NaCN (0.1 mol) was dissolved in 10 mL water. After the NaCN was fully dissolved, 25 mL of MTBE were added and the mixture was cooled on ice with stirring. Slowly, 10 mL of 30 % aqueous HCL were added with a dropping funnel over 15 minutes. Subsequently, the mixture was equilibrated to room temperature for approximately 30 minutes. The phases were separated and 7 mL of MTBE were added twice. The generated 2 M HCN – MTBE solution was stored in a darkened bottle over a small amount of 100 mM sodium acetate buffer pH 5.0.

Preparation of derivatisation reagent

Fresh derivatisation solution for later GC analysis was prepared in a glass bottle. It was composed of 85 % dichloromethane, 10 % acetic acid (anhydride) and 5 % pyridine.

Experimental set-up

Distilled benzaldehyde in various concentrations (500 mM, 400 mM, 350 mM, 300 mM, 250 mM, 200 mM, 150 mM, 125 mM, 100 mM, 50 mM, 25 mM, 10 mM) and the internal standard triethylbenzene (approx. 2 % v/v) were dissolved in the HCN / MTBE solution. A sample was taken before starting the reaction as the initial time point 0. The cyanohydrin formation reaction was carried out in 2 mL Eppendorf Safe-Lock tubes containing magnetic stirring bars at 4°C and 1000 rpm. One mL of the respective stock solution containing substrate, internal standard, HCN and MTBE was pipetted first. The reaction was started by adding 500 µL of purified enzyme (acidified with 1 M NaOAc buffer, pH 4.0) in a final concentration of 0.1 mg/mL per reaction vial. Per reaction, one mL derivatisation reagent was prepared in labelled glass vials. At respective time-points (5, 10, 15, 20 and 30 minutes) reactions were stopped by transferring 50 µl of the organic phase to the prepared derivatisation reagent. Derivatisation was done for at least 1 hour at room temperature.

Gas chromatography

Gas chromatography for the detection of converted benzaldehyde was performed with a temperature programme of 60°C with 10°C min^{-1} to 140°C and 2 min at 140°C. Carrier gas (H_2) was set to constant pressure mode at 100kPa and the injector temperature was set to 250°C. Retention times for aldehyde were 4.5 min, for (*R*)-cyanohydrin acetate 9.6 min and for (*S*)-cyanohydrin acetate 10.3 min. The substrate conversion was calculated based on the decrease of the benzaldehyde peak area compared to the peak of the internal standard. The enantiomeric excess was calculated based on the relative areas of the (*R*)- and (*S*)-mandelonitrile peaks.

Activity determination was obtained by observing the formation of (*R*)-mandelonitrile during the first 30 minutes of reaction, a period where a linear increase of product formation takes place. A linear slope during these first 30 minutes was ensured by an appropriate enzyme concentration. The slope (reaction velocity (µmol/min/mg)), of the linear equation at each substrate concentration was used for calculation of K_m and V_{max} with SigmaPlot^{TM}.

The calculation of k_{cat} was done by division of V_{max} [mM/s] through the de facto enzyme concentration [mM] present in the aqueous phase of the biphasic reaction system (figure 12).

$$\mathrm{Kcat} = \frac{\frac{Vmax\ (mM)}{(\mathrm{sec}\ )}}{DtHNL1\ (mM)}$$

Figure 12: Calculation of enzyme activity k_{cat} [s^{-1}]. V_{max} = maximal reaction velocity. *Dt*HNL1= Amount of enzyme, present in the buffer phase (0.5 mL).

4 Results and Discussion

Since DtHNLs offer the potential as biocatalysts for the synthesis of enantiomeric pure cyanohydrins, an overall biochemical characterization enlightens their optimal reaction requirements for further industrial applications. Four different E.coli strains, each constructed to produce one of the four DtHNL isoenzymes are reported in my thesis. After expression and purification the isoenzymes were characterized with respect to specific activity and behaviour at different pH and temperature conditions. Their tolerance against several supposed inhibiting compounds gave information about structural features that are involved in the reaction mechanism. The thermal stability and their acceptance for utilizing various substrates were evaluated, followed by their detailed kinetic characterization by the determination of their respective Michalis–Menten parameters.

4.1 Protein purification of *Dt*HNL isoenzymes produced by *E. coli*

Histidine-tagged *Dt*HNL isoenzymes, expressed by *E. coli* Top10F´ (re*Dt*HNL) were purified by Ni^{2+} - affinity chromatography, using a gradient of increasing imidazole in sodium phosphate buffer. Fractions containing purified re*Dt*HNL protein were assessed according to their UV detection signal at 280 nm and confirmed by SDS-Page (figures 13-16).

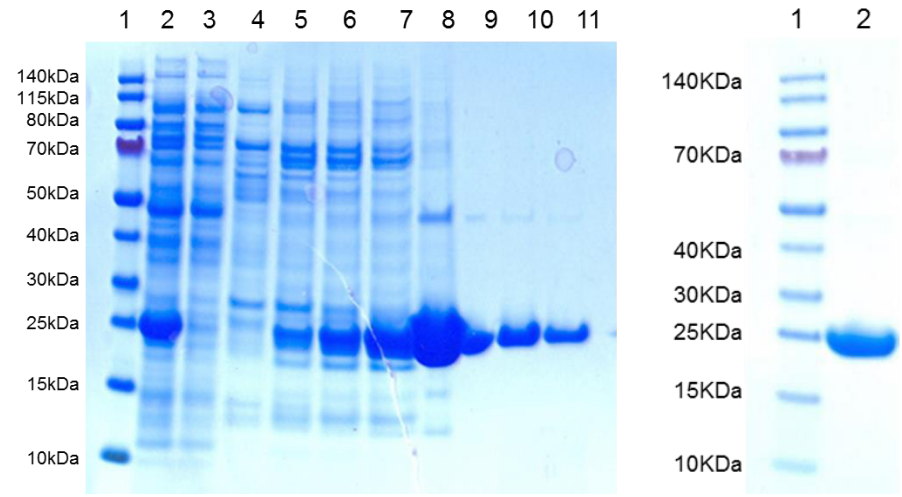

Figure 13: SDS-PAGE of recombinant re*Dt*HNL1 expressed by *E. coli* Top10F´ and purified by affinity chromatography. Left gel: Lane 1: PageRuler™ Prestained Protein Ladder, Lane 2: cell free lysate, Lane 3: Flow through, Lanes 4 – 11: different fractions of the purification process by increasing amount of imidazole in the elution buffer (15 µL each). Lane 7 – 11 were combined for desalting by size exclusion chromatography. Right gel: Lane 1: Protein standard, Lane 2: desalted, purified *Dt*HNL1. Tagged re*Dt*HNL MW = 23 kDa.

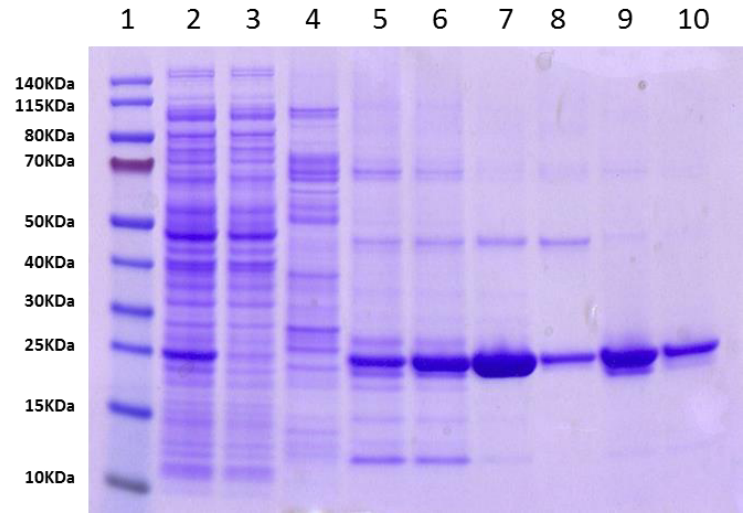

Figure 14: SDS-PAGE of re*Dt*HNL2 purified by affinity chromatography. Lane 1: PageRuler™ Prestained Protein Ladder, Lane 2: cell free lysate, Lane 3: Flow through, Lanes 4 – 8: best elution fractions (15 µL each). Tagged re*Dt*HNL MW = 23 kDa.

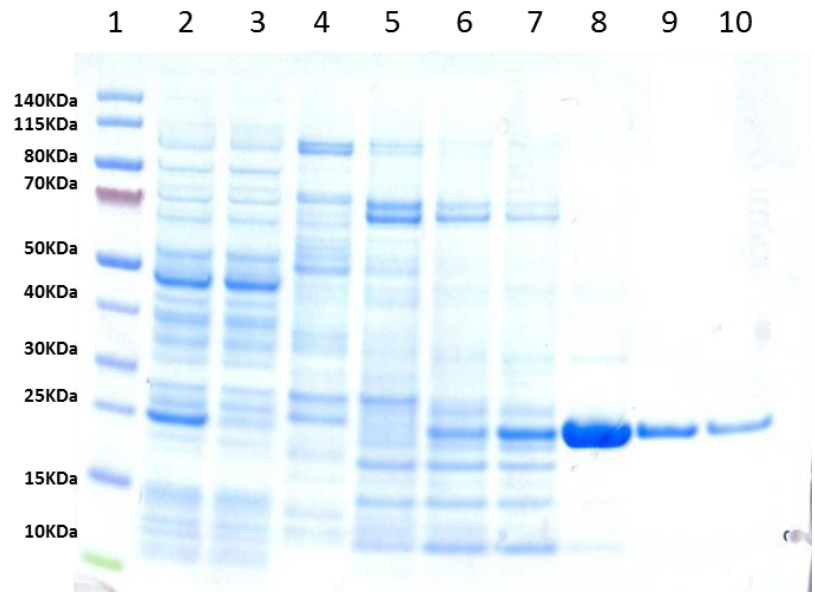

Figure 15: SDS-PAGE of re*Dt*HNL3 purified by affinity chromatography. Lane 1: PageRuler™ Prestained Protein Ladder, Lane 2: cell free lysate, Lane 3: Flow through, Lanes 4 – 10: best elution fractions (15 µL each). Tagged re*Dt*HNL MW = 23 kDa.

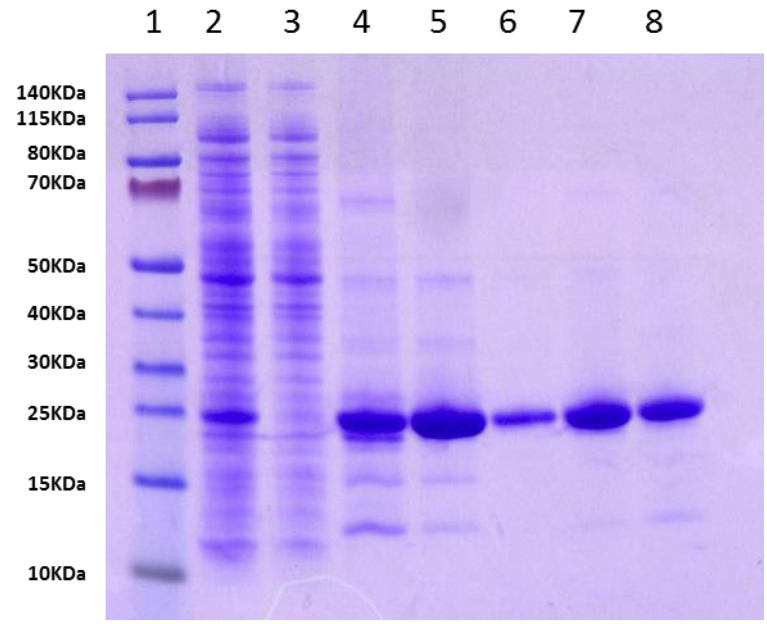

Figure 16: SDS-PAGE of re*Dt*HNL4 purified by affinity chromatography. Lane 1: PageRuler™ Prestained Protein Ladder, Lane 2: cell free lysate, Lane 3: Flow through, Lanes 4 – 6: best elution fractions, Lanes 7, 8: desalted fractions (7, 8) (15 µL each). Tagged re*Dt*HNL MW = 23 kDa.

The His trapTM FF (5 mL) column was eluted at an imidazole concentration between 25 – 40%. Fractions containing pure re*Dt*HNL were pooled, concentrated and desalted by size exclusion chromatography.

The protein concentration of the pooled fractions was measured using the BCA Assay. After initial activity determination, aliquots of 10 – 15 mg/mL were frozen at -80°C. SDS PAGE of desalted samples verified re*Dt*HNL1 (23.3 kDa), re*Dt*HNL2 (23.3 kDa), re*Dt*HNL3 (19.5 kDa) and re*Dt*HNL4 (20.0kDa) highly expressed and pure.

Specific activities achieved for (*R*/*S*)-MNL were 360 U/mg for re*Dt*HNL1, 393 U/mg for re*Dt*HNL2, 321 U/mg for re*Dt*HNL3 and 562 U/mg for re*Dt*HNL4.

4.2 Characterization of purified *Dt*HNL isoenzymes, recombinantly expressed in *Escherichia coli*

4.2.1 pH dependent activity and stability profiles of purified *Dt*HNLs

The specific activity of the four purified *Dt*HNL isoenzymes, re*Dt*HNL1, 2, 3 and 4, was recorded at different pH values from 2.0 to 7.0 (figure 17). The chemical degradation of the substrate, represented by the grey dashed line, significantly increases at pH higher than 6.0. Consequently a significant fraction of the substrate is lost by the chemical, non selective reaction. The optimum of the hydroxynitrile lyase activity was found to be at pH 5.0. All re*Dt*HNLs showed decreasing activities at pH higher than 6, though exact determination of the activity above this pH is difficult to measure since the substrate mandelonitrile underlies a rapid nonenzymatic dissociation. Activities lower than pH 5.0 followed an almost linearly decreasing profile until pH 2.5. At pH 4.0 still 80 % of activity remained at without any measureable nonenzymatic background conversion of mandelonitrile. No enzymatic activity was recordable at pH 2.0.

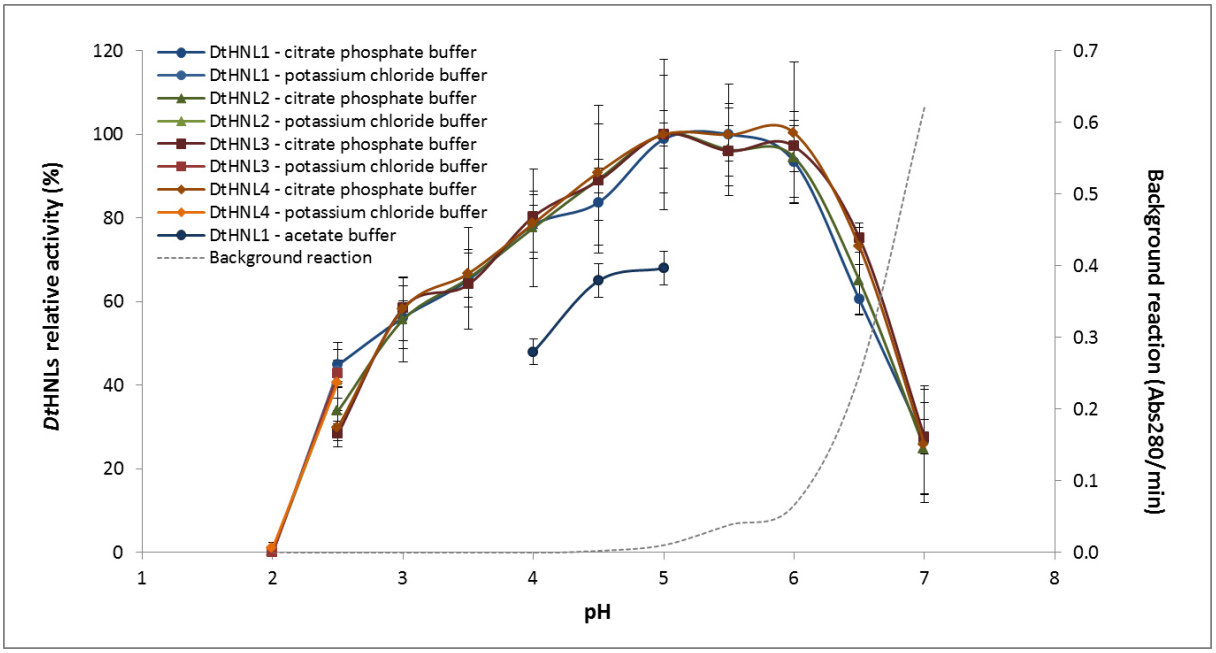

Figure 17: Effect of pH on the activity of purified re*Dt*HNL1 – 4. Cleavage of racemic mandelonitrile to benzaldehyde and HCN was observed. The initial reaction values in relative activity to the enzymes optimum at pH 5.0 are plotted against the respective pH. The nonenzymatic dissociation of (R/S)- mandelonitrile is shown in grey.

Activities in 50mM acetate buffer were determined to be 68% (pH 5.0), 65 % (pH 4.5) and 48% (pH 4.0), relative to 50mM citrate phosphate buffer at pH 5.0

Lower enzymatic activity of re*Dt*HNLs in acetate buffer might be a result of a competitive inhibition by acetate whereby the carbonyl group of the acetate may resemble the carbonyl of benzaldehyde and act as a competitive inhibitor, as described for *Me*HNL [6].

4.2.1.1 Stability of purified re*Dt*HNLs at different pH

Freshly thawed enzyme samples were diluted to a concentration of 1 mg/mL in the respective buffer and stored at 4°C (figures 18, 19).

Re*Dt*HNL1 is most stable in 50 mM sodium phosphate buffer at pH 6.5, which was chosen as storage buffer. Storage in potassium chloride buffer, pH 2.5 showed decreasing activities to 60% after 4 hours but led to an adaption of the enzymatic

activity with the result that after 312 hours still 80% residual activity were determined. Citrate phosphate buffer, pH 4.0 showed straight reduction of enzymatic activity to 57% over a time period of 312 hours. Worst stabilities were observed for storage in citrate phosphate buffer, pH 5.0 and pH 2.5. Reduced stabilities at pH 5.0 might are a result of precipitated and aggregated enzyme since re*Dt*HNL1 and 2 share the same isoelectric point (pH 4.77) as well as re*Dt*HNL3 and 4 (pH 5.12). When re*Dt*HNL1 was incubated at pH 2.0, it was still slightly active after 48 hours. The activity was immediately compromised after adjusting to the low pH. However, but the enzyme seemingly was not fully and irreversibly inactivated.

Re*Dt*HNL2 demonstrated constant activities for storage in citrate phosphate buffer pH 6.5, 5.0 and 4.0 after activity loss during the first 48 hours to 50 – 60 %. Moderate activity was measured for potassium chloride buffer pH 2.5, however lower activities were determined for potassium chloride buffer pH 2.0 and citrate phosphate buffer pH 2.5. Almost the same characteristics as for re*Dt*HNL2 were measured for re*Dt*HNL3 and re*Dt*HNL4. However, their residual activity stayed in higher ranges of 70 – 80%.

Activity determination of purified re*Dt*HNLs after 4 months of storage at 4°C in the respective buffer showed moderate activities in citrate phoshate buffer pH 5.0 with 39% of residual activity for re*Dt*HNL1, 22% for re*Dt*HNL2, 25 % for re*Dt*HNL3 and 16% for re*Dt*HNL4. Storage in citrate phosphate buffer at pH 6.5 showed actually lower enzymatic activities.

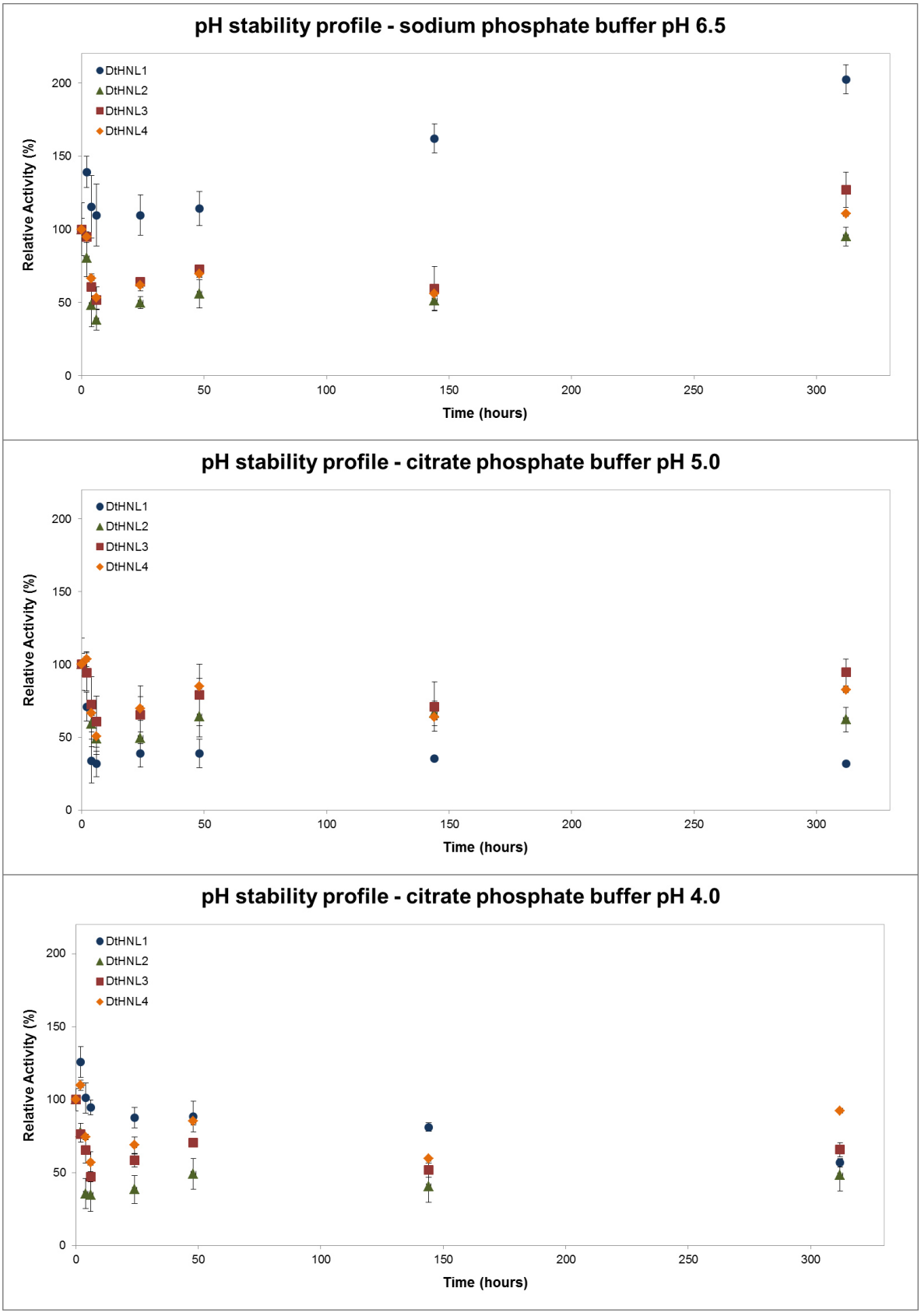

Figure 18: Stability profile of purified re*Dt*HNLs in 50mM sodium phosphate buffer pH 6.5 and 50mM citrate phosphate buffer 5.0 and 4.0. Re*Dt*HNLs were stored in concentrations of 1 mg/mL. The relative activities are plotted against the respective time of storage at 4°C.

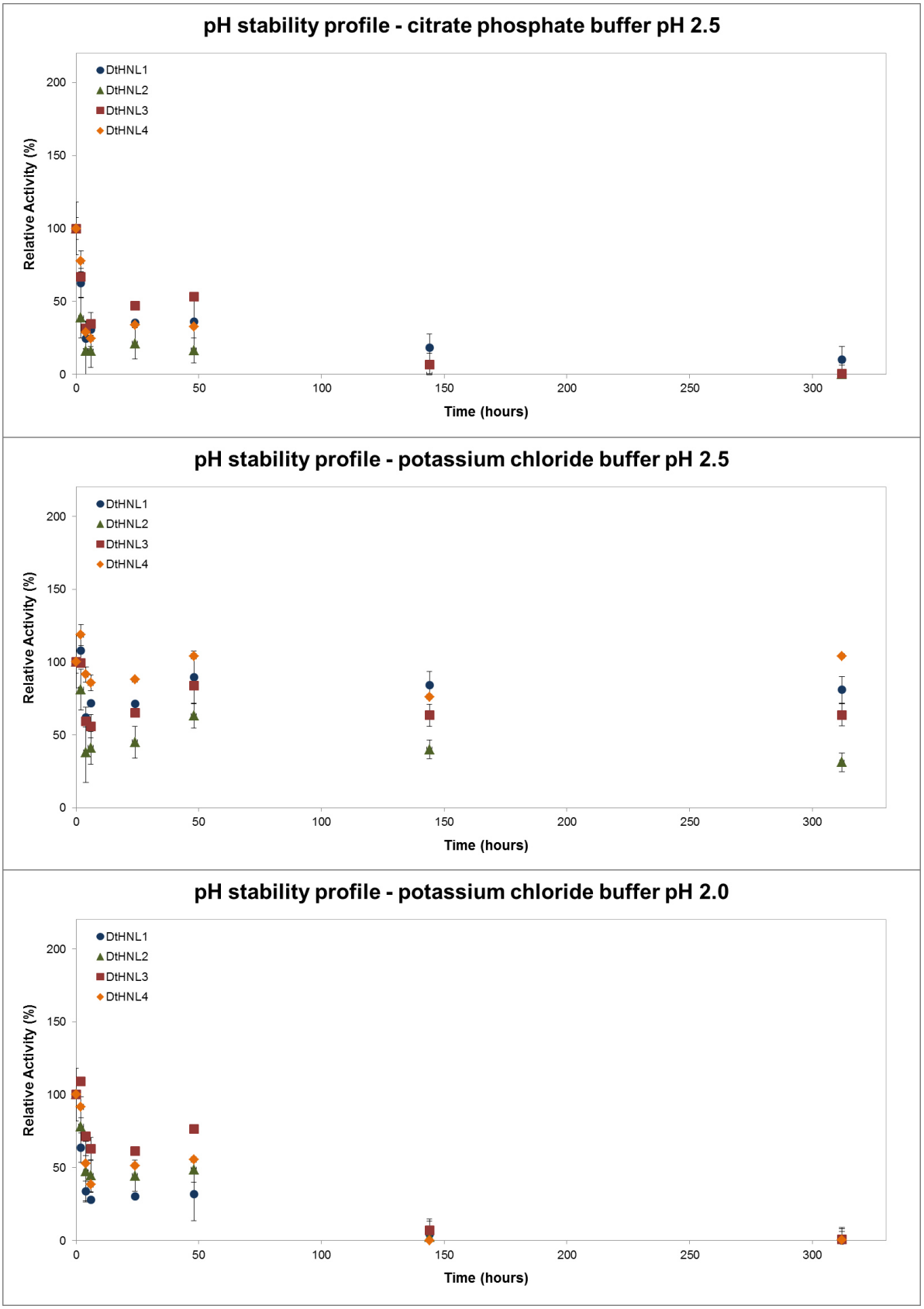

Figure 19: Stability profile of purified re*Dt*HNLs in 50mM citrate phosphate buffer pH 2.5 and 50mM potassium chloride buffer 2.5 and 2.0. Re*Dt*HNLs were stored in concentrations of 1 mg/mL. The relative activities are plotted against the respective time of storage at 4°C.

4.2.2 Temperature activity and stability profiles of purified re*Dt*HNLs

4.2.2.1 Activity of purified re*Dt*HNLs at varying temperature

Re*Dt*HNL1 and re*Dt*HNL3 both had their optimum temperature at 40°C, whereas the optimum for re*Dt*HNL2 was found to be at 35°C and for re*Dt*HNL4 at 45°C (figure 20). Since higher temperatures lead to competitive conditions between thermal degradation of mandelonitrile and available substrate for enzymatically conversion, a strong decrease of activity was observed at temperatures higher than the optimum. The enzymes intrinsic activity might additionally get reduced by the effect that higher reaction temperatures lower the actual pH of a buffer that was prepared at room temperature.

The nonenzymatic degradation of mandelonitrile was not measurable at 10°C, however re*Dt*HNL1 showed 35% of its maximum activity and re*Dt*HNL2, re*Dt*HNL3 and re*Dt*HNL4 still showed about 15- 20%. A reaction temperature of 20°C showed 65% activity for re*Dt*HNL1 and 35-40% residual activity for re*Dt*HNL2-4. HNL activity measurements for *Pat*HNL were done at 25°C [12] and at 22°C for *Chua*HNL [10]. However, for conversion of (*R/S*)-mandelonitrile by re*Dt*HNLs a reaction temperature of 20°C offered a reasonable compromise between low substrate degradation and catalytic activity and was therefore set as the optimal reaction temperature for activity determination in further experiments.

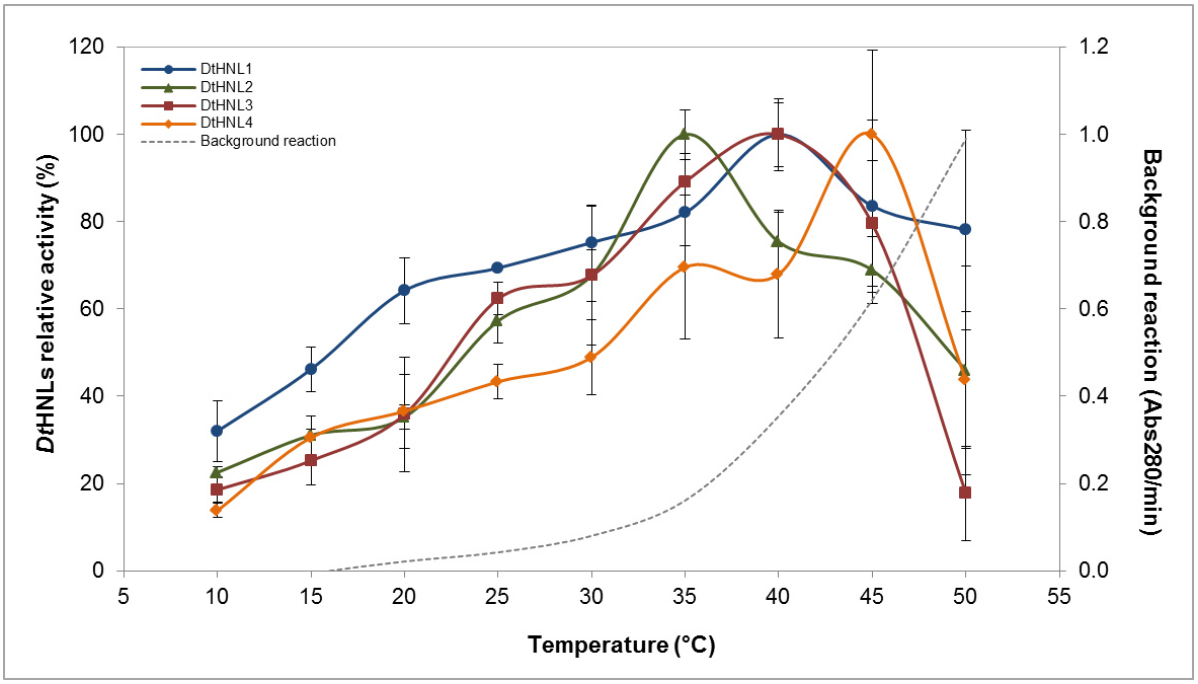

Figure 20: Effect of temperature on the activity of purified re*Dt*HNLs. Relative activities of re*Dt*HNL isoenzymes are plotted against the respective temperatures. The optimum temperature of each enzyme was set as 100%. The nonenzymatic production of benzaldehyde by spontaneous dissociation of mandelonitrile rises constantly from 20°C upwards.

Cleavage reactions of mandelonitrile to the corresponding benzaldehyde and HCN (cyanogenesis) were performed at 20°C. Synthesis reaction experiments were done at 8-10°C (table 9), since a lower reaction temperature in cyanohydrin synthesis reduces the chemical formation of product while conserving the enzymes catalytic activity. Minimization of this non-enzymatic background reaction improves thereby the enantio purity of the cyanohydrin product.

Table 9: Specific activities of purified re*Dt*HNL's in cyanogenesis reaction at certain temperatures.

Purified re*Dt*HNLs	Optimum			20°C	10°C
	U/mg	Temperature	$Abs_{280/min}$ background reaction	U/mg	U/mg
re*Dt*HNL1	501±42	40°C	0.380	323±49	159±30
re*Dt*HNL2	565±57	35°C	0.165	198±18	127±7
re*Dt*HNL3	588±83	40°C	0.376	253±139	120±44
re*Dt*HNL4	812±141	45°C	0.525	288±50	111±14

4.2.2.2 Determination of purified re*Dt*HNL's temperature stability

The impact of various storage temperatures between 8°C – 40°C on re*Dt*HNL´s stability was measured after incubating the single, purified enzymes in a concentration of 1 mg/mL in sodium phosphate buffer at the certain temperature (figures 21-24).

All enzymes showed similar stability after storage at 10°C, whereby re*Dt*HNL4 seemed to be most robust (figure 21). Re*Dt*HNL2 showed lowest tolerance to 30 °C and 40 °C and re*Dt*HNL3 and 4 were most stable until 30 °C for at least 312 hours (figure 23). Inactivation of re*Dt*HNL1 and re*Dt*HNL2 after 2 hours at 40°C was observed, whereas re*Dt*HNL3 and re*Dt*HNL4 were still active after 144 hours of incubation at this temperature (figure 24).

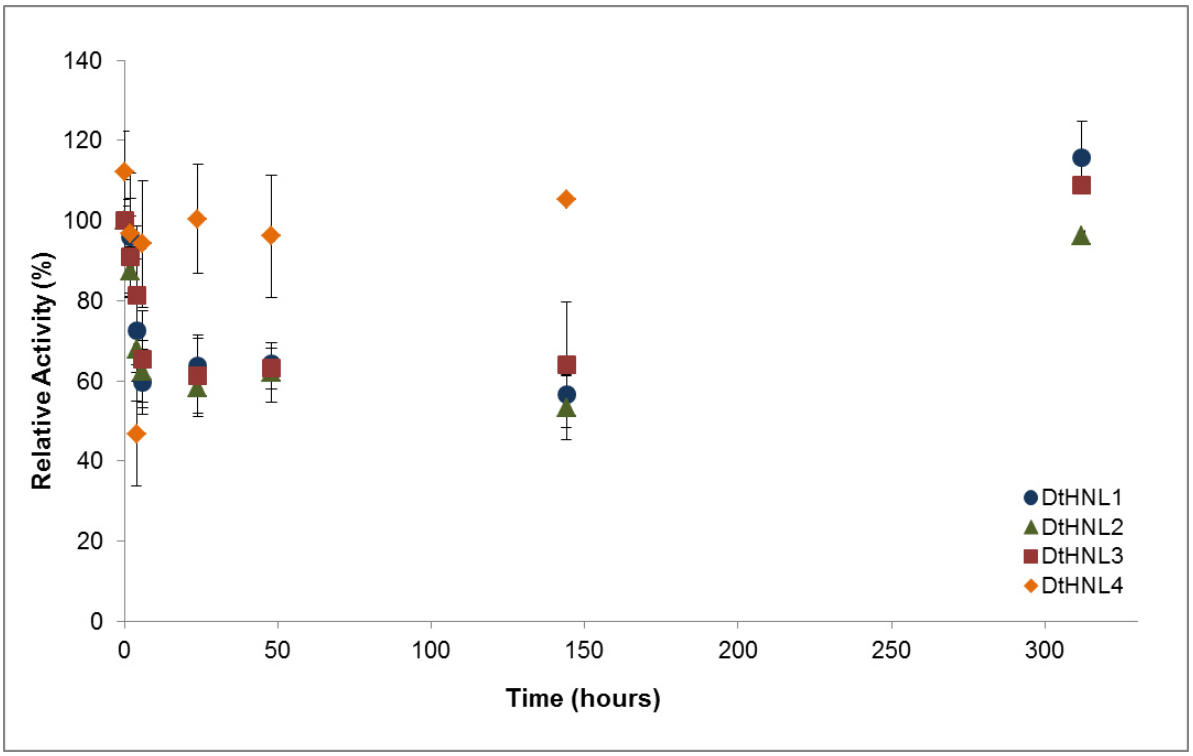

Figure 21: Temperature stability profile of purified re*Dt*HNLs at 10°C. Samples were stored in concentrations of 1 mg/mL in 50 mM citrate phosphate buffer pH 6.5. The relative activities are plotted against the respective time of storage.

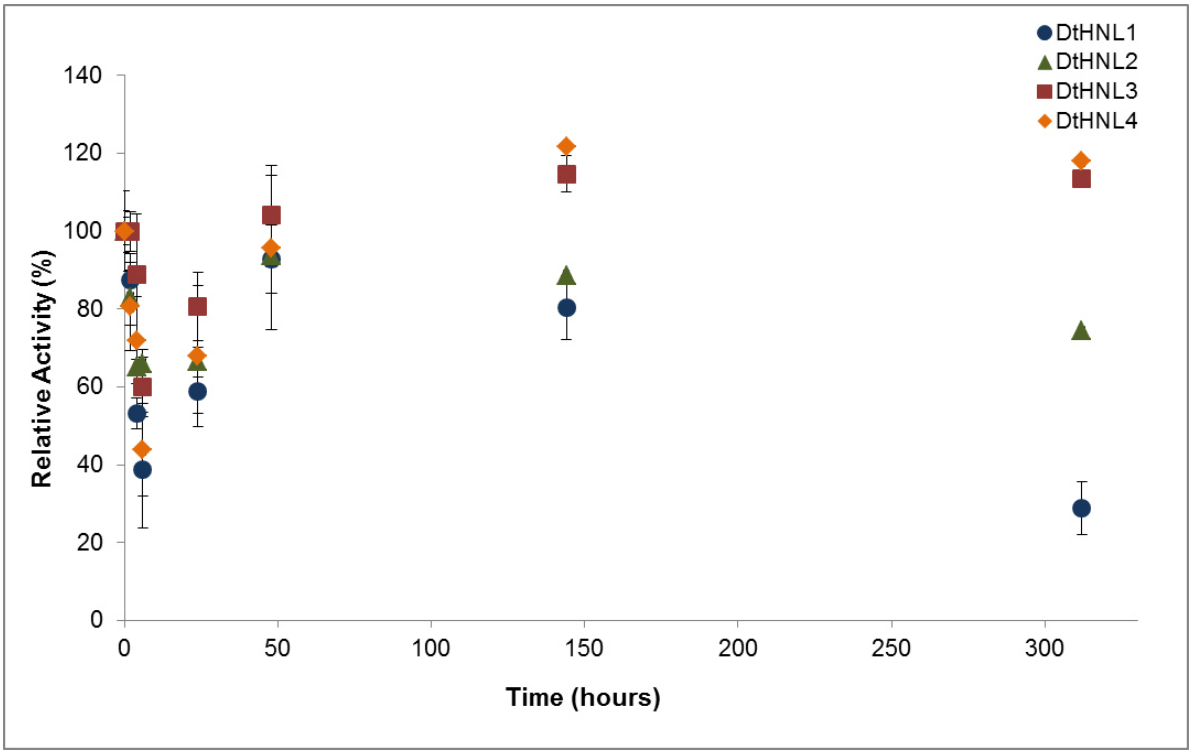

Figure 22: Temperature stability profile of purified re*Dt*HNLs at 20°C. Samples were stored in concentrations of 1 mg/mL in 50 mM citrate phosphate buffer pH 6.5. The relative activities are plotted against the respective time of storage.

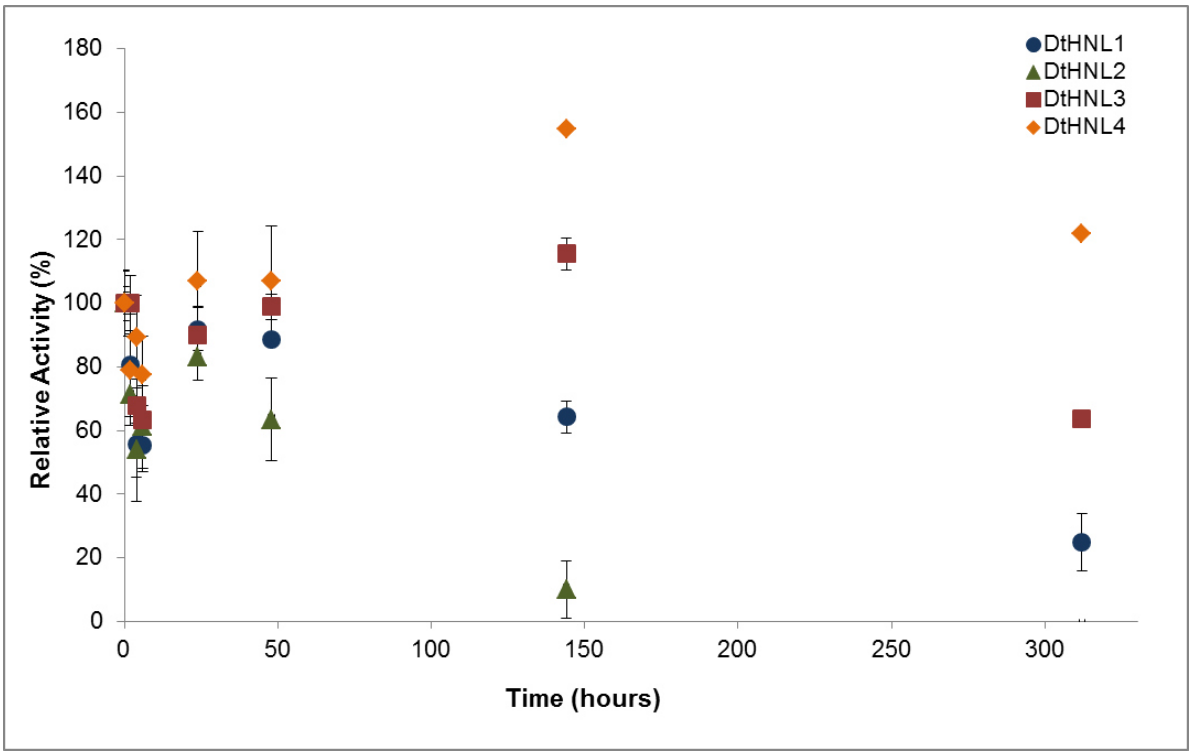

Figure 23: Temperature stability profile of purified re*Dt*HNLs at 30°C. Samples were stored in concentrations of 1 mg/mL in 50 mM citrate phosphate buffer pH 6.5. The relative activities are plotted against the respective time of storage.

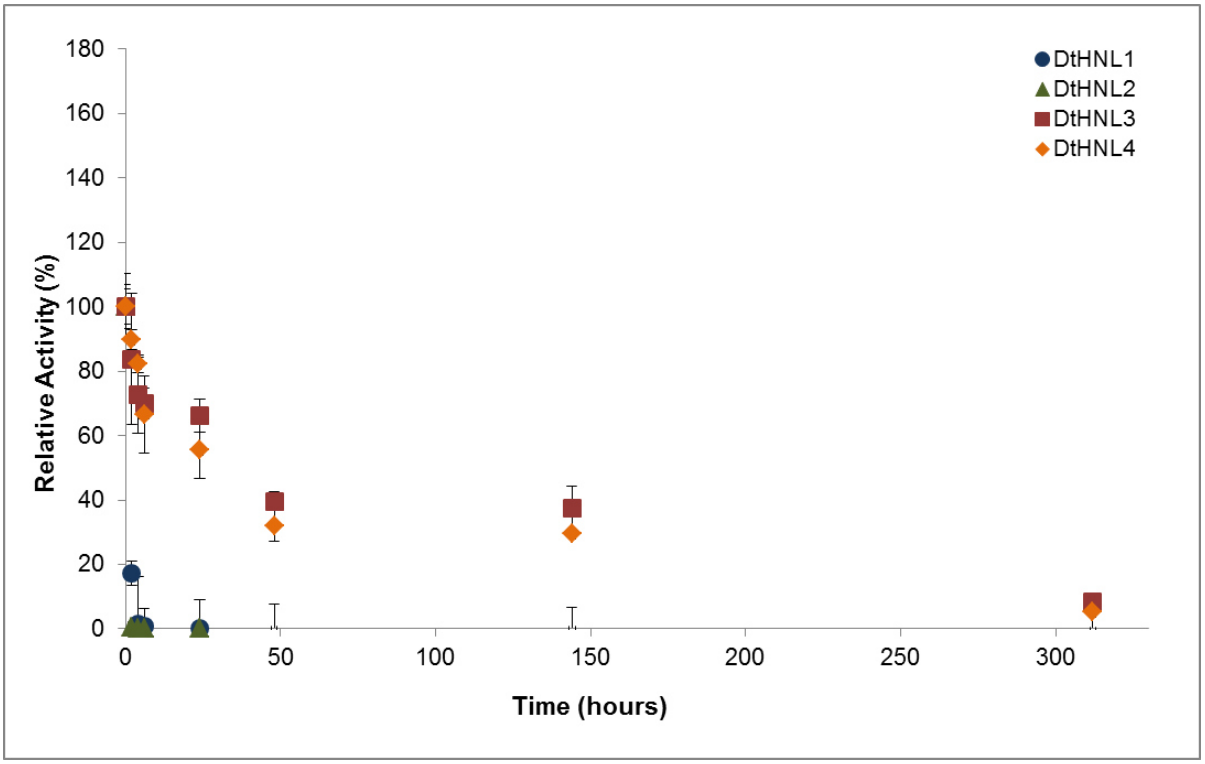

Figure 24: Temperature stability profile of purified re*Dt*HNLs at 40°C. Samples were stored in concentrations of 1 mg/mL in 50 mM citrate phosphate buffer pH 6.5. The relative activities are plotted against the respective time of storage.

After four months of storage in sodium phosphate buffer at 4°C the residual activities were 79 % for re*Dt*HNL4, 45 % for re*Dt*HNL3 and 14 % for re*Dt*HNL1. There was no residual activity measurable for re*Dt*HNL2. Comparison of these results with the activities measured for samples of pH-stability (table 10) indicated that a sodium phosphate buffer system might support the enzymatic stability of re*Dt*HNL3 and 4. Though these results were not observed for re*Dt*HNL1 and 2. Enzymes stored in citrate phosphate buffer kept stability values of 16 – 39 %.

Table 10: Residual activities of re*Dt*HNLs stored in sodium phosphate buffer pH 6.5 and citrate phosphate buffer p 5.0 for 4 months at 4°C.

***Dt*HNLs residual activities after 4 months of storage at 4°C (%)**				
50mM Buffer system	*Dt*HNL1	*Dt*HNL2	*Dt*HNL3	*Dt*HNL4
Sodium phosphate pH 6.5	14	0	45	79
Citrate phosphate pH 5.0	39	22	25	16

4.2.3 Determination of the melting temperature of purified re*Dt*HNL's by protein thermal shift assay

Re*Dt*HNL's thermal stabilities were measured using the protein thermal shift assay. Calculations were done by plotting the temperature against their correlating relative fluorescent units (RFU) of the TAMRA reporter signal. Highest fluorescent units indicated complete unfolding of the protein and the associated temperature was concluded to be the respective melting temperature.

Highest melting temperatures for re*Dt*HNL1 in citrate phosphate buffer at pH 4.5 were determined to be 60°C. Higher pH values as well as lower ones led to a decrease of the protein's melting temperature to 48.5°C (pH 6.5) and to 32°C (pH 2.5). Acetate buffer (pH 4.5) seemed to raise the stability of re*Dt*HNL1 by causing a thermal shift with partially unfolded structure at 50°C and complete unfolding at 60.5°C. Figure 25 depicts the melting curves of re*Dt*HNL1 in citrate phosphate buffer and acetate buffer pH 4.5.

This stabilizing effect might be the result of binding acetate that accumulates with the partially unfolded protein and therefore increases the temperature that is needed for complete denaturation. This effect was not observed for re*Dt*HNL2, 3 and 4 which might be a result of additional basic amino acids in the protein sequence of re*Dt*HNL1.

Basic amino acids as lysine, arginine and histidine are positively charged (protonated) at pH-values lower than the pK of the amino acids functional group. An increased amount of these amino acids would therefore ease the bondage of acetate anions.

Comparison of the enzymes protein sequence, however, showed that actually re*Dt*HNL3 and 4 contain most basic amino acids with an additional Lys64 and His137 instead of Gln64 and Tyr137 in *Dt*HNL1. Further re*Dt*HNL2 contains an Arg5 in place of Gly5.

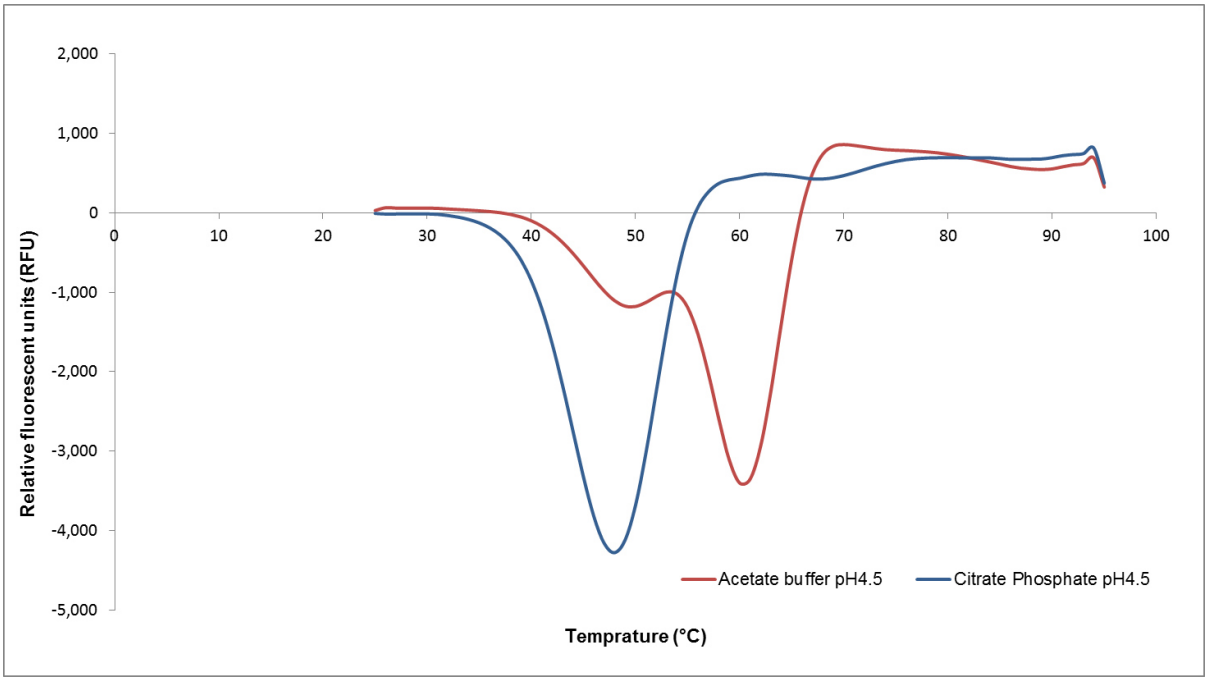

Figure 25: Melting curves of purified re*Dt*HNL1 in acetate and citrate phosphate buffer systems. Melting points are plotted against their respective temperatures.

Comparing all the four isoenzymes, re*Dt*HNL3 and re*Dt*HNL4 were more stable compared to re*Dt*HNL1 and re*Dt*HNL2. Overall it was observed that the higher the pH, the higher was the thermal stability difference among re*Dt*HNL3 and 4 and re*Dt*HNL1 and 2. Whereas highest differences of 9 °C were observed in citrate phosphate buffer pH 5.0 with an unfolding temperature of 64°C and 66°C, respectively (table 11). The melting curves of purified re*Dt*HNL1 for all tested buffers are depicted in the supplementary data (figure S1).

Table 11: Melting temperatures of re*Dt*HNL isoenzymes in citrate phosphate buffer, potassium chloride buffer and acetate buffer of various pH. n.m.= not measured, [1]thermal shift with partially unfolded structure at 50°C and complete unfolding at 60.5°C.

re*Dt*HNL´s melting temperatures (°C)					
Buffer	**pH**	**re*Dt*HNL1**	**re*Dt*HNL2**	**re*Dt*HNL3**	**re*Dt*HNL4**
Citrate phosphate	6.5	48.5 ± 0.5	48	55 ± 1	55.5 ± 0.5
	5	59 ± 2	57.5 ± 0.5	64	66
	4.5	60 ± 1	56 ± 1	61.5 ± 0.5	63 ± 1
	4	57.5 ± 1.5	52	54.5 ± 0.5	52.5 ± 1
	3.5	49	43	43	37.5 ± 1
	3	39 ± 1	35	34.5 ± 0.5	36 ± 1
	2.5	32	25	25	25
Potassium chloride	2	37	33	33.5 ± 0.5	34
Acetate	5	49	n.m.	n.m.	n.m.
	4.5	50 | 60.5[1] ± 1	n.m.	n.m.	n.m.
	4	54.5 ± 0.5	51	54	54

Results of re*Dt*HNL's melting temperature in citrate phosphate buffer pH 5.0 furthermore confirmed observations during online-measurements of re*Dt*HNL's activities at different temperatures (figure 20). It is shown that especially re*Dt*HNL4 was highly active at 45°C and despite all the enzymes activity decreased at 50°C it was not caused by complete thermal unfolding but was a competitive effect by spontaneous degradation of mandelonitrile.

The effect of benzaldehyde on re*Dt*HNLs thermal stability was attempted to test by adding 0.3 mM benzaldehyde per reaction. However, interactions of benzaldehyde with the Sypro orange fluorescent dye led to a constantly decreasing reporter signal and did not lead to reliable results

The absorption maxima for the SYPRO orange fluorescent dye are at λ = 300 nm and 470 nm, the emission has its maximum at λ = 570 nm [52]. Benzaldehyde shows a UV absorption spectrum between 252 and 368nm with a maxima at 284 nm [53]. It can be suggested that due to the superposition of the two absorption spectra the detection of the fluorescent signal by real time PCR is not possible.

4.2.4 Kinetic characterization of re*Dt*HNLs

Kinetic parameters (K_m, k_{cat}, k_{cat}/K_m) were determined by measuring re*Dt*HNLs' initial reaction rates using different concentrations of substrates. Measurements of cyanogenesis were performed for all four enzymes using enantiopure (*R*) – mandelonitrile as the substrate, monitoring the production of benzaldehyde by spectrophotometric screening. Kinetic parameters of the synthesis reaction were determined for re*Dt*HNL1 using various concentrations of benzaldehyde and a specific amount of HCN. The formation of the respective products was monitored by GC over time.

4.2.4.1 Michaelis Menten parameters of (*R*)-mandelonitrile cleavage reaction

Michaelis – Menten parameters of the hydroxynitrile lyase cleavage reactions for (*R*)-mandelonitrile were calculated by SigmaPlot 13.0 from the initial reaction rates dependent on different substrate concentrations.

Kinetic parameters were determined by varying the (*R*) – mandelonitrile concentrations from 0.009 mM to 18 mM with an enzyme amount of 0.01 µg per reaction. Specific activities of *Dt*HNLs at the respective substrate concentrations are listed in the supplementary data (table S1). Each reaction was performed in biological and technical triplicates. References containing all components except re*Dt*HNL were determined twice.

All re*Dt*HNLs showed high affinity to the substrate (*R*)-mandelonitrile with 0.297 ± 0.029 mM for re*Dt*HNL1, 0.451 ± 0.047 mM for re*Dt*HNL2, 0.639 ± 0.079 mM re*Dt*HNL3 and 0.591 ± 0.089 mM for re*Dt*HNL4. Re*Dt*HNL3 showed the highest maximum reaction rate (v_{max}) of 922 ± 24 µmol $min^{-1}mg^{-1}$ and a turn over number (k_{cat}) of 319.8 s^{-1}. Turn over numbers observed for re*Dt*HNL1, 2 and 4 were 141.9 s^{-1}, 173.2 s^{-1} and 231.9 s^{-1}, respectively.

However, all the four enzymes showed similar catalytic efficiency with an average of 438.5 ± 58.8 s^{-1} mM^{-1} (table 12).

Table 12: Michaelis – Menten parameters of re*Dt*HNLs for cleavage of (*R*) – mandelonitrile.

	v_{max}	$K_{M\ R\text{-}MNL}$	k_{cat}	k_{cat}/K_M
	(µmol/min/mg)	**(mM)**	**(s^{-1})**	**(s^{-1} mM^{-1})**
re*Dt*HNL1	373± 7	0.297 ± 0.029	141.9	487.5
re*Dt*HNL2	404 ± 8	0.451 ± 0.047	173.2	340.4
re*Dt*HNL3	922 ± 24	0.639 ± 0.079	319.8	510.3
re*Dt*HNL4	641 ± 20	0.591 ± 0.089	231.9	377.0

Certainly comparison of k_{cat}/K_m is not a reliable indicator to determine which enzyme is a better catalyst. Eisenthal *et al.* have shown that enzymes with higher catalytic efficiencies than with lower catalytic efficiencies catalysed identical reactions at lower rates at certain substrate concentrations. The ratio of two reaction rates is therefore not a constant but depends on the ratio of [S]/K_M [54].

Thus, the experimental set up kinetic parameter determination of re*Dt*HNLs was performed on the same substrate with identical concentrations, with the same enzyme amount and equal active sites, the ratio of k_{cat} to K_M gives an indication of the catalytic potential among the four re*Dt*HNLs. Based on this comparison, re*Dt*HNL3 seems to be the most efficient catalyst in Cyanogenesis.

4.2.4.2 Michaelis Menten parameters of (*R*)-mandelonitrile synthesis reaction

Michaelis – Menten parameters for the synthesis of (*R*)-mandelonitrile of re*Dt*HNL1 were determined in a biphasic system with strong agitation. Varying concentrations of benzaldehyde in buffer phase were used from 0.1 – 7.9 mM with a constant concentration of 2 M HCN in MTBE. Thereof, the enzyme amount per reaction was constantly 0.05 mg.

The maximal velocity for benzaldehyde conversion of 376.9 ± 88.9 µmol min^{-1} mg^{-1} (table 13) is virtually identical to the v_{max} measured for (*R*)-mandelonitrile cleavage (373 ± 7 µmol min^{-1} mg^{-1}). However, the affinity to benzaldehyde determined with 13.4 mM was lower than observed for the cleavage of mandelonitrile (0.297 mM).

The turn over number was 71.6 sec^{-1} and the consequential enzymatic efficiency k_{cat}/K_m was calculated to be 5.3 sec^{-1} mM^{-1}.

Table 13: Kinetic parameters for benzaldehyde for DtHNL1 synthesis reaction.

	V_{max}	$K_{M\text{ - Benzaldehyde}}$	k_{cat}	k_{cat}/K_M
	(µmol/min/mg)	(mM)	(s^{-1})	(s^{-1} mM^{-1})
re*Dt*HNL1	376.9 ± 88.9	13.4	71.6	5.3

Conversion rates of re*Dt*HNL1 at the respective substrate concentrations are listed in the supplementary data (table S11). The graphical representation of the Michaelis – Menten kinetic curve is shown in figure 26.

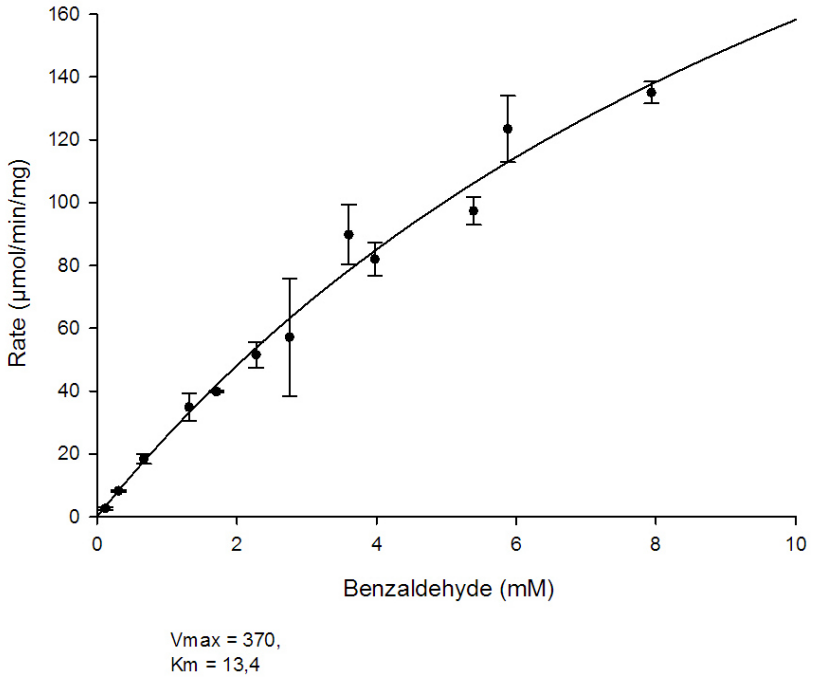

Figure 26: Graphical representation of Michaelis – Menten parameters for the synthesis of mandelonitrile from benzaldehyde by re*Dt*HNL1. Benzaldehyde concentrations varied from 0.1 – 7.9 mM in aqueous phase are plotted against respective conversion rates of re*Dt*HNL1.

Synthesis of (*R*)-mandelonitrile took place in a biphasic system of MTBE and acetate buffer. The benzaldehyde concentration in the organic phase cannot reach concentrations below 10 mM or above 500 mM, hence, the measurement range was restricted. Therefore, the v_{max} could not be reached in these experiments and prevented a more accurate determination of the kinetic parameters.

Advantages of the biphasic system for preparative synthetic applications are higher substrate concentrations due to a higher solubility of substrates. Enzyme inhibition and chemical side-reactions are avoided since the substrate concentration in the aqueous phase is much lower and the organic layer is almost water-free. Further, the catalyst can be reused by simple separation of the two phases.

However, disadvantages of this system are low enzymatic conversion rates especially for substrates with high K_M values, due to high partition coefficients and probably low substrate concentrations in the aqueous phase. Increasing the surface area between the two phases by intensive stirring is working around this problem but might reduce the enzyme stability [2].

4.2.5 Determination of inhibition effects on re*Dt*HNLs activities

The influence of various reagents on catalytic activity of re*Dt*HNLs was performed to identify amino acid residues that may potentially be involved in the reaction. Interaction with the respective reagent can result in enzymatically inhibiting effects. The two reducing agents 2-mercaptoethanol and dithiothreitol (DTT) were chosen in order to break possible disulphide bonds of the enzymes tertiary and quaternary structure [55]. Influences of $AgNO_3$ or phenylmethylsulfonyl fluoride (PMSF) would indicate the participation of a cysteine or a serine in the catalytic reaction, respectively [56]. Further, benzoic acid, known for inhibiting the hydroxynitrile lyase from *Sorghum bicolor*, and acetone were tested.

Certain amounts of reagent were added to 50 mM citrate phosphate buffer pH 5.0 that was used as standard reaction buffer for kinetic activity determination. After incubating the enzymes with the respective reagents, conversion of (*R/S*)-mandelonitrile to benzaldehyde was followed spectrophotometrically.

Components that showed little influence on the catalytic activity of re*Dt*HNLs according to the standard kinetic assay were incubated for 7 min at 30°C with the respective inhibitor prior to the kinetic activity determination. However, the additional incubation step hardly showed any influence on the effect of the inhibiting compounds (figure 27).

Significant inhibition was observed for the metabolite benzoic acid with 60 % residual activity at 1 mM and 45 % at 2.5 mM. The presence of 1 mM $AgNO_3$ caused complete inhibition. Moderate activities were observed for the serine modifying agent PMSF (5 mM) as well as for 5 mM acetone and 5 mM DTT with 90, 85, 80 % residual activity, respectively. The sulfhydryl reagent 2-mercaptoethanol (5 mM) inhibited the activity by 5 %, caused by the reductive cleavage of potential disulfide bonds.

In comparison, a typical alpha/beta-hydrolase fold HNLs as *Hb*HNL is known to get inhibited by compounds as diisopropyl fluorophosphates (DFP) (3MM, 93% inhibition) and diethyl dicarbonate (3 MM, 93% inhibition) [11], hexafluoroacetone and acetone [57]. Benzaldehyde acts as strong competitive inhibitor against mandelonitrile [58]. However PMSF does not influence the enzymes catalytic activity [59]. *Me*HNL, also belonging to the alpha/beta-hydrolase fold superfamily gets inhibited by PMSF, DFP [24], acetone, benzaldhyde, propanol, propionaldehyde and phenol [60].

Since $AgNO_3$ is known for interacting with the sulfhydryl group of cysteine, the results indicate that a cysteine is involved in re*Dt*HNLs catalysis or located near the active site of the enzyme [56]. Further agarose gel electrophoresis might reveal more information about the influence of $AgNO_3$ and could enlighten whether a dimer- or multimerization takes place as an effect of disulphide bond formation. Inhibition effects might also be a result of a blockade of cyanides entrance tunnel by $AgNO_3$ or an oxidation of involved cysteines.

However, analysis of re*Dt*HNLs amino acid conformation identified six residues that are involved in substrate binding and catalysis. Both Arg69 and Tyr101 are directly involved in the catalysis as well as Tyr117, Asp85, Ser87 and Tyr161 [8].

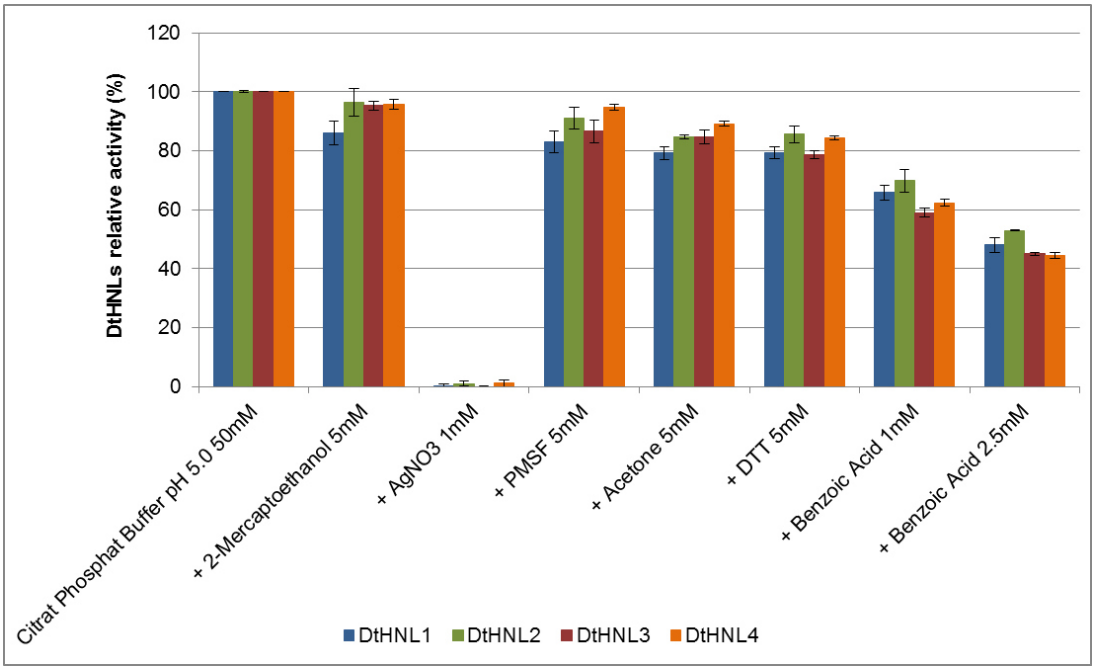

Figure 27: Influence of different inhibitors on enzymatic activity of re*Dt*HNLs. The residual activities for inhibitor containing reactions are given relative to citrate phosphate buffer, pH 5.0.

4.2.6 Re*Dt*HNL activity with aliphatic substrates

The cleavage reaction was additionally performed with different substrates in order to explore the enzymes acceptance for utilizing various cyanohydrins using the endpoint assay. The substrate concentrations were set to 300 mM of (*R*/*S*)-mandelonitrile, acetone cyanohydrin and hydroxypivaldehyde cyanohydrin (see chapter 3.6.9).

Relative to cyanogenesis of (*R*/*S*)-mandelonitrile that was set to 100%, activities for acetone cyanohydrin cleavage were determined between 4 to 7%. Cyanogenesis of hydroxypivaldehyde cyanohydrin was shown to be about 1% relative to (*R*/*S*)-mandelonitrile (table 14).

Table 14: Acceptance of re*Dt*HNLs for acetone cyanohydrin and hydroxypivaldehyde cyanohydrin relative to (*R/S*)-mandelonitrile.

	(*R/S*) – Mandelonitrile		Acetone Cyanohydrin		Hydroxypivaldehyde	
	Relative activitiy (%)	Abs_{280}/min	Relative activitiy (%)	Abs_{280}/min	Relative activitiy (%)	Abs_{280}/min
re*Dt*HNL1	100	1.875	4.0	0.075	0.9	0.017
re*Dt*HNL2	100	1.819	7.1	0.128	1.0	0.019
re*Dt*HNL3	100	0.653	3.6	0.023	0.3	0.002
re*Dt*HNL4	100	1.932	4.4	0.084	0.0	0.001

It is shown that re*Dt*HNLs hardly accept substrates as acetone cyanohydrin and hydroxypivaldehyde cyanohydrin. The enzymes substrate scope might further be extended by different protein engineering strategies but at least the enzymes seem to be most active with aromatic substrates. Variations of substrate binding and affinity or modification of amino acids that are involved in the catalytic mechanism would be another approach in order to broaden the enzymes substrate range.

4.3 Characterization of glycosylated *Dt*HNL isoenzymes produced in *Pichia pastoris*

In addition to the biochemical characterization of purified re*Dt*HNL isoforms, intracellular isoenzymes *Dt*HNL2, 3 and 4 (rp*Dt*HNLs) and extracellular *Dt*HNL1, 2, 3 and 4 (rs*Dt*HNLs) were produced in *Pichia pastoris* CBS 7435 Mut^S using the wildtype AOX1-promoter.

Glycosylated samples of rs*Dt*HNL enzymes were delivered by a third party and additional partner in the Kyrobio project (VTU technologies). Proprietary secretion signals for secretion of expressed protein were added to preordered synthetic genes by PCR and afterwards cloned into wildtype AOX1 promoter variants. In order to select transformants of highest activity, two consecutive screening rounds were performed [61].

The four enzymes have four predicted *N*-glycosylation sites and thereby differ slightly among each other. The first glycosylation site of rs*Dt*HNL3 and 4 has a lysine instead of glutamine at position 67 (figures 28 - 31). Further differences of the enzymes protein sequence that are not supposed to be influencing the enzymes glycosylation pattern, include a basic Arg5 in rs*Dt*HNL2 instead of an aliphatic glycine, whereby rs*Dt*HNL3 and 4 appear to be more basic since they both have a Lys64 and His137 instead of Gln64 and Tyr137. Further they share an aliphatic Gly183 instead of the acidic Asp138 of rs*Dt*HNL1 and 2 (table 15).

Table 15: Differences in rs*Dt*HNLs protein sequence. [1]predicted *N*-glycosylation site.

	Position						
	5	**10**	**64[1]**	**78**	**136**	**137**	**183**
rs*Dt*HNL1	Gly	Gln	Gln	Glu	Phe	Tyr	Asp
rs*Dt*HNL2	Arg	Glu	Gln	Asp	Phe	Tyr	Asp
rs*Dt*HNL3	Gly	Glu	Lys	Glu	Leu	His	Gly
rs*Dt*HNL4	Gly	Glu	Lys	Glu	Phe	His	Gly

The enzymes show similar molecular weights with 20.14 kDa, 20.21 kDa, 19.95 kDa and 20.01 kDa respectively. Rs*Dt*HNL1 and 2 have the same calculated isoelectric point (pH 4.77) as well as rs*Dt*HNL3 and 4 (pH 5.12). Despite their similarities it has

to be considered that not each glycosylated enzyme shows the same glycosylation pattern. Rather, the additional sugar residues are a heterogenic mixture of diverse length and number that may show different influence on the enzymes catalytic activity.

MAGTGGGAEQFQLRGVLWGKAYSWKITGTTIDKVWSIVGDYVRVDNWVSSVVKSS
HVVSGEA**NQT**GCVRRFVCYPASEGESETVDYSELIHMNAAAHQYMYMIVGG**NIT**GF
SLMKNYVS**NIS**LSSLPEEDGGGVIFYWSFTAEPAS**NLT**EQKCIEIVFPLYTTALKDLC
THLSIPESSVTLLDD

Figure 28: **Amino acid sequence of rs*Dt*HNL1. Predicted N-glycosylation sites shown in bold.**

MAGTRGGAEEFQLRGVLWGKAYSWKITGTTIDKVWSIVGDYVRVDNWVSSVVKSS
HVVSGDA**NQT**GCVRRFVCYPASDGESETVDYSELIHMNAAAHQYMYMIVGG**NIT**G
FSLMKNYVS**NIS**LSSLPEEDGGGVIFYWSFTAEPAS**NLT**EQKCIEIVFPLYTTALKDL
CTHLSIPESSVTLLDD

Figure 29: Amino acid sequence of rs*Dt*HNL2. Predicted N-glycosylation sites shown in bold.

MAGTGGGAEEFQLRGVLWGKAYSWKISGTTIDKVWAIVGDYVRVDNWVSSVVKSS
HVVSGDA**NKT**GCVRRFVCYPASEGESETVDYSELIHMNAAAHQYMYMIVGG**NIT**GF
SLMKNYVS**NIS**LNSLPEADGGGVILHWSFTAEPAS**NLT**EQKCIEIVFPLYTTALKDLC
THLSIPESSVTLLGD

Figure 30: Amino acid sequence of rs*Dt*HNL3. Predicted N-glycosylation sites shown in bold.

MAGTGGGAEEFQLRGVLWGKAYSWKITGTTIDKVWSIVGDYVRVDNWVSSVVKSS
HVVSGDA**NKT**GCVRRFVCYPASEGESETVDYSELIHMNAAAHQYMYMIVGG**NIT**GF
SLMKNYVS**NIS**LNSLPEADGGGVIFHWSFTAEPAS**NLT**EQKCIEIVFPLYTTALKDLC
THLSIPESSVTLLGD

Figure 31: Amino acid sequence of rs*Dt*HNL4. Predicted N-glycosylation sites shown in bold.

VTU delivered rs*Dt*HNLs which had been produced in fermenters with a total volume of 0.5 L. Cultivations ran for 100 hours whereof cells were fed with 60% glycerol solution over the first 5 h and with methanol for the remaining time. After filtration of the reaction broth, supernatants were screened for HNL activity. Frozen samples were afterwards delivered at -20°C.

Characterization experiments of glycosylated rs*Dt*HNL isoenzymes included the determination of their specific activities and behaviour at different pH and temperature. The protein amount of all the four enzymes, determined using the Bradford protein assay, was observed to be about 5 mg/mL. All rs*Dt*HNLs showed similar activities for (*R/S*)-mandelonitrile around 100 U/mg and almost 60% higher activity for enantiopure (*R*)-mandelonitrile (table 16). Specific activities of glycosylated rs*Dt*HNL1 were about 30% of the purified enzyme.

Table 16: Glycosylated rs*Dt*HNLs protein amount and specific activities for (*R/S*)- and (*R*)-mandelonitrile.

Glycosylated rs*Dt*HNLs	Total protein amount (mg/mL)	Specific activity (U/mg)	
		(*R/S*)-mandelonitrile	(*R*)-mandelonitrile
rs*Dt*HNL1	5.5	96.5 ± 1.2	270.7 ± 1.5
rs*Dt*HNL2	5.7	94.8 ± 1.2	259.6 ± 16.1
rs*Dt*HNL3	5.5	85.5 ± 0.9	180.6 ± 4.9
rs*Dt*HNL4	5.1	111.4 ± 2.2	274.0 ± 10.9

Samples measured with racemic mandelonitrile contained 0.5 µg; samples measured with (*R*)-mandelonitrile contained 0.25 µg of enzyme. Due to the uneven enzyme amount of the two different samples no doubled enzymatic activity for (*R*)-mandelonitrile is observed (figure 32).

Activity measurements performed with various enzyme amounts showed that activities for measurements containing 0.2 µg of enzyme reach 80% of activity of reactions containing 0.4 µg. Considering this coherence and the doubled activity for enantiopure substrate, the activity for (*R*/*S*)-mandelonitrile fits to the expected values of about 50%.

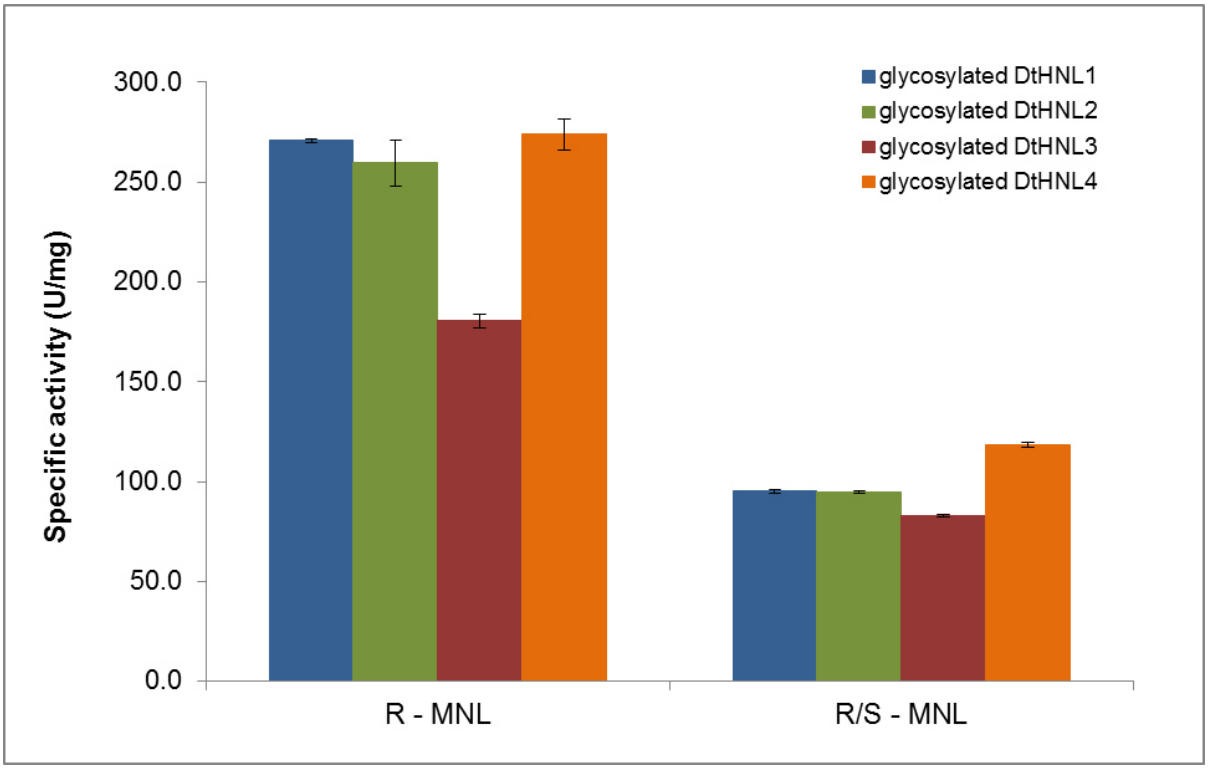

Figure 32: Specific activities achieved for conversion of (*R*) – MNL and (*R*/*S*) – MNL by glycosylated rs*Dt*HNLs.

As reported by company partner VTU, activity values for mandelonitrile cleavage, obtained from culture supernatants, all secreted rs*Dt*HNLs showed comparable levels of activity. Regarding the estimated concentration of the particular rs*Dt*HNL isoforms in the culture supernatant (measured by mCE after deglycosylation) in combination with the determined activities, results have shown that re*Dt*HNL3 exhibits a higher "specific activity" compared to the other rs*Dt*HNLs [61].

4.3.1 SDS – PAGE of glycosylated rs*Dt*HNL isoenzymes

Visualization of glycosylated (figure 33 B) and deglycosylated (figure 33 A) rs*Dt*HNLs was performed by SDS-PAGE. After deglycosylation, all the four enzymes migrate corresponding to their original size of about 23 kDa. A control of endoglycosidase H was added as control in lane 5 (figure 33 A) and migrated to a size of 29kDa. The supernatant of a *P. pastoris* Mut^S strain was used as the negative control. Since generally low amounts of endogenous proteins are produced by *P. pastoris* [40] there are now visible bands occurring in lane 6.

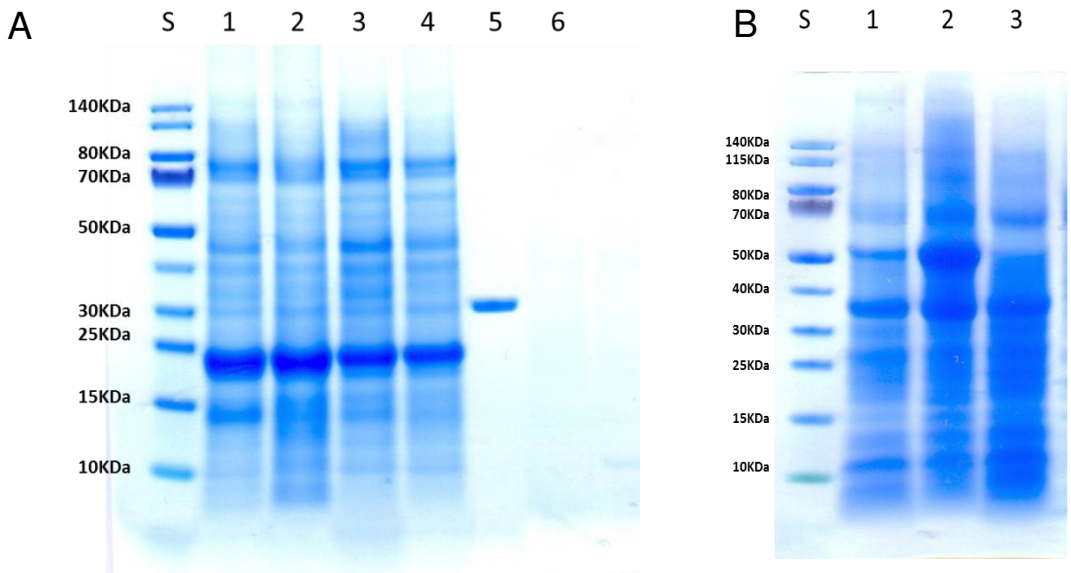

Figure 33: A: SDS-Page of deglycosylated rs*Dt*HNL isoenzymes after *Endo*H treatment. MW deglycosylated rs*Dt*HNLs= 23 kDa. S: PageRulerTM Prestained Protein Ladder; Lane 1: rs*Dt*HNL1 (44µg); Lane 2: rs*Dt*HNL2 (45µg); Lane 3: rs*Dt*HNL3 (49µg); Lane 4: rs*Dt*HNL4 (39µg); Lane 5: *Endo* H (5U); Lane 63: MutS (40µg). **B: SDS-Page of glycosylated rs*Dt*HNL2-4.** S: PageRulerTM Prestained Protein Ladder; Lane 1: rs*Dt*HNL2; Lane 2: rs*Dt*HNL3; Lane 3: rs*Dt*HNL4 (15µl each);

Glycosylated rs*Dt*HNLs2-4 (figure 33 B) migrated to a size of 35 kDa. Comparison with electropherograms performed by company partner VTU (figures 34 – 37) showed that a small fractions of rs*Dt*HNLs1, 2 and 4 and a considerable fraction of rs*Dt*HNL3 are secreted in a non-glycosylated form (peak present without EndoH-treatment) while still the vast majority of the enzyme is only visualizable after deglycosylation.

Upon comparison of the peak area of the entire peak bump for deglycosylated rs*Dt*HNLs with the peak area of Cytochrome c, a theoretical yield of ~ 900mg/L rs*Dt*HNL1, ~ rs*Dt*HNL2, ~530mg/L rs*Dt*HNL3 and ~ rs*Dt*HNL were calculated [62].

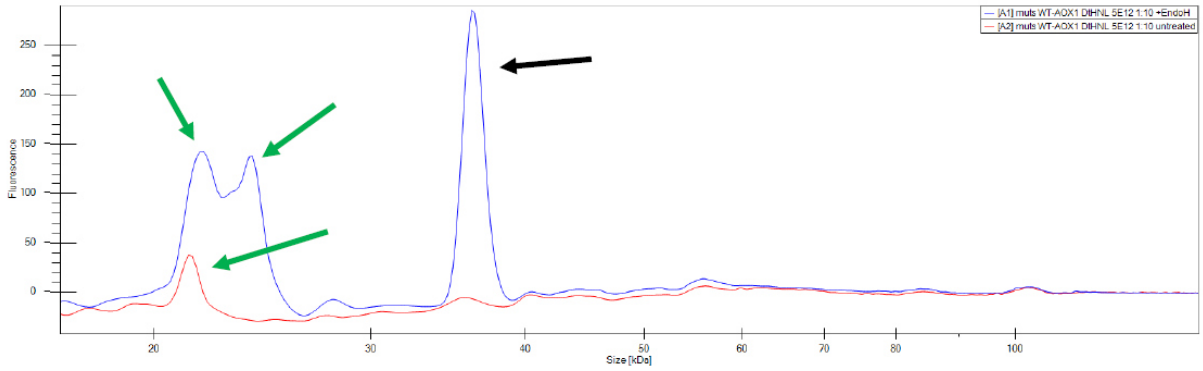

Figure 34: Electropherogram overlay of filtrate with (blue line) and without (red line) treatment with EndoH; green arrows point at (presumable) deglycosylated rs*Dt*HNL-peaks (also present in untreated sample, red line), while black arrow marks the EndoH-signal [62].

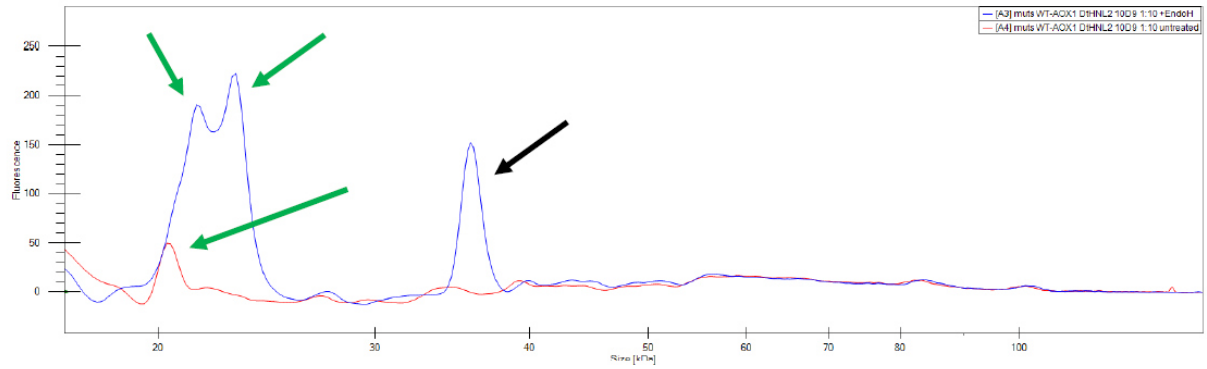

Figure 35: Electropherogram overlay of filtrate with (blue line) and without (red line) treatment with EndoH; green arrows point at (presumable) deglycosylated rs*Dt*HNL-peaks (also present in untreated sample, red line!), while black arrow marks the EndoH-signal [62].

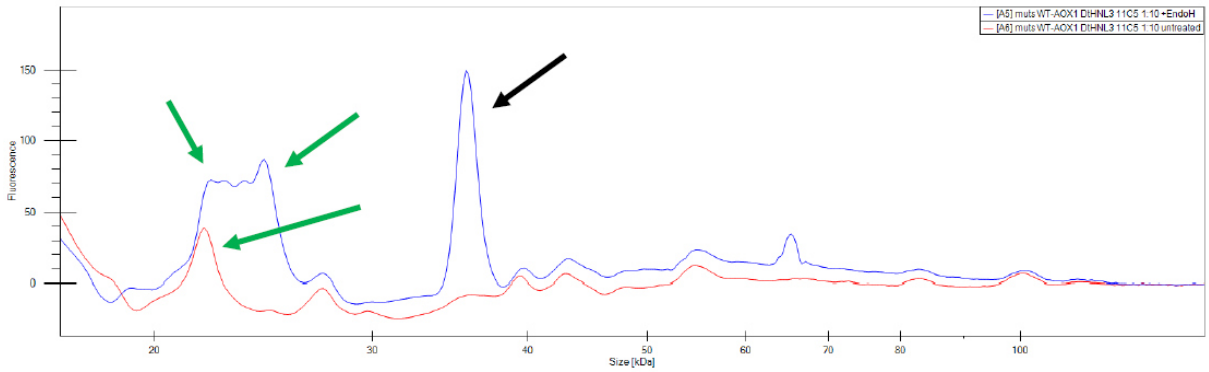

Figure 36: Electropherogram overlay of filtrate with (blue line) and without (red line) treatment with EndoH; green arrows point at (presumable) deglycosylated rs*Dt*HNL-peaks (also present in untreated sample, red line!), while black arrow marks the EndoH-signal [62].

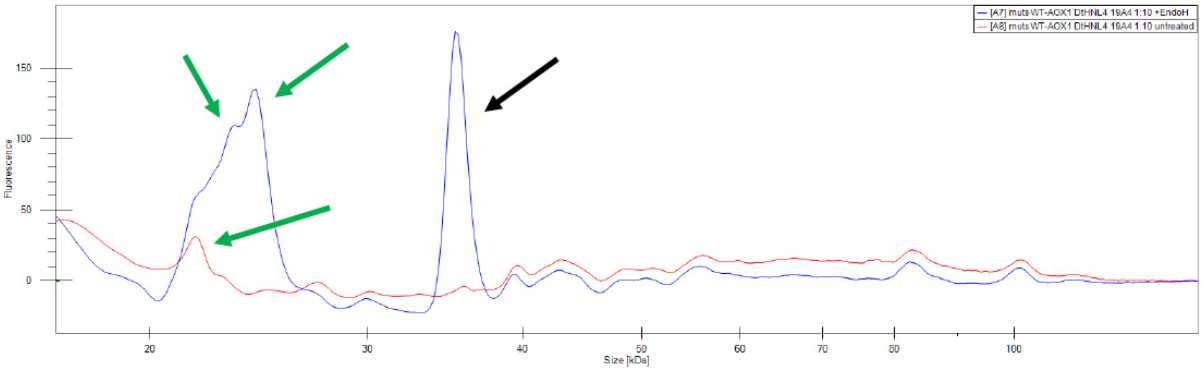

Figure 37: Electropherogram overlay of filtrate with (blue line) and without (red line) treatment with EndoH; green arrows point at (presumable) deglycosylated rs*Dt*HNL-peaks (also present in untreated sample, red line!), while black arrow marks the EndoH-signal [62].

4.3.2 Activity at different pH and stability profiles of glycosylated rs*Dt*HNLs

4.3.2.1 Activity determination of glycosylated rs*Dt*HNLs at different pH values

The specific activity of the four glycosylated rs*Dt*HNLs was determined at various pH values from pH 2.0 to pH 7.0, whereby a conytantly increacing reaction rate was observed along with the raising pH. A maxiumum was reached at pH 5.0 and pH 5.5. Along with higher pH values, the nonenzymatic formation of benzaldehyde was observed due to spontanous decomposition of mandelonitrile (figure 38). The enzyme amount per reaction was constantly 0.5 Units with 15 mM substrate per well.

Activities in acetate buffer (1 µg enzyme/well), relative to citrate phosphate buffer pH 5.0 were determined to be 94% (pH 5.0), 81 % (pH 4.5) and 68% (pH 4.0). Consequently, glycosylated rs*Dt*HNL isoforms showed 20% higher conversion in acetate buffer compared to their non-glycosylated counterparts.

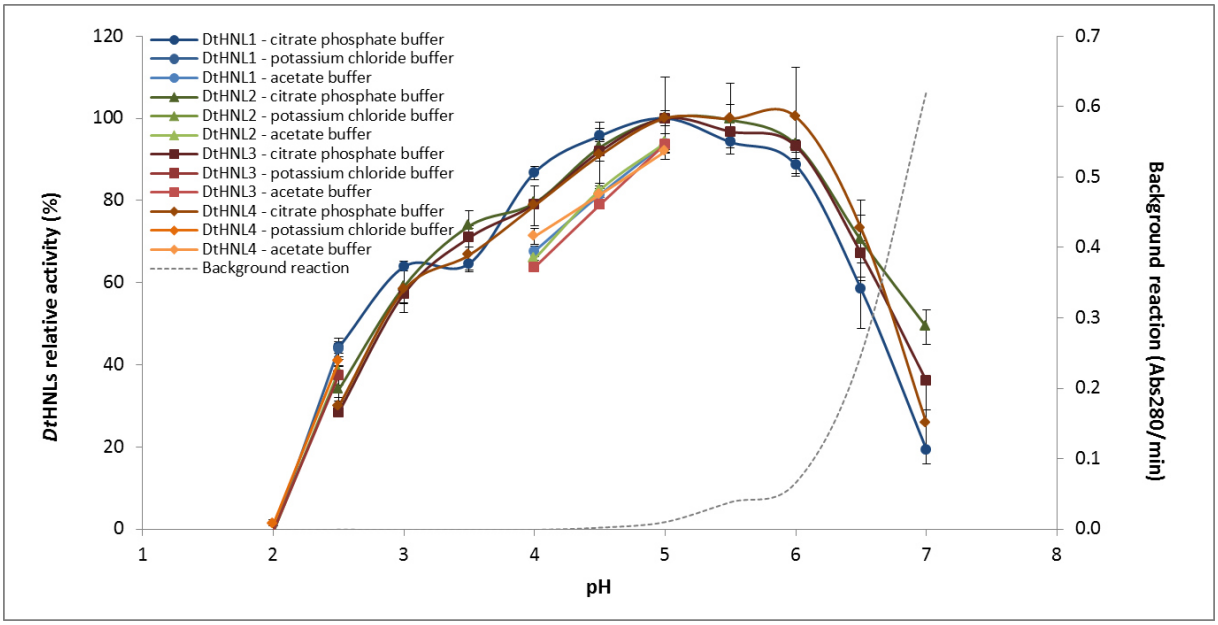

Figure 38: pH activity profile of glycosylted rs*Dt*HNL. Rs*Dt*HNLs' relative activities are plotted against the respective pH. The enzyme amount per reaction was 0.5 Units. Reaction buffers used for the determination were 50 mM citrate phosphate buffer pH 2.5 to pH 6.5, acetate buffer pH 4.0 to pH 5.0 and potassium chloride buffer pH 2.0, pH 2.5. The chemical degradation of the substrate is represented by the grey dashed line.

The pH activity of purified re*Dt*HNLs(see 4.2.1.1) and glycosylated rs*Dt*HNLs is highly similar. Hundred % of activity was observed at pH 5.0 and 5.5. An acidic pH of 2.5 led to activities of 35 – 40% for both citrate phosphate and potassium chloride buffer, and for both purified and glycosylated samples activities of 80 % were observed.

4.3.2.2 Stability of rs*Dt*HNL isoenzymes at different pH values

Enzymes were stored in concentrations of 10 mg/mL in the respective buffer at 8°C. All isoenzymes showed constant activities for at least 312 hours (figure 39, 40).

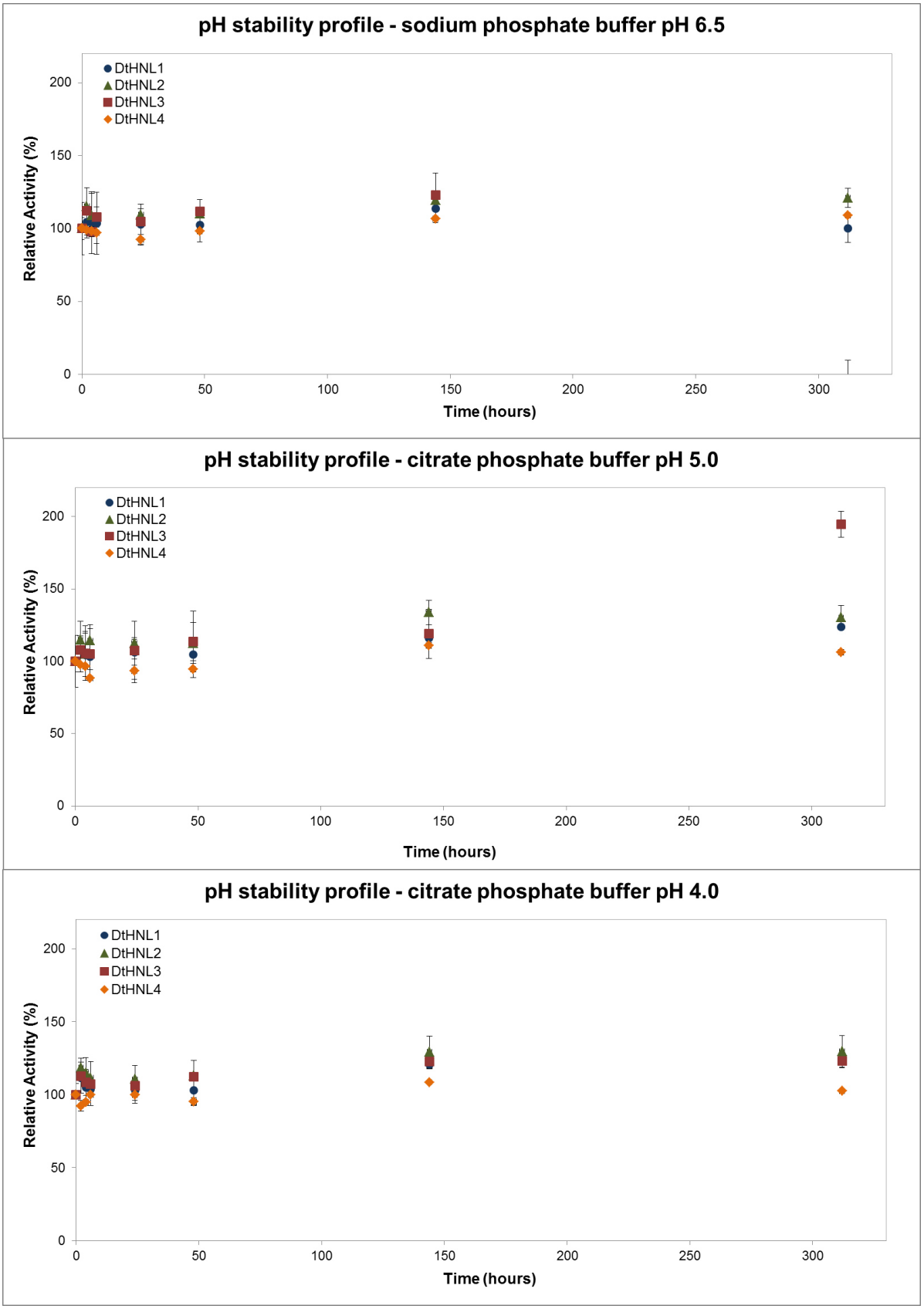

Figure 39: pH stability profile of glycosylated rs*Dt*HNLs in sodium phosphate buffer pH 6.5 and citrate phosphate buffer pH 5.0 and 4.0. The relative activities are plotted against the respective time of storage at 8°C.

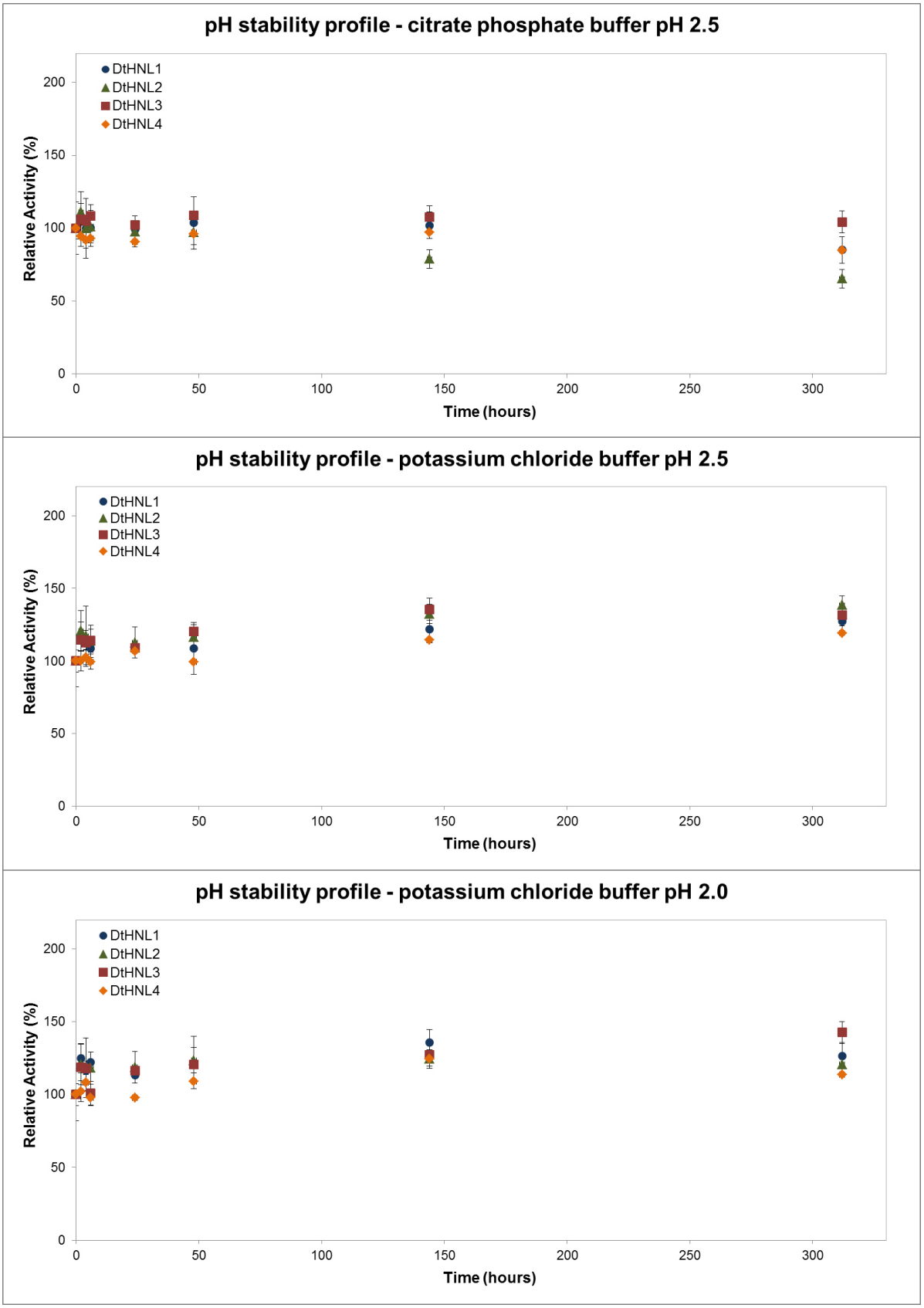

Figure 40: pH stability profile of glycosylated rs*Dt*HNLs in citrate phosphate buffer pH 2.5 and potassium chloride buffer pH 2.0 and 2.5. The relative activities are plotted against the respective time of storage at 8°C.

After 4 months of storage at pH 6.5, rs*Dt*HNL1 showed 90%, rs*Dt*HNL3 and 4 80% and rs*Dt*HNL2 20% of remaining activity, respectively. Similar values were also obtained for storage at pH 4.0 and pH 5.0. Notably, *Dt*HNL2 showed similar stabilities for both glycosylated and purified version.

4.3.3 Temperature activity and stability profiles of glycosylated rs*Dt*HNL

4.3.3.1 Temperature optimum of rs*Dt*HNLs

Glycosylated rs*Dt*HNL2, 3 and 4 demonstrated their maximum activity at 40°C, however rs*Dt*HNL1 showed its optimum at 35 °C. Activities above these optima decreased sharply, which is partly caused by increasing non-enzymatic degradation of mandelonitrile and the enzyme's denaturation (figure 41).

Higher activities then for the purified versions were observed for the glycosylated variants at 10°C. Rs*Dt*HNL1 showed 40%, isoforms 2 and 3 showed about 30% and rs*Dt*HNL4 20% of remaining activity. Thus, the glycosylation seemed to increase the relative activities in a range of 5 - 10%.

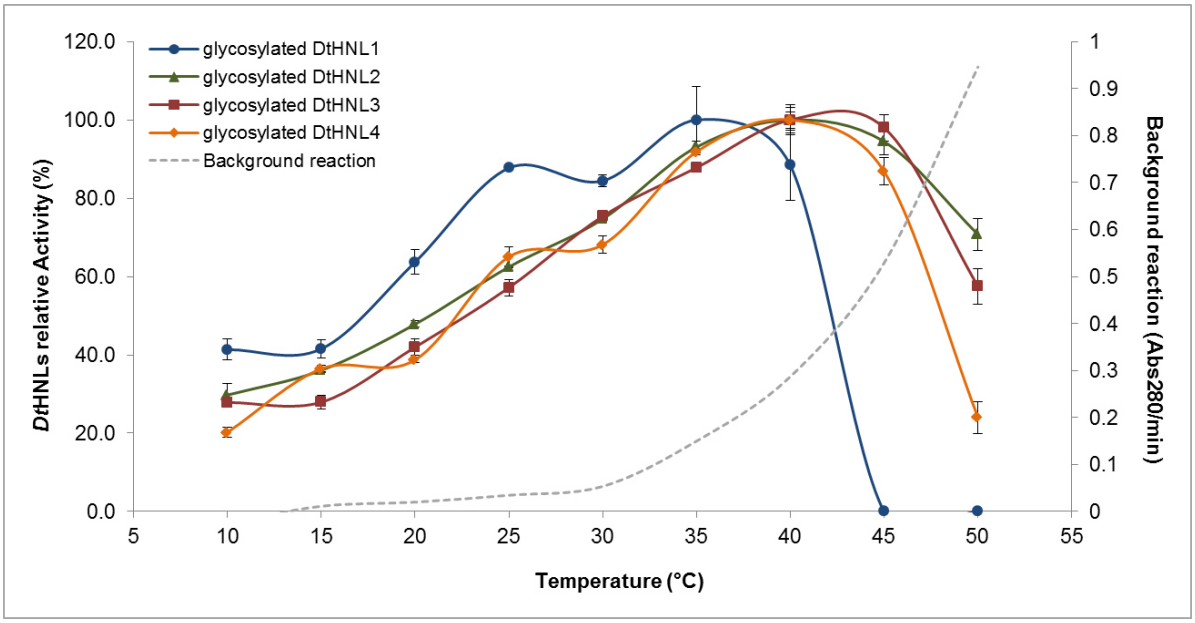

Figure 41: Effect of temperature on the activity of glycosylated rs*Dt*HNL1, 2, 3 and 4. Relative activities of rs*Dt*HNL isoenzymes are plotted against the respective temperatures. The optimum temperature of each enzyme was set as 100%. The non-enzymatic production of benzaldehyde by spontaneous dissociation of mandelonitrile is represented by the grey dashed line that rises constantly from 20°C.

Specific activities determined for glycosylated isoforms (table 17) reached about 30% of the maximal activities of purified re*Dt*HNLs (table 9). Purified re*Dt*HNL1 reached highest activities at 40°C with 500 ± 42 U/mg, whereas the optimal temperature for its glycosylated variant was determined with 35°C and 154 ± 23 U/mg. Almost the same ratio was observed for purified re*Dt*HNL2 with 565 ± 57 U/mg and glycosylated rs*Dt*HNL2 with 195 ± 7 U/mg. The same correlations were observed for *Dt*HNL3 and *Dt*HNL4, whereby both had their optimum at 40 °C with 177 ± 11 U/mg from rs*Dt*HNL3 and 231±13 U/mg from rs*Dt*HNL4.

Table 17: Specific activities of glycosylated rs*Dt*HNL isoenzymes in cyanogenesis reaction at optimal temperatures.

Glycosylated rs*Dt*HNLs	Optimum			
	U/mg	Temperature	$Abs_{280/min}$ cyanogenesis reaction	$Abs_{280/min}$ background reaction
rs*Dt*HNL1	154 ± 23	35°C	0.533	0.462
rs*Dt*HNL2	195 ± 7	40°C	0.670	0.257
rs*Dt*HNL3	177 ± 11	40°C	0.608	0.287
rs*Dt*HNL4	232 ± 13	40°C	0.797	0.290

A reaction temperature of 20°C showed similar correlation to the purified versions as observed at the temperature optimum. Thirty % of activity was achieved for rs*Dt*HNL1 (198 ± 8 U/ mg), rs*Dt*HNL3 (74 ± 6 U/ mg) and rs*Dt*HNL4 (90 ± 3 U/mg). Rs*Dt*HNL2 showed similar specific activities (93 ± 3 U/mg) with 47% remaining activity compared to its purified counterpart. A reaction temperature of 10 °C further halved the activities of all the four isoenzymes (table 18).

Table 18: Specific activities of glycosylated rs*Dt*HNL isoenzymes in cyanogenesis reaction at certain temperatures. [1] temperature used for cyanogenesis reaction assay. [2]temperature, that would be used for synthesis reaction.

Glycosylated rs*Dt*HNLs	20°C [1]	10°C [2]
	U/mg	U/mg
rs*Dt*HNL1	98 ± 8	64 ± 7
rs*Dt*HNL2	93 ± 3	58 ± 10
rs*Dt*HNL3	74 ± 6	49 ± 4
rs*Dt*HNL4	90 ± 3	47 ± 5

4.3.3.2 Stability of glycosylated rs*Dt*HNLs at different temperatures

The impact of glycosylation on rs*Dt*HNLs stability was measured after incubating the single enzymes in a dilution of 1000 U/mL in sodium phosphate buffer at certain temperatures (figures 42-45). Rs*Dt*HNL1, 2, 3 and 4 demonstrated constant stabilities at 10 °C for 312 hours (figure 42), at 20 °C for 48 hours (figure 43) and at 30 °C for 24 hours (figure 44). Increasing stabilities at 4°C might are a result of the enzymes adaptation to the aqueous buffer system since freshly defrosted samples need time for adjusting the right conformation of amino acids.

*Rs*Dt*HNL1 and 2 showed less stability, since their activities decreased at 20°C after 144 hours, whereas rs*Dt*HNL3 and 4 were still stable. After 144 hours of incubation at 30°C rs*Dt*HNLs3 and 4 showed residual activities of about 40%.

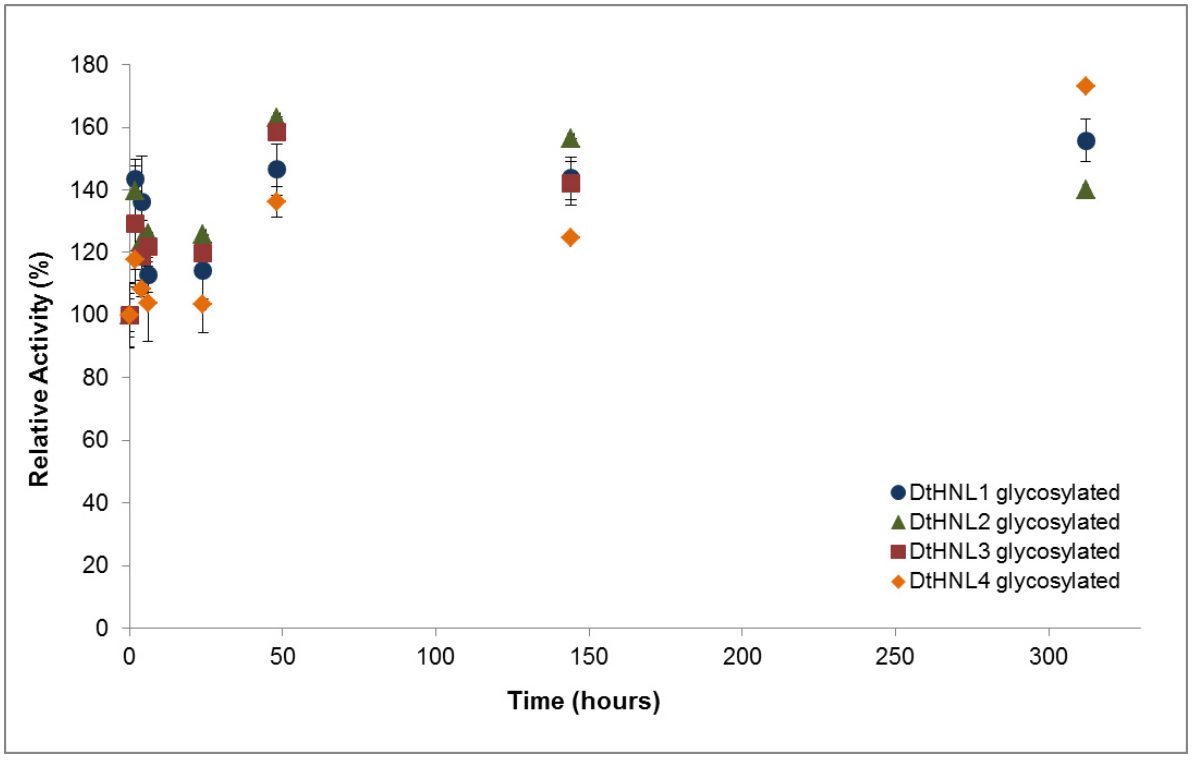

Figure 42: Time dependent temperature stability profile of glycosylated rs*Dt*HNLs at 10°C. Samples were stored at the respective temperature in dilutions of 100 U/mL in 50 mM sodium phosphate buffer pH 6.5. Aliquots were taken at certain time points and activities measured using the standard assay for *Dt*HNLs. The relative activities compared to the activity at 0 hours are plotted against the respective time of storage.

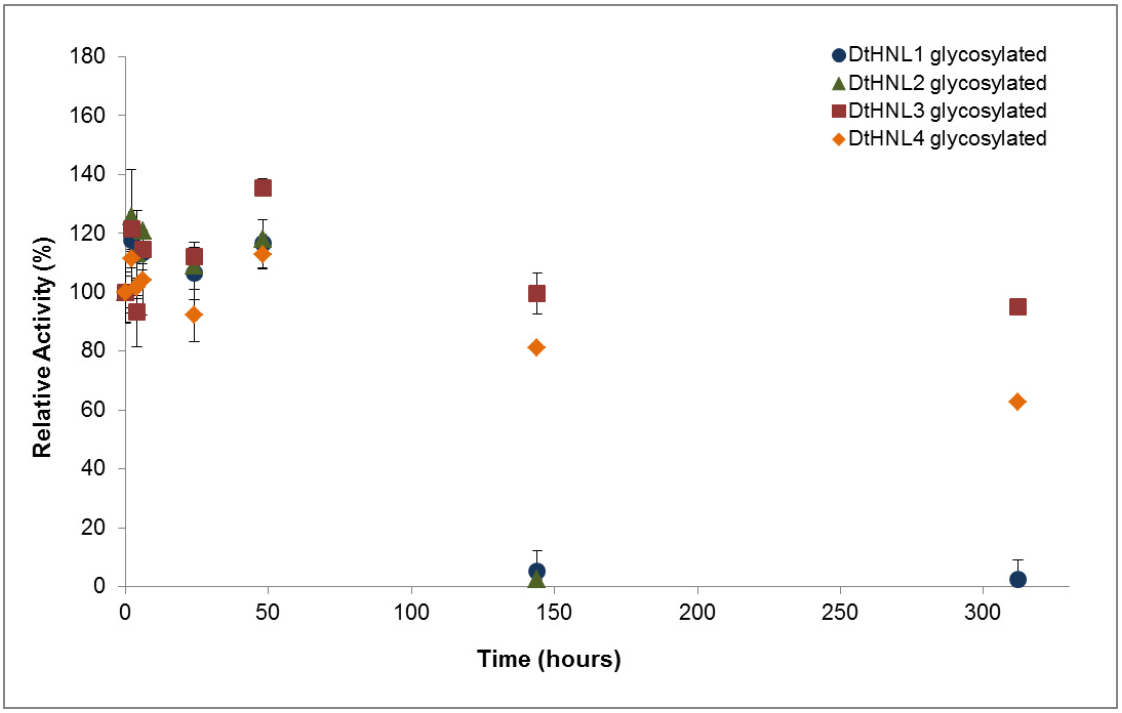

Figure 43: Time dependent temperature stability profile of glycosylated rs*Dt*HNLs at 20°C. Samples were stored at the respective temperature in dilutions of 100 U/mL in 50 mM sodium phosphate buffer pH 6.5. Aliquots were taken at certain time points and activities measured using the standard assay for *Dt*HNLs. The relative activities compared to the activity at 0 hours are plotted against the respective time of storage.

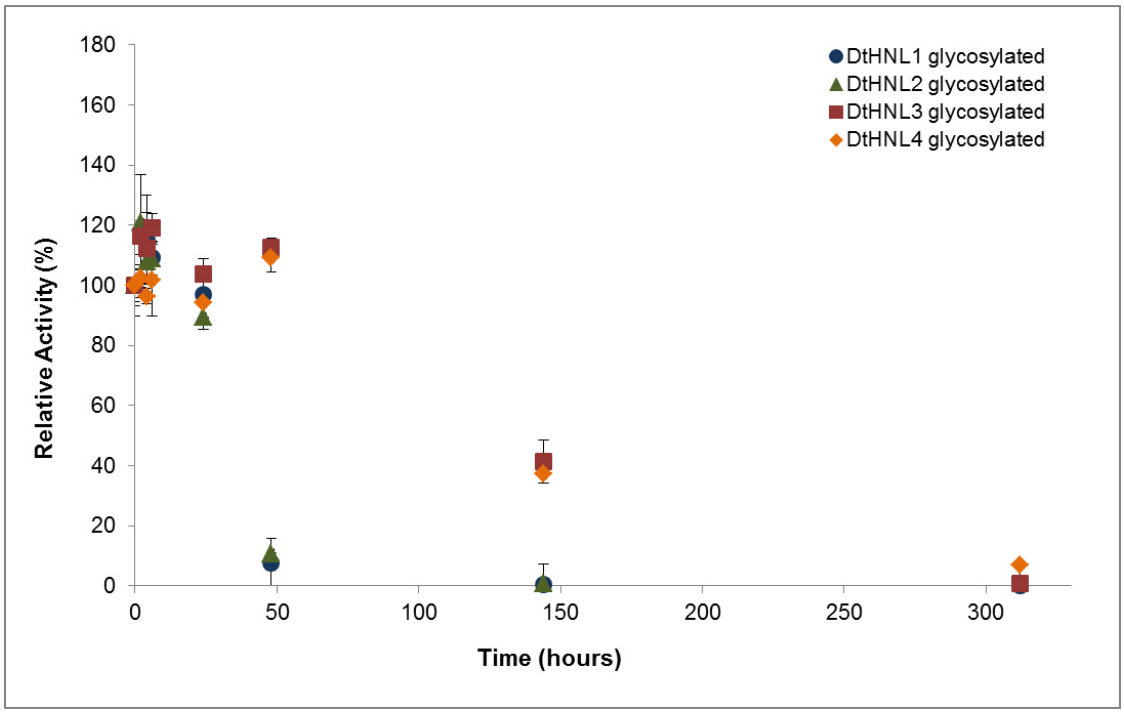

Figure 44: Time dependent temperature stability profile of glycosylated rs*Dt*HNLs at 30°C. Samples were stored at the respective temperature in dilutions of 100 U/mL in 50 mM sodium phosphate buffer pH 6.5. Aliquots were taken at certain time points and activities measured using the standard assay for *Dt*HNLs. The relative activities compared to the activity at 0 hours are plotted against the respective time of storage.

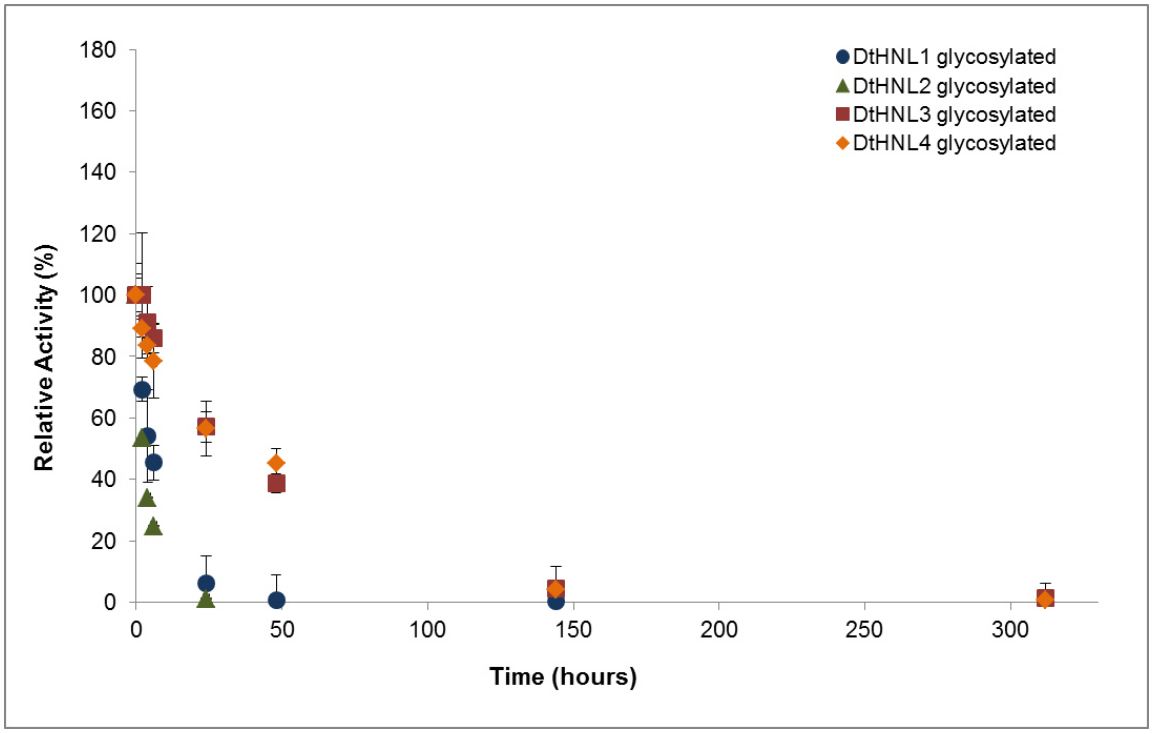

Figure 45: Time dependent temperature stability profile of glycosylated rs*Dt*HNLs at 40°C. Samples were stored at the respective temperature in concentrations of 100 U in 50 mM sodium phosphate buffer pH 6.5. Aliquots were taken at certain time points and measured according to the standard activity assay for *Dt*HNLs. The relative activities compared to the activity at 0 hours are plotted against the respective time of storage.

*RsDt*HNL3 and 4 showed to be more stable even at higher temperatures. Both demonstrated 40% of the original activity after 48 hours at 40°C. After 120 days of storage at 4°C only rs*Dt*HNL4 showed 10% of residual activity.

4.4 Cloning of *Dt*HNLs (rp*Dt*HNLs) for intracellular expression in *Pichia pastoris*

For the intracellular production, codon-optimized genes, ordered by company partner VTU, were cloned in both pPpT4- and pPpB1-based vectors. Generally, pPpB1-based vectors tend to multi copy gene integration, since the weak *ADH*1 promoter of *Saccharomyces cerevisiae* regulates the expression of the Zeocin™ resistance gene. Up to 60 gene copies per cell are possible and necessary to keep up the antibiotic resistance. However, pPpT4-based vectors favour low copy gene integration with a maximum of 7 gene copies per cell due to the stronger *ILV*5 promoter that drives expression of the Zeocin™ resistance cassette [46].

The two different plasmid strategies were chosen in order to obtain one clone per enzyme that generated possibly high HNL activity. The selection of the vector seemed to have minor influence in *Dt*HNL activity, however, constructs of pPpB1 showed on average slightly higher conversion rates, however, none of the strains reached the activity levels obtained for the rp*Dt*HNL1 reference strain obtained by E. Lanfranchi [25]. To improve the overall result, a plasmid amplification strategy of the best transformants was chosen. Clones that showed highest HNL activity were restreaked on YPD plates containing 0.5mg/ml Zeocin (5x), 0.75mg/ml Zeocin (10x) and 1.5mg/ml Zeocin (15x) with the aim to amplify their respective HNL coding cassettes. Conversion of (*R/S*)-mandelonitrile to benzaldehyde was detected for all positive clones (figure 46).

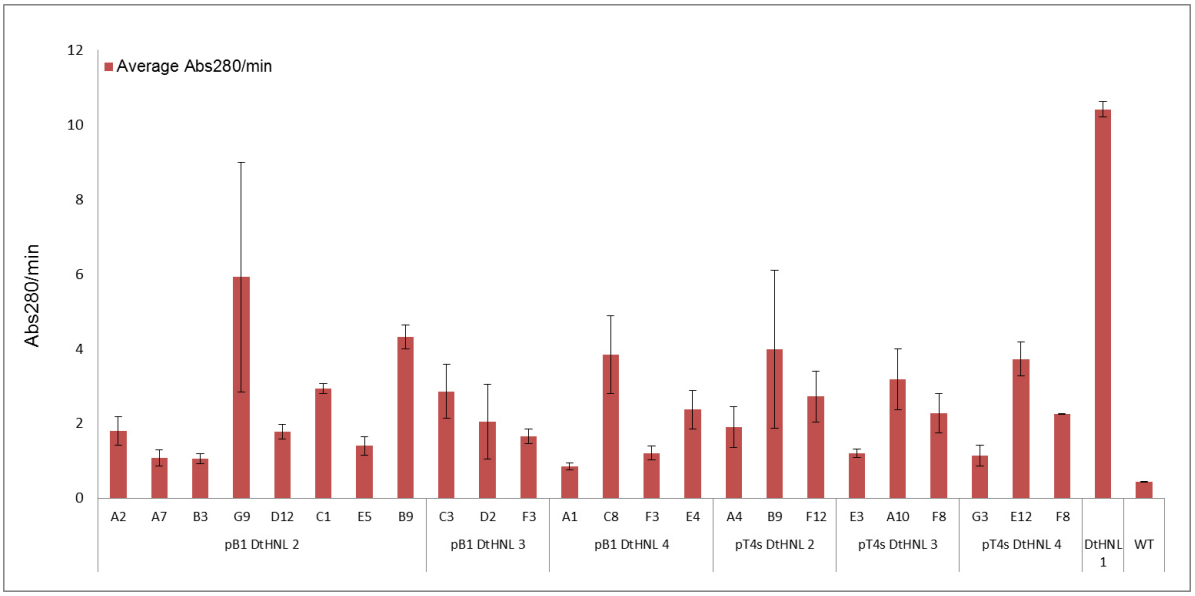

Figure 46: Activity screening of intracellular rp*Dt*HNL producing *P. pastoris* transformants after plasmid amplification on YPD plates containing 1.5 mg/ml zeocin.

Constructs pPpB1_*Dt*HNL2 B9, pPpB1_*Dt*HNL3 C3 and pPpB1_*Dt*HNL4 C8 showed highest catalytic activity with 0.5 µg/µl protein in the supernatant of pPpB1_*Dt*HNL2 B9, 0.7 µg/µl protein in the supernatant of pPpB1_*Dt*HNL3 C3 and 0.9 µg/µl protein in the supernatant of pPpB1_*Dt*HNL4 C8. The former created construct pPpB1_*Dt*HNL1 B1. G4 [25] achieved a protein amount of about 1.3 µg/µl.

Volumetric activities obtained were 146 ± 10 U/ml for rp*Dt*HNL1, 80 ± 5 U/ml for rp*Dt*HNL2 followed by rp*Dt*HNL 3 with 40 ± 5 U/ml and rp*Dt*HNL4 with 54 ± 6 U/ml.

Since the volume of DWP cultivation was limited, and the indicated protein amount was quite low, all supernatants were loaded with a maximum volume of 15 µl in order to visualize at least highest concentrated clones (figure 47). Based on the depicted bands with a size of about 23 kDa the successful protein production of all the three constructs was achieved.

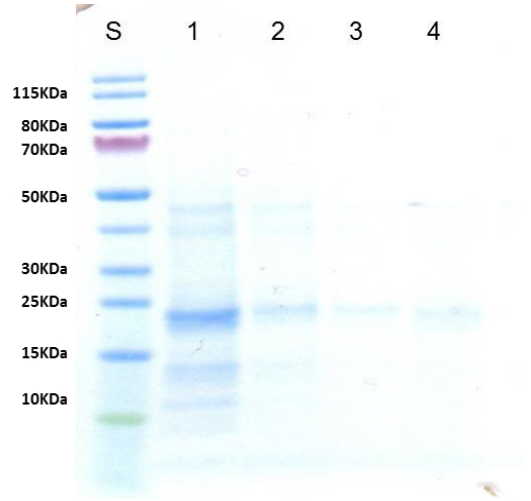

S	Standard
1	rp*Dt*HNL1 (19µg)
2	rp*Dt*HNL2 (8µg)
3	rp*Dt*HNL3 (10µg)
4	rp*Dt*HNL4 (13µg)

Figure 47: SDS-Page of intracellularly produced rp*Dt*HNL isoenzymes liberated with Y-PER solution from *P. pastoris* cultivations. Listed protein amounts are indications based on nano drop measurements of disrupted culture supernatants.

Differences of the production levels between rp*Dt*HNL1 and the constructs of rp*Dt*HNL2, 3 and 4 were suggested to be a result of diverse optimization strategies for *Pichia pastoris* codon usage. However, the alignment of rp*Dt*HNL1 and rp*Dt*HNL2 just showed slight differences as depicted in figure S10. Additional sequencing of the zeocin resistance cassette of all reporter plasmids also indicated no errors of the nucleotide sequence in this region.

Further bottlenecks in the recombinant system of *P. pastoris* are the transcription efficiency, the protein turn over due to proteolysis, protein processing and folding in endoplasmic reticulum and Golgi. The optimal gene copy number is depending on the product of interest and increase of the gene dosage might result in decreased yields. This effect owing to other bottlenecks of the expression pathway that are already limiting at low gene levels [63], [64].

In summary, rp*Dt*HNL2, 3 and 4 were successfully produced intracellularly in *P. pastoris*, however enzyme yield and activity have been moderate compared to rp*Dt*HNL1. Purification and visualization of intracellularly produced enzyme was further challenging due to little amounts of recombinant expressed proteins and showed no advantages compared to production by *E. coli*.

Hence, an important advantage of extracellular protein production in *P. pastoris* is an easier purification from undesired proteins. Only low levels of endogenous proteins are secreted from *P. pastoris* and procedures like disruption and separation of extraneous cell compartments are not necessary [40], [65], [66].

5 Conclusion and Outlook

Expression of *Dt*HNL1, 2, 3 and 4 in *E.coli* and *P.pastoris* as well as purification of *E.coli* produced enzymes was successfully performed. Subsequent characterization experiments of purified and glycosylated variants showed almost identical pH and temperature optima at pH 5.0 and 40°C. Slight deviations were observed for purified re*Dt*HNL 2 (35°C) and re*Dt*HNL4 (45°C). Despite *Dt*HNLs similarities in reaction optima, the glycosylation pattern showed considerable influence on the enzymes stabilities. Glycosylated enzyme expression variants were stable in all tested buffer systems for at least 312 hours. However, re*Dt*HNLs showed decreasing activities along with decreasing pH values. Temperature stability profiles showed, that rs*Dt*HNL3 and 4 were most stable even at temperatures up to 30°C. Nevertheless the glycosylation pattern seemed to decrease the enzymes' catalytic activity by 75%. It has to be considered that not each glycosylated enzyme shows the same glycosylation pattern. Rather, the additional sugar residues are a heterogenic mixture of diverse length and number that further show different influence on the enzymes catalytic activity.

Considering further applications of re*Dt*HNL enzymes, re*Dt*HNL3 would be the most interesting candidate. It showed the best substrate affinity for (*R*)-mandelonitrile (0.639 ± 0.079 mM), conversion rate (319.8s^{-1}) and favourable values considering pH and temperature stabilities.

With respect to applications of glycosylated variants, both rs*Dt*HNL3 and 4 showed most favourable characteristics. All the four glycosylated rs*Dt*HNLs showed similar catalytic activities and reaction optima, whereas both rs*Dt*HNL3 and 4 demonstrated improved stability values in temperatures higher than 30°C.

Overall, *Dt*HNL enzymes, purified as well as glycosylated, seem to be promising biocatalysts for industrial applications due to their activity at low pH and temperature, the most favourable conditions for cyanohydrin synthesis.

In contrast to the expectation that the vector backbone would show significant differences for the intracellular production of rp*Dt*HNL2, 3 and 4, the vector had only

minor influence on catalytic activity. Throughout only little amounts of protein were obtained for both pPpB1- and pPpT4-based plasmids. Yet, the PpB1- based constructs showed slightly better expression results since the weaker *ADH*1 promoter for Zeocin™ expression selects transformants with highest copy numbers but on the other hand forces the cells to use more resources to retain its resistance gene.

The yield and activity of former constructed rp*Dt*HNL1 have not been achieved, however even the well-produced rp*Dt*HNL1 did not show as high expression levels and activities as the extracellular produced enzymes in *P. pastoris*. Production as an extracellular enzyme further offers the advantage of easier purification without the risk of protein degradation due to the release of proteases during cell disruption. Challenges, as also observed for intracellular protein isolation in this thesis, could therefore be avoided.

It was shown that the purified, as well as extracellularly produced *Dt*HNLs offer a notable option as promising biocatalysts that are both easy to produce, to purify, and they also have good properties in view of the reaction conditions required for cyanohydrin synthesis reactions.

6 References

[1] M. A. Kassim and K. Rumbold, “HCN production and hydroxynitrile lyase: a natural activity in plants and a renewed biotechnological interest.,” *Biotechnol. Lett.*, vol. 36, no. 2, pp. 223–8, Mar. 2014.

[2] M. Winkler, A. Glieder, and K. Steiner, “C-X Bond Formation:Hydroxynitrile Lyases: From Nature to Application,” in *Comprehensive Chirality*, vol. 7, E. M. Carreira and H. Yamamoto, Eds. 2012, pp. 350–371.

[3] I. Hajnal, A. Łyskowski, U. Hanefeld, K. Gruber, H. Schwab, and K. Steiner, “Biochemical and structural characterization of a novel bacterial manganese-dependent hydroxynitrile lyase,” *FEBS J.*, vol. 280, no. 22, pp. 5815–5828, 2013.

[4] I. Dreveny, K. Gruber, A. Glieder, A. Thompson, and C. Kratky, “The hydroxynitrile lyase from almond: A lyase that looks like an oxidoreductase,” *Structure*, vol. 9, no. 9, pp. 803–815, 2001.

[5] S. Nakano, M. Dadashipour, and Y. Asano, “Structural and functional analysis of hydroxynitrile lyase from Baliospermum montanum with crystal structure, molecular dynamics and enzyme kinetics.,” *Biochim. Biophys. Acta*, vol. 1844, no. 12, pp. 2059–2067, 2014.

[6] J.-K. Guterl, J. N. Andexer, T. Sehl, J. von Langermann, I. Frindi-Wosch, T. Rosenkranz, J. Fitter, K. Gruber, U. Kragl, T. Eggert, and M. Pohl, “Uneven twins: comparison of two enantiocomplementary hydroxynitrile lyases with alpha/beta-hydrolase fold.,” *J. Biotechnol.*, vol. 141, no. 3–4, pp. 166–73, 2009.

[7] H. Lauble, B. Miehlich, S. Förster, H. Wajant, and F. Effenberger, “Crystal structure of hydroxynitrile lyase from Sorghum bicolor in complex with the inhibitor benzoic acid: A novel cyanogenic enzyme,” *Biochemistry*, vol. 41, no. 40, pp. 12043–12050, 2002.

[8] E. Lanfranchi, M. Winkler, T. Pavkov-Keller, E.-M. Koehler, M. Diepold, K. Steiner, B. Darnhofer, J. Hartler, T. V. D. B.-J. Joostenf, M. Gruber-Khadjawia, G. G. Thallingera, R. Birner-Gruenbergera, K. Gruber, and A. Glieder, “Manuscript in preperation.”

[9] K. Trummler, J. Roos, U. Schwaneberg, F. Effenberger, S. Förster, K. Pfizenmaier, and H. Wajant, “Expression of the Zn2+-containing hydroxynitrile lyase from flax (Linum usitatissimum) in Pichia pastoris- utilization of the recombinant enzyme for enzymatic analysis and site-directed mutagenesis,” *Plant Sci.*, vol. 139, no. 1, pp. 19–27, 1998.

[10] M. Dadashipour, Y. Ishida, K. Yamamoto, and Y. Asano, “Discovery and molecular and biocatalytic properties of hydroxynitrile lyase from an invasive millipede, *Chamberlinius hualienensis*,” *Proc. Natl. Acad. Sci.*, vol. 112, no. 34, pp. 10605–10610, 2015.

[11] H. Wajant, S. Forster, D. Selmar, F. Effenberger, and K. Pfizenmaier, “Purification and Characterization of a Novel (R)-Mandelonitrile Lyase from the Fern Phlebodium aureum.,” *Plant Physiol.*, vol. 109, no. 4, pp. 1231–1238, Dec. 1995.

[12] D. Alagöz, S. S. Tükel, and D. Yildirim, “Purification, immobilization and characterization of (R)-hydroxynitrile lyase from Prunus amygdalus turcomanica seeds and their applicability for synthesis of enantiopure cyanohydrins,” *J. Mol. Catal. B Enzym.*, vol. 101, pp. 40–46, Mar. 2014.

[13] G. W. Kuroki and E. E. Conn, “Mandelonitrile lyase from Ximenia americana L.: stereospecificity and lack of flavin prosthetic group.,” *Proc. Natl. Acad. Sci.*, vol. 86, no. 18, pp. 6978–6981, Sep. 1989.

[14] T. Ueatrongchit, T. Ohmiya, A. H-kittikun, and Y. Asano, “Enzyme and Microbial Technology Hydroxynitrile lyase from Passiflora edulis : Purification , characteristics and application in asymmetric synthesis of (R) -mandelonitrile,” vol. 46, pp. 456–465, 2010.

[15] M. Zagrobelny, S. Bak, and B. L. Møller, “Cyanogenesis in plants and arthropods,” *Phytochemistry*, vol. 69, no. 7, pp. 1457–1468, 2008.

[16] J. E. Poulton, “Cyanogenesis in plants.,” *Plant Physiol.*, vol. 94, no. 2, pp. 401–5, Oct. 1990.

[17] M. Zagrobelny, S. Bak, A. V. Rasmussen, B. Jørgensen, C. M. Naumann, and B. Lindberg Møller, “Cyanogenic glucosides and plant–insect interactions,” *Phytochemistry*, vol. 65, no. 3, pp. 293–306, 2004.

[18] T. E. Tappey H. Jones, William E. Conner, Jerrold Meinwald, Hans E. Eisner, “Benzoyl cyanide and mandelonitrile in the cyanogenetic secretion of a centipede,” *J. Chem. Ecol.*, vol. 2, no. 4, pp. 421–429, 1976.

[19] S. S. Duffey, “Cyanide and Arthropods.,” in *Cyanide in Biology.*, F. Vennesland, B., Conn, E.E., Knowles, C.J., Westley, J., Wissing, Ed. London: Academic Press, 1981, p. 385–414.

[20] B. Reece, J, Meyers, N, Urry, L, Cain, M, Wasserman, S, Minorsky, P, Jackson, R, Cooke, *Cambell Biology, 9th Edition*. Pearson, 2005.

[21] M. a. Kassim, S. a. Sooklal, R. Archer, and K. Rumbold, “Screening for hydroxynitrile lyase activity in non-commercialised plants,” *South African J. Bot.*, vol. 93, pp. 9–13, Jul. 2014.

[22] R. Weis, P. Poechlauer, R. Bona, W. Skranc, R. Luiten, M. Wubbolts, H. Schwab, and a Glieder, “Biocatalytic conversion of unnatural substrates by recombinant almond R-HNL isoenzyme 5,” *J. Mol. Catal. B Enzym.*, vol. 29, no. 1–6, pp. 211–218, Jun. 2004.

[23] M. Sharma, N. N. Sharma, and T. C. Bhalla, “Hydroxynitrile lyases: At the interface of biology and chemistry,” *Enzyme Microb. Technol.*, vol. 37, no. 3, pp. 279–294, Aug. 2005.

[24] M. Dadashipour and Y. Asano, “Hydroxynitrile Lyases: Insights into Biochemistry, Discovery, and Engineering,” *ACS Catal.*, vol. 1, no. 9, pp. 1121–1149, Sep. 2011.

[25] E. Lanfranchi, “NEW HYDROXYNITRILE LYASE FROM WHITE RABBIT’S FOOT FERN: The route from discovery to perspectives for applications,” 2015.

[26] G. E. Healthcare and L. Sciences, “Recombinant Protein Purification, Principles and Methods,” pp. 1–308, 2012.

[27] G. E. Healthcare and L. Sciences, “Size Exclusion Chromatography.”

[28] C. H. Hirs, “Gel filtration.,” *Methods Enzymol.*, vol. 47, pp. 97–107, 1977.

[29] L. Reinhard, A. Geerlof, J. Mueller-dieckmann, M. S. Weiss, G. W. Vej, and F.-G. Cedex, “laboratory communications Optimization of protein buffer cocktails using Thermofluor laboratory communications,” no. October 2012, pp. 209–214, 2013.

[30] M. D. Cummings, M. a Farnum, and M. I. Nelen, “Universal screening methods and applications of ThermoFluor.,” *J. Biomol. Screen. Off. J. Soc. Biomol. Screen.*, vol. 11, no. 7, pp. 854–863, 2006.

[31] M. W. Pantoliano, E. C. Petrella, J. D. Kwasnoski, V. S. Lobanov, J. Myslik, E. Graf, T. Carver, E. Asel, B. a Springer, P. Lane, and F. R. Salemme, “High-density miniaturized thermal shift assays as a general strategy for drug discovery.,” *J. Biomol. Screen. Off. J. Soc. Biomol. Screen.*, vol. 6, no. 6, pp. 429–440, 2001.

[32] M. C. Lo, A. Aulabaugh, G. Jin, R. Cowling, J. Bard, M. Malamas, and G. Ellestad, “Evaluation of fluorescence-based thermal shift assays for hit identification in drug discovery,” *Anal. Biochem.*, vol. 332, no. 1, pp. 153–159, 2004.

[33] Http://www.bio.anl.gov/molecular_and_systems_biology/Sensor/sensor_images/assay_theory_figure, “Thermal Shift Assay.” .

[34] Emerson, “Fundamentals of Gas Chromatography,” *85th Annu. Int. Sch. Hydrocarb. Meas.*, vol. 43, pp. 1–8, 2010.

[35] G. a Eiceman, H. H. Hill, and J. Gardea-Torresdey, “Gas chromatography.,” *Anal. Chem.*, vol. 70, no. 12, p. 321R–339R, 1998.

[36] Agilent, “LC AND LC / MS Your Essential Resource for Columns & Supplies.”

[37] J. E. Dowd and D. S. Riggs, “A Comparison of Estimates of Michaelis-Menten Kinetic Constants From Various Linear Transformations,” *J. Biol. Chem.*, vol. 240, no. 2, pp. 863–869, 1965.

[38] P. M. Doran, *Bioprocess Engineering Principles*, 2nd ed. Oxford: Academic Press, 2013.

[39] M. . Gleeson and P. Sudbery, “The methylotrophic yeasts,” *Yeast*, vol. 4, pp. 1–15, 1988.

[40] S. Macauley-Patrick, M. L. Fazenda, B. McNeil, and L. M. Harvey, “Heterologous protein production using the Pichia pastoris expression system,” *Yeast*, vol. 22, no. 4, pp. 249–270, 2005.

[41] W. Zhang, M. Inan, and M. M. Meagher, “Fermentation strategies for recombinant protein expression in the methylotrophic yeast Pichia pastoris .pdf,” *Biotechnol. Bioprocess Eng .*, vol. 5, no. 4, pp. 275–287, 2000.

[42] J. M. Cregg, J. L. Cereghino, J. Shi, and D. R. Higgins, “Recombinant Protein Expression in Pichia pastoris,” *Mol. Biotechnol.*, vol. 16, no. 1, pp. 23–52, 2000.

[43] F. S. Hartner and A. Glieder, “Regulation of methanol utilisation pathway genes in yeasts.,” *Microb. Cell Fact.*, vol. 5, no. 1, p. 39, 2006.

[44] G. Gellissen, “Heterologous protein production in methylotrophic yeasts,” *Appl. Microbiol. Biotechnol.*, vol. 54, no. 6, pp. 741–750, 2000.

[45] H. Rußmayer, M. Buchetics, C. Gruber, M. Valli, K. Grillitsch, G. Modarres, R. Guerrasio, K. Klavins, S. Neubauer, H. Drexler, M. Steiger, C. Troyer, A. Al Chalabi, G. Krebiehl, D. Sonntag, G. Zellnig, G. Daum, A. B. Graf, F. Altmann, G. Koellensperger, S. Hann, M. Sauer, D. Mattanovich, and B. Gasser, “Systems-level organization of yeast methylotrophic lifestyle,” *BMC Biol.*, 2015.

[46] L. Näätsaari, B. Mistlberger, C. Ruth, T. Hajek, F. S. Hartner, and A. Glieder, “Deletion of the Pichia pastoris KU70 Homologue Facilitates Platform Strain Generation for Gene Expression and Synthetic Biology,” *PLoS One*, vol. 7, no. 6, p. e39720, 2012.

[47] B. Krammer, K. Rumbold, M. Tschemmernegg, P. Pöchlauer, and H. Schwab, “A novel screening assay for hydroxynitrile lyases suitable for high-throughput screening.,” *J. Biotechnol.*, vol. 129, no. 1, pp. 151–61, Mar. 2007.

[48] J. Lin-cereghino, W. W. Wong, S. Xiong, W. Giang, T. Linda, J. Vu, S. D. Johnson, and G. P. Lin-cereghino, “Condensed protocol for competent cell preparation and transformation of the methylotrophic yeast Pichia pastoris,” *Biotechniques*, vol. 38, no. 1, pp. 48–52, 2005.

[49] Y. Fukuta, S. Nanda, Y. Kato, H. Yurimoto, Y. Sakai, H. Komeda, and Y. Asano, “Characterization of a New (R)-Hydroxynitrile Lyase from the Japanese Apricot Prunus mume and cDNA Cloning and Secretory Expression of One of the Isozymes in Pichia pastoris,” *Biosci. Biotechnol. Biochem.*, vol. 75, no. 2, pp. 214–220, May 2014.

[50] J. Andexer, J.-K. Guterl, M. Pohl, and T. Eggert, “A high-throughput screening assay for hydroxynitrile lyase activity.,” *Chem. Commun. (Camb).*, vol. 9, no. 40, pp. 4201–4203, 2006.

[51] R. Wiedner, B. Kothbauer, T. Pavkov-Keller, M. Gruber-Khadjawi, K. Gruber, H. Schwab, and K. Steiner, “Improving the Properties of Bacterial R -Selective Hydroxynitrile Lyases for Industrial Applications,” *ChemCatChem*, vol. 7, no. 2, pp. 325–332, 2015.

[52] Sigma-Aldrich, “SYPRO Orange Protein Gel Stain,” *http://www.sigmaaldrich.com/catalog/product/Sigma/S5692?lang=de&region=AT (10.10.2015)*. .

[53] G. Thiault, a Mellouki, G. Le Bras, a Chakir, N. Sokolowski-Gomez, and D. Daumont, “UV-absorption cross sections of benzaldehyde, ortho-, meta-, and para-tolualdehyde,” *J. Photochem. Photobiol. A Chem.*, vol. 162, no. 2–3, pp. 273–281, 2004.

[54] R. Eisenthal, M. J. Danson, and D. W. Hough, “Catalytic efficiency and kcat/KM: a useful comparator?,” *Trends Biotechnol.*, vol. 25, no. 6, pp. 247–249, 2007.

[55] C. E. Aitken, R. A. Marshall, and J. D. Puglisi, “An Oxygen Scavenging System for Improvement of Dye Stability in Single-Molecule Fluorescence Experiments,” *Biophys. J.*, vol. 94, no. 5, pp. 1826–1835, 2008.

[56] T. Ueatrongchit, A. Kayo, H. Komeda, Y. Asano, and A. H-Kittikun, “Purification and Characterization of A Novel (R)-Hydroxynitrile Lyase from Eriobotrya japonica (Loquat),” *Biosci. Biotechnol. Biochem.*, vol. 72, no. 6, pp. 1513–1522, May 2014.

[57] J. Zuegg, K. Gruber, M. Gugganig, U. G. Wagner, and C. Kratky, “Three-dimensional structures of enzyme – substrate complexes of the hydroxynitrile lyase from Hevea brasiliensis,” pp. 1990–2000, 2000.

[58] M. Bauer, H. Griengl, and W. Steiner, “Kinetic studies on the enzyme (S)-hydroxynitrile lyase from Hevea brasiliensis using initial rate methods and progress curve analysis,” *Biotechnol. Bioeng.*, vol. 62, no. 1, pp. 20–29, 1999.

[59] M. Hasslacher, C. Kratky, H. Griengl, H. Schwab, and S. D. Kohlwein, “Hydroxynitrile lyase from Hevea brasiliensis: Molecular characterization and mechanism of enzyme catalysis,” *Proteins Struct. Funct. Bioinforma.*, vol. 27, no. 3, pp. 438–449, 1997.

[60] S. Chueskul and M. Chulavatnatol, “Properties of a -Hydroxynitrile Lyase from the Petiole of Cassava (Manihot esculenta Crantz),” vol. 334, no. 2, pp. 401–405, 1996.

[61] R. Weis, “Expression feasibility of Dt HNL isozymes 1 , 2 , 3 and 4 extracellularly in Pichia pastoris using the wildtype AOX1-promoter Microscale and bioreactor cultivations,” 2014.

[62] R. Weis, “KYROBIO Expression feasibility of Dt HNL intracellularly and extracellularly in Pichia pastoris using VTU ´ s expression technology.”

[63] M. D. Hohenblum H, Gasser B, Maurer M, Borth N, “Effects of gene dosage, promoters, and substrates on unfolded protein stress of recombinant Pichia pastoris.,” *Biotechnol. Bioeng.*, vol. 85, pp. 367–75, 2004.

[64] Q. Shen, M. Wu, H. Bin Wang, H. Naranmandura, and S. Q. Chen, “The effect of gene copy number and co-expression of chaperone on production of albumin fusion proteins in Pichia pastoris,” *Appl. Microbiol. Biotechnol.*, vol. 96, no. 3, pp. 763–772, 2012.

[65] M. Yang, S. Teymorian, P. Olivares, and P. P. N. Murthy, “Extracellular expression of alkaline phytase in Pichia pastoris: Influence of signal peptides, promoters and growth medium,” *Biotechnol. Reports*, vol. 6, pp. 112–118, 2015.

[66] D. Mattanovich, A. Graf, J. Stadlmann, M. Dragosits, A. Redl, M. Maurer, M. Kleinheinz, M. Sauer, F. Altmann, and B. Gasser, “Genome, secretome and glucose transport highlight unique features of the protein production host Pichia pastoris.,” *Microb. Cell Fact.*, vol. 8, p. 29, 2009.

7 Abbreviations

96 DWP	96- well footprint deep well plate
AOX	alcohol oxidase gene
Arg	arginine
Asp	aspartic acid
BCA	bicinchoninic acid
Bet v 1	pollen allergen of *Betula pendula*
BMD	buffered minimal glucose medium
BMM	buffered minimal methanol medium
CCD	Charge Coupled Devices
ddH_2O	double distilled water
dH_2O	deionized water
DNA	deoxyribonucleic acid
dNTP	deoxyribonucleotide
Dt	*Davallia tyermanii*
DTT	dithiothreitol
*Endo*H	endoglycosidase H
EtBr	ethidium bromide
FAD	Flavin adenine dinucleotide
FPLC	fast protein liquid chromatography
G6P	glucose-6-phosphate
G6PDH	glucose-6-phosphate dehydrogenase
GAP	glycerinealdehyde-3-phosphate
GC	gas chromatography
Gln	glutamine
Glu	glutamic acid
Gly	glycine
HCN	hydrogen cyanide
His	histidine
HNL	hydroxyl nitrile lyase
LB	Luria Bertani
Lys	lysine
MeOH	methanol
MES	2-(N-morpholino)ethanesulfonic acid
MNL	mandelonitrile

MTBE	Methyl-tert-butylether
MUT	methanol utilization
Mut^+	methanol utilization plus phenotype
Mut^S	methanol utilization slow phenotype
$NAD(P)^+$	nicotinamide adenine dinucleotide (phosphate), oxidized
NAD(P)H	nicotinamide adenine dinucleotide (phosphate), reduced
NaCN	sodium cyanide
OD	optical density
PCR	polymerase chain reaction
Phe	phenylalanine
PMSF	phenylmethanesulfonyl fluoride
PPB	potassium phosphate buffer
RFU	relative fluorescent units
RNA	ribonucleic acid
Ser	serine
SDS-PAGE	sodium dodecyl sulfate- polyacrylamide gel electrophoresis
Tyr	tyrosine
WT	wild type
YNB	yeast nitrogen base
YPD	yeast extract peptone dextrose
Y-PER	Dialyzable Yeast Protein Reagent
Zeo	Zeocin™

8 Supplementary data

8.1 Melting curve analysis of purified *Dt*HNL1

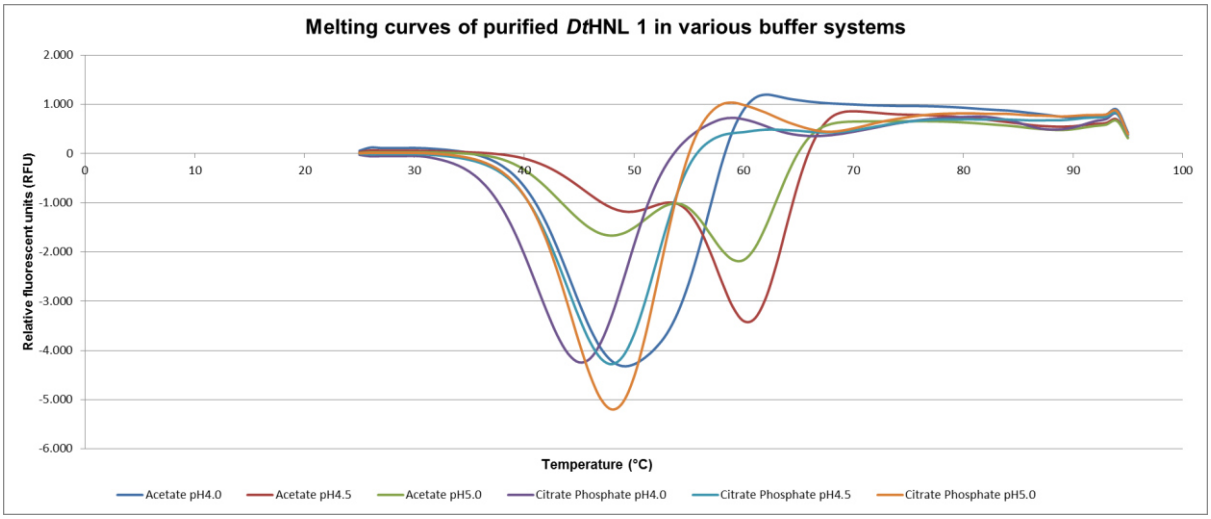

Figure S1: Melting curves of purified *Dt*HNL1 in acetate and citrate phosphate buffers of various pH. The relative fluorescent units of the TAMRA reporter signal are plotted against the respective pH.

8.2 Kinetic Parameters of purified *Dt*HNLs

Table S1: Specific activities of *Dt*HNLs for cleavage of (*R*)-MNL taken as basis for determination of kinetic parameters.

Specific activity *Dt*HNLs				
R-MNL	**Mean V *Dt*HNL1**	**Mean V *Dt*HNL2**	**Mean V *Dt*HNL3**	**Mean V *Dt*HNL4**
(mM)	**(µmol/min/mg)**	**(µmol/min/mg)**	**(µmol/min/mg)**	**(µmol/min/mg)**
0.009	10.9 ± 1.9	8.5 ± 1.0	10.9 ± 1.4	7.7 ± 1.6
0.045	44 ± 5.9	37.8 ± 6.5	52.4 ± 11.7	40.9 ± 3.2
0.09	80.2 ± 13.3	70.3 ± 8.7	100.1 ± 14.8	76.3 ± 6.4
0.225	154.5 ± 18.3	134.8 ± 15.7	218.3 ± 33.7	167.9 ± 13.5
0.45	223.1 ± 20.9	193.8 ± 18.9	361.5 ± 52.3	254.7 ± 16.5
0.9	304.9 ± 26.8	274.2 ± 25.3	546.8 ± 64.4	420.5 ± 65.3
2.25	321.9 ± 37.9	337.1 ± 24.9	734.0 ± 53.7	512.2 ± 60.5
3.6	-	363.8 ± 34.0	883.4 ± 27.8	559.9 ± 61.1
4.5	360.8 ± 29.7	366.9 ± 32.8	791.5 ± 65.5	574.4 ± 70.2
6.75	357.6 ± 21.6	361.7 ± 15.9	815.5 ± 72.5	585.6 ± 52.9
9	358.6 ± 15.9	390.9 ± 30.3	834.2 ± 101.7	575.9 ± 65.0
13.5	366.8 ± 22.7	393.8 ± 39.1	857.4 ± 71.3	621.3 ± 103.5

*Dt*HNL1 for cyanogenesis

Table S2: Initial reaction rates of *Dt*HNL1 depending on different R-Mandelonitrile concentrations. Reactions were performed in 50 mM citrate phosphate buffer pH 5.0

Specific activity *Dt*HNL1			
R-MNL	**V Replicate 1**	**V Replicate 2**	**V Replicate 3**
(mM)	**(µmol/min/mg)**	**(µmol/min/mg)**	**(µmol/min/mg)**
0.009	13.1	11.1	8.4
0.045	50.3	45.5	36.0
0.09	93.6	84.7	62.1
0.225	172.2	162.0	129.2
0.45	238.5	237.2	193.3
0.9	331.1	315.5	267.9
2.25	375.2	300.0	290.5
4.5	402.6	341.8	337.7
6.75	388.0	340.9	343.7
9	378.3	339.4	357.9
13.5	380.5	385.0	334.7
18	343.4	359.3	366.1

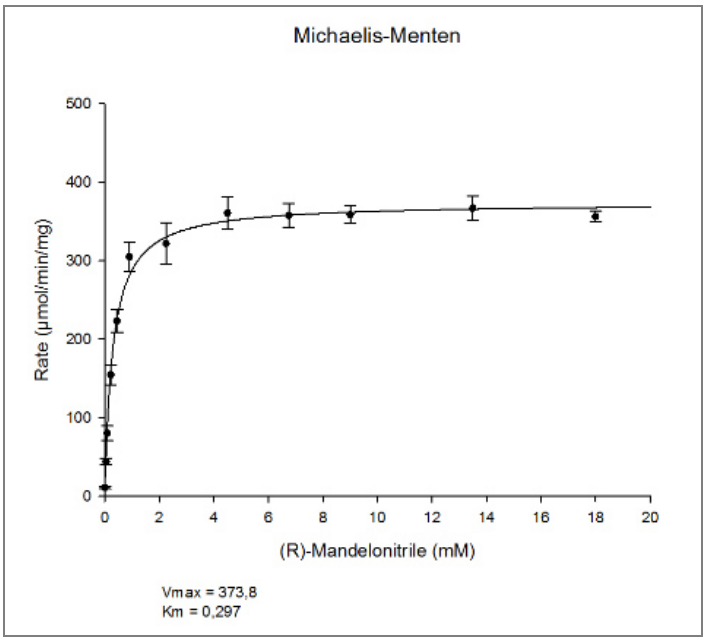

Figure S2: Graphical representation of Michaelis – Menten parameters for R- mandelonitrile for *Dt*HNL1 cyanogenesis. R-Mandelonitrile concentrations were varied from 0.009 – 18 mM. Amount of enzyme used in the reaction was 0.1 µg. Calculations were done with SigmaPlot 13.0

Table S3: **Kinetic parameters for R- mandelonitrile in *Dt*HNL1 cyanogenesis reaction.**

	V_{max}	$K_{M\ R\text{-}MNL}$	k_{cat}	k_{cat}/K_M
	(µmol/min/mg)	**(mM)**	**(s^{-1})**	**(s^{-1} mM^{-1})**
*Dt*HNL 1	373.8	0.297	144.8	487.5

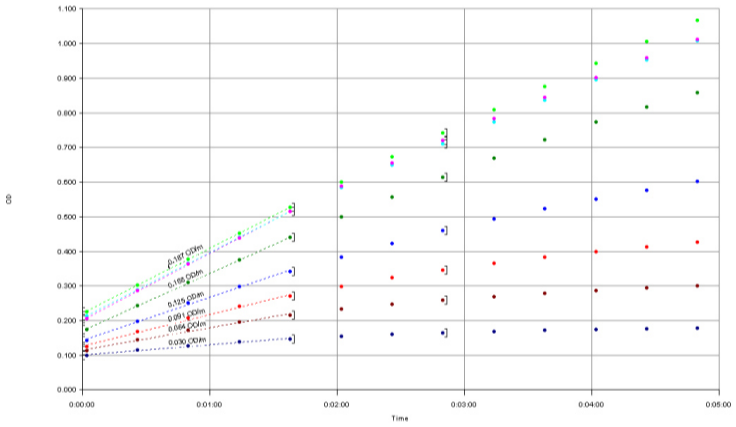

Figure S3: **Graphical representation of the different initial reaction rates of *Dt*HNL 1 converting R-mandelonitrile of various concentrations.**

*Dt*HNL2 for cyanogenesis

Table S4: Initial reaction rates of *Dt*HNL2 depending on different R-Mandelonitrile concentrations. Reactions were performed in 50 mM citrate phosphate buffer pH 5.0

Specific activity *Dt*HNL2			
R-MNL	**V Replicate 1**	**V Replicate 2**	**V Replicate 3**
(mM)	**(µmol/min/mg)**	**(µmol/min/mg)**	**(µmol/min/mg)**
0.009	9.8	7.4	8.2
0.045	46.9	33.6	32.7
0.09	81.7	60.6	68.6
0.225	156.9	122.9	124.5
0.45	217.7	171.4	192.2
0.9	310.0	256.6	255.9
2.25	372.0	323.4	315.9
3.6	411.8	337.9	341.5
4.5	411.0	332.3	357.4
6.75	358.7	343.8	382.4
9	393.0	352.7	426.9
13.5	423.0	338.5	419.9

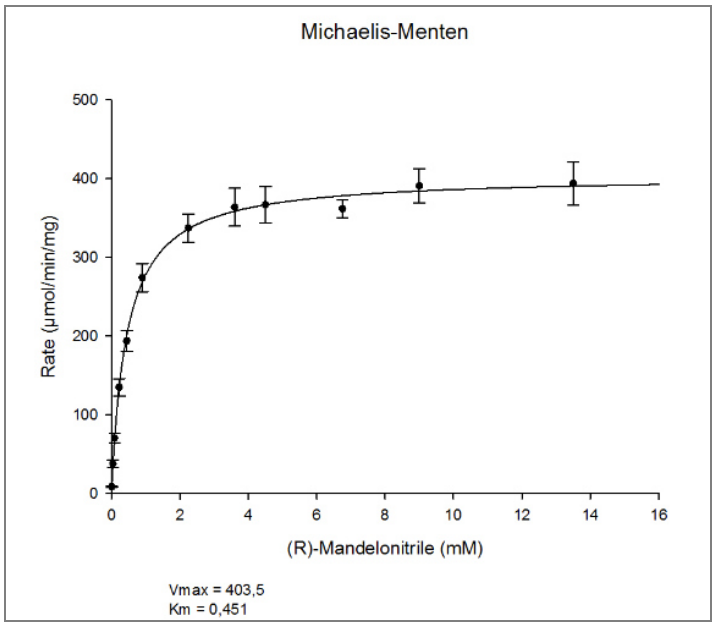

Figure S4: Graphical representation of Michaelis – Menten parameters for R- mandelonitrile in *Dt*HNL2 cyanogenesis reaction. R-Mandelonitrile concentrations were varied from 0.009 – 18 mM. Amount of enzyme used in the reaction was 0.1 µg. Calculations were done with SigmaPlot 13.0

Table S5: Kinetic parameters for R- mandelonitrile in *Dt*HNL2 cyanogenesis reaction.

	V_{max}	$K_{M\ R\text{-}MNL}$	k_{cat}	k_{cat}/K_M
	(µmol/min/mg)	**(mM)**	**(s^{-1})**	**(s^{-1} mM^{-1})**
*Dt*HNL 2	403.5	0.451	156.9	347.8

*Dt*HNL3 for cyanogenesis

Table S6: Initial reaction rates of *Dt*HNL 3 depending on different R-Mandelonitrile concentrations. Reactions were performed in 50 mM citrate phosphate buffer pH 5.0

Specific activity *Dt*HNL3			
R-MNL	**V Replicate 1**	**V Replicate 2**	**V Replicate 3**
(mM)	**(µmol/min/mg)**	**(µmol/min/mg)**	**(µmol/min/mg)**
0.009	10.2	9.4	12.8
0.045	45.7	42.6	68.
0.09	93.8	85.9	120.4
0.225	190.8	198.1	265.7
0.45	320.7	328.4	435.2
0.9	478.9	528.2	633.2
2.25	682.0	711.9	808.0
3.6	915.2	847.4	887.6
4.5	702.0	856.8	815.6
6.75	715.0	847.8	883.6
9	692.7	882.5	927.3
13.5	757.0	915.6	899.5

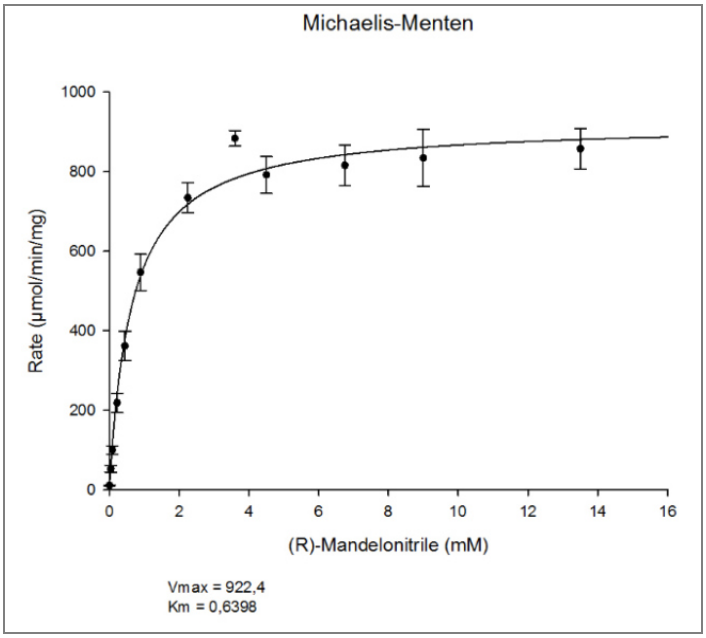

Figure S5: Graphical representation of Michaelis – Menten parameters for R- mandelonitrile in *Dt*HNL3 cyanogenesis reaction. R-Mandelonitrile concentrations were varied from 0.009 – 18 mM. Amount of enzyme used in the reaction was 0.1 µg. Calculations were done with SigmaPlot 13.0

Table S8: Kinetic parameters for R- mandelonitrile for *Dt*HNL 3 cyanogenesis.

	V_{max}	$K_{M\ R\text{-}MNL}$	k_{cat}	k_{cat}/K_M
	(µmol/min/mg)	**(mM)**	**(s^{-1})**	**($s^{-1}\ mM^{-1}$)**
*Dt*HNL 3	922.4	0.640	306.7	479.4

*Dt*HNL4 for cyanogenesis

Table S9: Initial reaction rates of *Dt*HNL4 depending on different R-Mandelonitrile concentrations. Reactions were performed in 50 mM citrate phosphate buffer pH 5.0

Specific activity *Dt*HNL4			
R-MNL	**V Replicate 1**	**V Replicate 2**	**V Replicate 3**
(mM)	**(µmol/min/mg)**	**(µmol/min/mg)**	**(µmol/min/mg)**
0.009	9.3	8.3	5.5
0.045	45.3	37.7	39.6
0.09	85.0	70.2	73.4
0.225	186.3	162.9	154.4
0.45	272.6	258.7	232.7
0.9	456.6	475.9	328.8
2.25	548.0	561.6	427.1
3.6	582.6	620.8	476.3
4.5	579.6	657.5	485.9
6.75	583.5	651.4	521.9
9	542.3	666.8	518.8
13.5	654.8	727.8	481.1

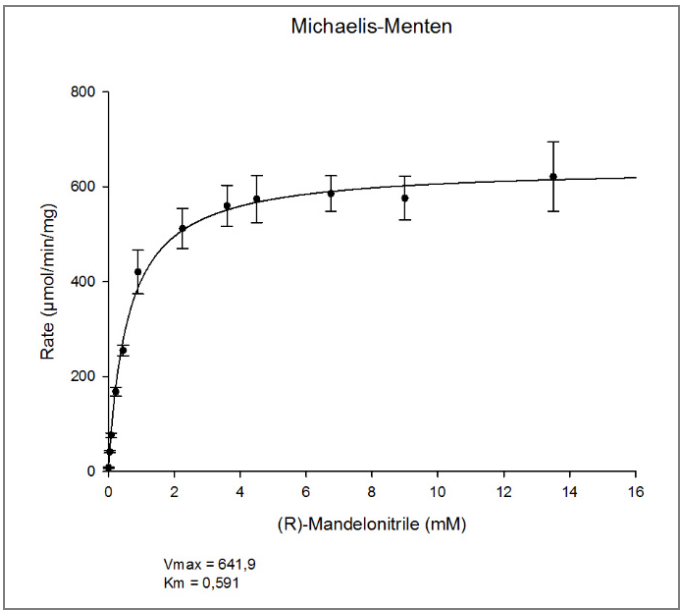

Figure S6: Graphical representation of Michaelis – Menten parameters for R- mandelonitrile in *Dt*HNL4 cyanogenesis reaction. R-Mandelonitrile concentrations were varied from 0.009 – 18 mM. Amount of enzyme used in the reaction was 0.1 µg. Calculations were done with SigmaPlot 13.0

Table S10: **Kinetic parameters for R- mandelonitrile in *Dt*HNL4 cyanogenesis reaction.**

	V_{max}	$K_{M\ R\text{-}MNL}$	k_{cat}	k_{cat}/K_M
	(µmol/min/mg)	(mM)	(s^{-1})	(s^{-1} mM^{-1})
*Dt*HNL 4	641.9	0.591	214.1	362.3

*Dt*HNL1 for synthesis reaction

Table S11: **Initial reaction rates of *Dt*HNL1 for synthesis reaction with respective substrate concentrations of benzaldehyde.**

Specific activities *Dt*HNL 1						
Replicate 1 include zero			Replicate 2 include zero			Average
BA Organic phase	BA Buffer phase	V	BA Organic phase	BA Buffer phase	V	BA Buffer phase
(mM)	(mM)	(µmol/min/mg)	(mM)	(mM)	(µmol/min/mg)	(mM)
468.9	6.9	131.6	611.2	9.0	138.5	7.9
417.5	6.1	134.1	382.9	5.6	112.9	5.9
401.6	5.9	101.8	332.1	4.9	93.0	5.4
276.1	4.1	87.3	265.1	3.9	76.7	4.0
247.0	3.6	80.3	243.2	3.6	99.3	3.6
182.0	2.7	38.4	193.1	2.8	75.9	2.8
138.4	2.0	55.6	171.5	2.5	47.5	2.3
114.4	1.7	39.5	118.4	1.7	40.1	1.7
91.9	1.4	30.5	87.6	1.3	39.3	1.3
45.6	0.7	16.8	45.2	0.7	20.1	0.7
21.4	0.3	8.6	20.4	0.3	7.9	0.3
8.5	0.1	3.0	7.9	0.1	2.3	0.1

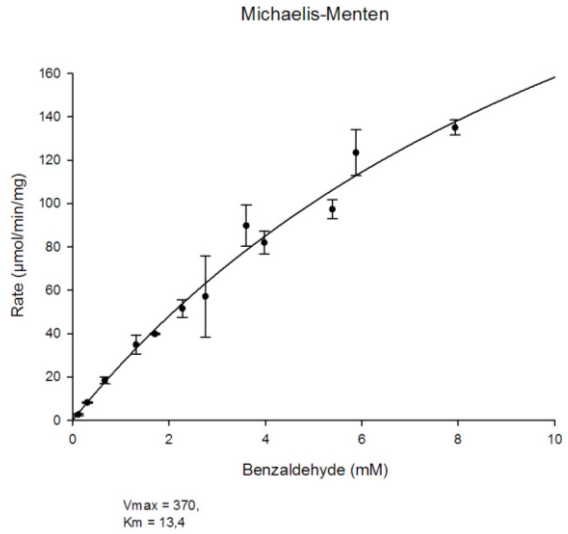

Figure S7: Graphical representation of Michaelis – Menten parameters for benzaldehyde for *Dt*HNL1 synthesis reaction. Benzaldehyde concentrations were varied from 0.1 – 6.9 mM in aqueous phase. Amount of enzyme used in the reaction was 0.05 mg. Calculations were done with SigmaPlot 13.0

Table S12: Kinetic parameters for benzaldehyde for *Dt*HNL1 synthesis reaction.

	V_{max}	$K_{M\ -\ Benzaldehyde}$	k_{cat}	k_{cat}/K_M
	(µmol/min/mg)	(mM)	(s^{-1})	(s^{-1} mM^{-1})
*Dt*HNL1	376.9 ± 88.9	13.4	71.6	5.3

8.3 Comparison of optimized *Dt*HNL1 and *Dt*HNL2

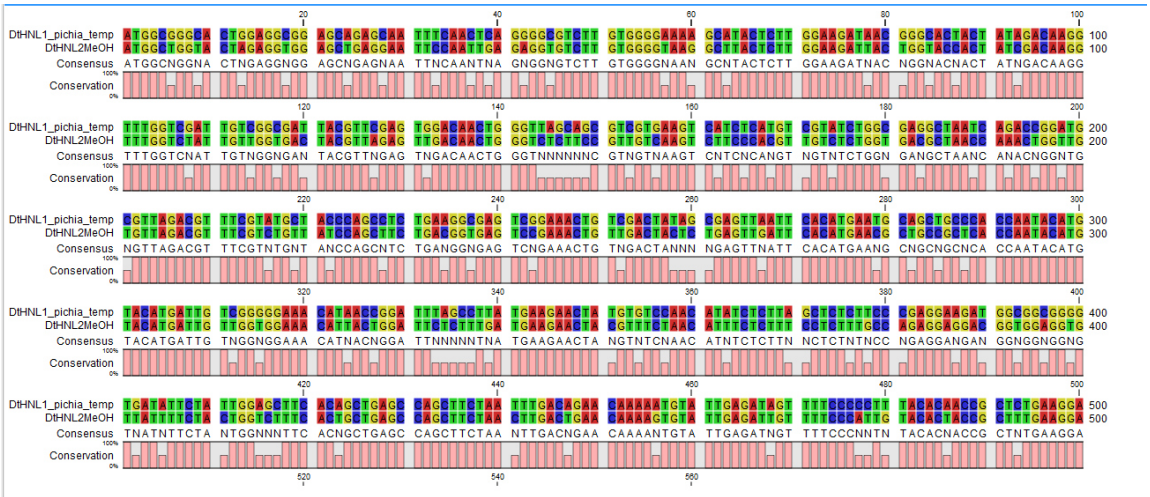

Figure S10: Alignment of *P. pastoris* optimized *Dt*HNL1 and *Dt*HNL2.

8.4 Glycerol stock list

Table S13: List of glycerol stocks that are related to this thesis or were generated during this work.

Box	Eppis N.	Host strain	Vector	Strain N.	Date	cc # strain colleczion
1	60	E. coli BL21 (DE3) Gold	pET_HNL02643_Davallia		21.08.2013	7164
1	80	E. coli Top10F'	pPpT4_S_DtHNL02643 Pichia opt		13.12.2013	7166
1	82	E. coli Top10F'	pPpB1_DtHNL Pichia opt		13.12.2013	7165
2	112	P. pastoris CBS 7435 MutS	pPpB1_DtHNL026543 Pichia opt	B1.G4	13.12.2013	7167
2	113	P. pastoris CBS 7435 MutS	pPpB1_DtHNL026543 Pichia opt	B1.G4	13.12.2013	7164
2	114	P. pastoris CBS 7435 MutS	pPpT4_S_DtHNL02643 Pichia opt	T4.F1	13.12.2013	7169
2	115	P. pastoris CBS 7435 MutS	pPpT4_S_DtHNL02643 Pichia opt	T4.F1	13.12.2013	7169
2	116	P. pastoris CBS 7435 MutS	pPpT4_S_DtHNL02643 Pichia opt	T4.B7	13.12.2013	7168
2	117	P. pastoris CBS 7435 MutS	pPpT4_S_DtHNL02643 Pichia opt	T4.B7	13.12.2013	7168
2	122	P. pastoris CBS 7435 MutS	pPpB1_DtHNL026543 Pichia opt	B1.G4	14.01.2014	7167
2	123	P. pastoris CBS 7435 MutS	pPpB1_DtHNL026543 Pichia opt	B1.G4	14.01.2014	7164
2	124	P. pastoris CBS 7435 MutS	pPpT4_S_DtHNL02643 Pichia opt	T4.F1	14.01.2014	7169
2	125	P. pastoris CBS 7435 MutS	pPpT4_S_DtHNL02643 Pichia opt	T4.F1	14.01.2014	7169
2	136	E. Coli BL21 star (DE3)	pEHisTEV DtHNL 02641		25.02.2014	7171
2	137	E. Coli BL21 star (DE3)	pEHisTEV DtHNL 02641		25.02.2014	7171
2	138	E. Coli BL21 star (DE3)	pEHisTEV DtHNL 07602		25.02.2014	7172
2	139	E. Coli BL21 star (DE3)	pEHisTEV DtHNL 07602		25.02.2014	7172
2	140	E. Coli BL21 star (DE3)	pEHisTEV DtHNL 00751		25.02.2014	7173
2	141	E. Coli BL21 star (DE3)	pEHisTEV DtHNL 00751		25.02.2014	7173
2	142	E. Coli BL21 star (DE3)	pEHisTEV DtHNL 02643 opt		25.02.2014	7170
2	143	E. Coli BL21 star (DE3)	pEHisTEV DtHNL 02643 opt		25.02.2014	7170
2	162	E. Coli TOP 10 F'	pPpT4_S_DtHNL2_opt		30.07.2014	
2	163	E. Coli TOP 10 F'	pPpT4_S_DtHNL2_opt		30.07.2014	
2	164	E. Coli TOP 10 F'	pPpT4_S_DtHNL3_opt		30.07.2014	
2	165	E. Coli TOP 10 F'	pPpT4_S_DtHNL3_opt		30.07.2014	
2	166	E. Coli TOP 10 F'	pPpT4_S_DtHNL4_opt		30.07.2014	
2	167	E. Coli TOP 10 F'	pPpT4_S_DtHNL4_opt		30.07.2014	
2	168	E. Coli TOP 10 F'	pPpB1_DtHNL2_opt		30.07.2014	
2	169	E. Coli TOP 10 F'	pPpB1_DtHNL2_opt		30.07.2014	
2	170	E. Coli TOP 10 F'	pPpB1_DtHNL3_opt		30.07.2014	
2	171	E. Coli TOP 10 F'	pPpB1_DtHNL3_opt		30.07.2014	
2	172	E. Coli TOP 10 F'	pPpB1_DtHNL4_opt		30.07.2014	
2	173	E. Coli TOP 10 F'	pPpB1_DtHNL4_opt		30.07.2014	
3	198	P. pastoris CBS 7435 MutS	pPpB1_DtHNL2_opt		09.03.2015	
3	199	P. pastoris CBS 7435 MutS	pPpB1_DtHNL3_opt		09.03.2015	
3	200	P. pastoris CBS 7435 MutS	pPpB1_DtHNL4_opt		09.03.2015	